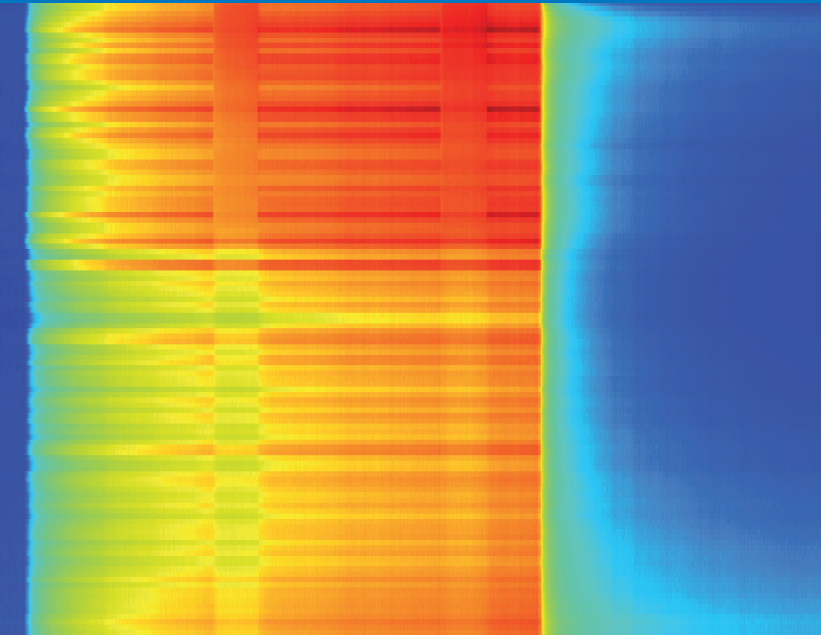


Distributed thermal response tests – New insights on U-pipe and Coaxial heat exchangers in groundwater-filled boreholes

JOSÉ ACUÑA



Doctoral Thesis in Energy Technology
Stockholm, Sweden 2013



KTH Industrial Engineering
and Management



KTH Industrial Engineering
and Management

Distributed thermal response tests – New insights on U-pipe and Coaxial heat exchangers in groundwater-filled boreholes

José Acuña

Doctoral Thesis 2013
KTH School of Industrial Engineering and Management
Division of Applied Thermodynamics and Refrigeration
SE-100 44 STOCKHOLM

Trita REFR Report 13/01
ISSN 1102-0245
ISRN KTH/REFR/13/01-SE
ISBN 978-91-7501-626-9

© José Acuña

Preface

A substantial amount of new insights about the operation and thermal response testing of U-pipe and Coaxial heat exchangers installed in groundwater filled boreholes are revealed in this experimental thesis work. I feel that I just planted one more seed to lots of further research to be done with the measurements presented here, but I can proudly say that ground source cooling and heating systems can be improved if the methods demonstrated in this thesis are implemented on existing and/or new installations.

This achievement is not only mine and it is hard to see how much work there is behind the measurements presented here. I would like to acknowledge those who helped me on this journey:

The first credit goes to the Swedish Energy Agency for financing this project through the EFFSYS+ and EFFSYS2 programs. This would have been impossible without our sponsors: Alfa-Laval, Ahlsell, Aska rör, AVANTI, Brage Broberg, Brunata, COMSOL, COOLY, Cupori, Ekofektiv, Energi-Montage, ETM Kylteknik, Extena, Geosigma, GRUNDFOS, Hydroresearch, Högalids elektriska, IVT, LAFOR Energientreprenader, LOWTE, Lämpöässä, Mateve Oy, Merinova, GEOTEC, MuoviTech, Neoenergy, NIBE, Nowab, PEMTEC, PMAB, Prof. Richard Beier, SEEC, Stures Brunnborrningar, SUST, SVEP, SWECO, THERMIA, Tibnor, Thoren VP, Tommy Nilsson, UPONOR, Viessmann, Willy's cleantech, WILO. Thanks also to Prof. Eric Granryd, Erik Björk, Martin Forsén, and Anders Nilsson, and other members of the EFFSYS board, for coordinating these research programs.

Manil Bygg, Nordahl Fastigheter, Klas Andersson, Kenneth Weber, and JM, are specially acknowledged for kindly allowing us to carry out this research at their installations and for their support during this work. I would like to extend a very sincere gratitude to Tommy Nilsson who significantly helped to materialize many of these installations, and to Sam Johansson who introduced me to the fascinating world of distributed temperature measurements.

For their help during installations, I would also like to recognize the important contributions of Peter Hill, Benny Sjöberg, Hans Alexandersson,

Karl-Åke Lundín, John Ljungqvist, Peter Platell, and Brage Broberg. I will always remember the magic phrase: *AKTA fibern!*

Thanks also to my dad José G. Acuña, to Michael Klasson, Åke Melinder, Erik Lindstein, Björn Kyrk, Mauri Lieskoski, Johan Wasberg, Jussi, Claudi, Samer, Bo Jansson, Jan Cederström, Willy Ociasson, Jan-Erik Nowacki, Rashid, Stina, Hatef, Carl, Julia, Jesus, Patricia, Tomas, Leoni, Maria, Andreas, Lukas, Tommy, Charles, Klaes, Eduard, Marcos, and Francois. You all gave me a hand at some point.

I would like to remember and acknowledge some people who no longer are physically with us but who helped and motivated me at different moments along this journey: Benny Andersson, Nabil Kasem, Olle Hellman, Stanislaw (Slawek), Abuelo Sequera, and Abuela Carmen.

A special recognition to my supervisor Prof. Björn Palm, whose humbleness and dedication inspired me day after day. Björn, thanks for trusting me, for your support and wise advices. Thanks also to you and Prof. Per Lundqvist for selecting me as a PhD student. I take the chance to greet our EITT family, it is a pleasure to be part of it! A special salutation to all my colleague PhD students for many moments together, especially to Monika and Hatef whom I had the pleasure to be roommate with.

A very particular gratitude to Palne Mogensen, the pioneer of thermal response testing and the most precise person I have ever met. Thanks for teaching me among other things the secrets of TRTs, and for all your valuable critics. You are a professional role model to me. Thank you also for showing me a bit more of Sweden, a beautiful country that is now part of me.

Mamá, Papá, Abuela Mercedes, María, Miguel, Fatima, Eduardo, little princess Natalia, primos y tíos, thanks for your support. I feel you often walk with me despite the distance that separates us!

And the most special credit goes to my beautiful wife, Dominika, for her infinite understanding, support and patience. This achievement is also yours! And to our daughters, Emilia and Amanda, for giving me even more reasons to finish this thesis. I love you!

It has been a fantastic journey thanks to all of you! May god give you health for many years to come!

Thank you!

José Acuña

Abstract

U-pipe Borehole Heat Exchangers (BHE) are widely used today in ground source heating and cooling systems in spite of their less than optimal performance. This thesis provides a better understanding on the function of U-pipe BHEs and investigates alternative methods to reduce the temperature difference between the circulating fluid and the borehole wall, including one thermosyphon and three different types of coaxial BHEs.

Field tests are performed using distributed temperature measurements along U-pipe and coaxial heat exchangers installed in groundwater filled boreholes. The measurements are carried out during heat injection thermal response tests and during short heat extraction periods using heat pumps. Temperatures are measured inside the secondary fluid path, in the groundwater, and at the borehole wall. These type of temperature measurements were until now missing.

A new method for testing borehole heat exchangers, Distributed Thermal Response Test (DTRT), has been proposed and demonstrated in U-pipe, pipe-in-pipe, and multi-pipe BHE designs. The method allows the quantification of the BHE performance at a local level.

The operation of a U-pipe thermosyphon BHE consisting of an insulated down-comer and a larger riser pipe using CO₂ as a secondary fluid has been demonstrated in a groundwater filled borehole, 70 m deep. It was found that the CO₂ may be sub-cooled at the bottom and that it flows upwards through the riser in liquid state until about 30 m depth, where it starts to evaporate.

Various power levels and different volumetric flow rates have been imposed to the tested BHEs and used to calculate local ground thermal conductivities and thermal resistances. The local ground thermal conductivities, preferably evaluated at thermal recovery conditions during DTRTs, were found to vary with depth. Local and effective borehole thermal resistances in most heat exchangers have been calculated, and their differences have been discussed in an effort to suggest better methods for interpretation of data from field tests.

Large thermal shunt flow between down- and up-going flow channels was identified in all heat exchanger types, particularly at low volumetric flow rates, except in a multi-pipe BHE having an insulated central pipe where the thermal contact between down- and up-coming fluid was almost eliminated.

At relatively high volumetric flow rates, U-pipe BHEs show a nearly even distribution of the heat transfer between the ground and the secondary fluid along the depth. The same applies to all coaxial BHEs as long as the flow travels downwards through the central pipe. In the opposite flow direction, an uneven power distribution was measured in multi-chamber and multi-pipe BHEs.

Pipe-in-pipe and multi-pipe coaxial heat exchangers show significantly lower local borehole resistances than U-pipes, ranging in average between 0.015 and 0.040 Km/W. These heat exchangers can significantly decrease the temperature difference between the secondary fluid and the ground and may allow the use of plain water as secondary fluid, an alternative to typical antifreeze aqueous solutions. The latter was demonstrated in a pipe-in-pipe BHE having an effective resistance of about 0.030 Km/W.

Forced convection in the groundwater achieved by injecting nitrogen bubbles was found to reduce the local thermal resistance in U-pipe BHEs by about 30% during heat injection conditions. The temperatures inside the groundwater are homogenized while injecting the N₂, and no radial temperature gradients are then identified. The fluid to groundwater thermal resistance during forced convection was measured to be 0.036 Km/W. This resistance varied between this value and 0.072 Km/W during natural convection conditions in the groundwater, being highest during heat pump operation at temperatures close to the water density maximum.

Keywords: Borehole Heat Exchangers, Distributed Thermal Response Test, Ground Source Heat Pumps, Coaxial, U-pipe, Multi-pipe, Pipe-in-pipe, Multi-chamber, Groundwater, Thermosyphon.

Nomenclature

α	Thermal diffusivity of the surrounding ground [m ² /s]
ΔT	Temperature difference [K]
h	Enthalpy [kJ/kg]
λ	Thermal conductivity of secondary fluid [W/(m K)]
λ_{rock}	Thermal conductivity of the surrounding ground [W/(m K)]
λ_{PE}	Thermal conductivity of polyethylene pipes [W/(m K)]
m_{dot}	Mass flow rate of CO ₂ in thermosyphon BHE [kg/s]
Nu	Nusselt number [-]
q'	Power per meter [W/m]
q_{1-12}	Heat flow through the peripheral pipes in Multi-pipe BHE [W]
q_0	Heat flow through the central pipe in Multi-pipe BHE [W]
q_{total}	Sum of heat flows through central and peripheral pipes [W]
Pr	Prandtl number [-]
R	Thermal resistance [Km/W]
R_{an-bw}	Annulus-to-borehole wall thermal resistance [Km/W]
R_b	Local borehole resistance [Km/W]
R_b^*	Effective borehole resistance [Km/W]
R_b^{*t}	Resistance based on true mean fluid temperature [Km/W]

R_{fgw}	Secondary fluid-to-groundwater thermal resistance [Km/W]
R_{gw-bw}	Groundwater-to-borehole wall thermal resistance [Km/W]
Re	Reynolds number [-]
T_{amb}	Ambient temperature [$^{\circ}\text{C}$]
T_{an}	Secondary fluid temperature inside the annular flow channel [$^{\circ}\text{C}$]
T_{bottom}	Fluid temperature at the bottom of a heat exchanger [$^{\circ}\text{C}$]
T_{bw}	Temperature of the borehole wall [$^{\circ}\text{C}$]
$T_{bw\ mean}$	Average borehole wall temperature vs. depth [$^{\circ}\text{C}$]
T_{ϕ}	Secondary fluid temperature inside the central pipe [$^{\circ}\text{C}$]
T_{in}	Temperature at the inlet of the borehole heat exchanger [$^{\circ}\text{C}$]
T_f	Secondary fluid temperature [$^{\circ}\text{C}$]
T_{gw}	Temperature of the groundwater [$^{\circ}\text{C}$]
T_{mean}	Average between inlet and outlet fluid temperature [$^{\circ}\text{C}$]
T_{out}	Temperature at the outlet of a borehole heat exchanger [$^{\circ}\text{C}$]
T_{rock}	Temperature of the surrounding ground [$^{\circ}\text{C}$]
ν	Kinematic viscosity [m^2/s]

Note: The appended articles contain other symbols which are explained in each specific paper

Structure of the thesis

Chapter 1 presents the general objective and gives a broad context to the subject of this research together with a brief explanation about the distributed temperature measurement technique. Chapter 2 gives background knowledge based on relevant previous work on borehole heat exchangers.

Chapters 3 to 7 aim at studying the specific objectives of this thesis, each on a particular borehole heat exchanger type. The specific objectives are presented at the beginning of each chapter, followed by a short summary of one published scientific paper (appended at the end of this thesis), as well as some new experiments and unpublished results. Each of the chapters presents individual conclusions based on the specific objectives set for the corresponding borehole heat exchanger type.

Publications

The papers appended to this thesis are the following:

Paper I: *J. Acuña, P. Mogensen, B. Palm.* Distributed Thermal Response Test on a U-pipe Borehole Heat Exchanger. The 11th International Conference on Energy Storage EFFSTOCK, Stockholm 2009.

Paper II: *J. Acuña, B. Palm, R. Khodabandeh, K. Weber.* Distributed Temperature Measurements on a U-pipe Thermosyphon Borehole Heat Exchanger with CO₂. 9th Gustav Lorentzen Conference. Sydney 2010.

Paper III: *J. Acuña, B. Palm.* Distributed Thermal Response Tests on Pipe-in-Pipe Borehole Heat Exchangers. Accepted for publication. In press. Applied Energy, 2013.

Paper IV: *J. Acuña, P. Mogensen, B. Palm.* Evaluation of a Coaxial Borehole Heat Exchanger Prototype. 14th ASME IHTC International Heat Transfer Conference, Washington D.C 2010.

Paper V: *J. Acuña, P. Mogensen, B. Palm.* Distributed thermal response tests on a multi-pipe coaxial borehole heat exchanger, HVAC&R Research, 17:6, 1012-1029. 2011.

Other publications by the author during the PhD studies but not included in this thesis are:

1. R. Beier, J. Acuña, P. Mogensen, B. Palm. 2013. Borehole resistance and vertical temperature profiles in coaxial borehole heat exchangers. *Applied Energy* 102 (2013), 665-675.
2. J. Acuña. Vatten som köldbärare i svenska bergvärmepumpar! Är det möjligt? KYLA Värmepumpar No 6 2012.
3. J. Acuña, M. Fossa, P. Monzó, B. Palm. Numerically Generated g-functions for Ground Coupled Heat Pump Applications. COMSOL Multiphysics Conference, Milano 2012.
4. E. Johansson, J. Acuña, B. Palm. Use of Comsol as a Tool in the Design of an Inclined Multiple Borehole Heat Exchanger. COMSOL Multiphysics Conference, Milano 2012.
5. R. Beier J. Acuña, P. Mogensen, B. Palm. Vertical temperature profiles and borehole resistance in a U-tube borehole heat exchanger, 2012. *Geothermics* 44 (2012), 23-32.
6. P. Monzó, J. Acuña, B. Palm. Analysis of the influence of the heat power rate variations in different phases of a DTRT. Innostock - The 12th International Conference on Energy Storage, Lleida, 2012.
7. J. Acuña, B. Palm. Distributed Temperature Measurements on a Multi-pipe Coaxial Borehole Heat Exchanger. The 10th IEA Heat Pump Conference, Tokyo, 2011.
8. J. Acuña, B. Palm. First Experiences with Coaxial Borehole Heat Exchangers. IIR Conference on Sources/Sinks alternative to the outside Air for HPs and AC techniques, Padua, 2011.
9. J. Acuña. Framtidens värmesystem med borrhålvärmeväxlare. Energi&Miljö nr 2 februari 2011.
10. J. Acuña, B. Palm. Comprehensive Summary of Borehole Heat Exchanger Research at KTH. Conference on Sustainable Refrigeration and Heat Pump Technology, Stockholm, 2010.
11. J. Acuña. Effektivare Utnyttjande av Energibrunnar för Värmepumpar Undersöks på KTH. KYLA Värmepumpar No 6 2010.
12. H. Madani, J. Acuña, J. Claesson, P. Lundqvist, B. Palm. The Ground Source Heat Pump: A System Analysis with a Particular Focus on the U-pipe Borehole Heat Exchanger. 14th ASME IHTC International Heat Transfer Conference, Washington D.C 2010.
13. J. Acuña, B. Palm. A Novel Coaxial Borehole Heat Exchanger: Description and First Distributed Thermal Response Test Measurements. IGA World Geothermal Congress, Bali 2010.
14. J. Acuña. Optimera med rätt kollektortyp. Borrvägen nr. 2/2010.
15. J. Acuña, B. Palm. Local Heat Transfer in U-pipe Borehole Heat Exchangers. COMSOL Multiphysics Conference, Milano 2009.

16. J. Acuña. Efficient Use of Energy Wells for Heat Pumps. GeoConneXion Magazine. Canada, Fall 2009.
17. J. Acuña. Slang intill bergväggen ger effektivare värmeväxling. Husbyggaren, nr 6 2009.
18. J. Acuña. Bergvärmepumpar Kan Göras Ännu Mer Effektiva, Energi&Miljö no 3, 2008.
19. Hur bra kan ett borrhål bli? Interview. SVEP NYTT nr 3, 2008.
20. J. Acuña, B. Palm. Experimental Comparison of Four Borehole Heat Exchangers. 8th IIR Gustav Lorentzen Conference, Copenhagen 2008.
21. J. Acuña, B. Palm, P. Hill. Characterization of Boreholes: Results from a U-pipe Borehole Heat Exchanger Installation. 9th IEA Heat Pump Conference, Zurich 2008. s4-p19.

Besides this, the author has during his PhD studies supervised 18 Master theses from the Energy Department at KTH and collaborated with thesis supervision at Uppsala University, Karlstad University, Chalmers University of Technology, and University of Genoa.

Oral and poster presentations about this project have also been given by the author at seminars organized by Energi&Miljö Tekniska föreningen (EMTF), University of Genoa, Swedish Heat Pump association (SVEP), Kyltekniska Föreningen, Nordbygg 2008 and 2012, GeoEnergiTag 2011, the EU projects GEOPOWER and GroundMed, AVANTI, Swedish Energitinget 2009, GEOTEC, Geothermal PhD student day, University of Zagreb, EFFSYS2 and EFFSYS+ days, Sveriges energiting 2009, Nordic Climate Solutions conference 2008, Vasas energilösningar 2008 and 2009, Astech workshop Bilbao 2008, Exportrådet, and Näringslivets internationella råd.

Most publications and more information about this project can be found at <http://www.energy.kth.se/energibrunnar>, <http://www.effsys2.se> and <http://www.effsysplus.se>.

Table of Contents

ABSTRACT	3
NOMENCLATURE	5
STRUCTURE OF THE THESIS	7
PUBLICATIONS	7
TABLE OF CONTENTS	10
INDEX OF FIGURES	12
INDEX OF TABLES	19
1 INTRODUCTION	20
1.1 GENERAL OBJECTIVE	20
1.2 CONTEXT OF THE RESEARCH	20
1.3 DISTRIBUTED TEMPERATURE SENSING IN BHEs	22
2 PREVIOUS WORK	25
2.1 THE GROUND THERMAL RESPONSE	25
2.2 GROUNDWATER-FILLED BOREHOLES	29
2.3 THE COLLECTOR PIPES	30
2.3.1 <i>U-pipe BHEs</i>	31
2.3.2 <i>Coaxial BHEs</i>	32
2.3.3 <i>Thermosyphon BHE pipes</i>	34
2.4 THE SECONDARY FLUID	34
2.4.1 <i>Aqueous antifreeze solutions</i>	35
2.4.2 <i>Fluids for thermosyphons</i>	35
3 MEASUREMENTS ON U-PIPE BHEs	37
3.1 SPECIFIC OBJECTIVES	37
3.2 THE EXPERIMENTAL RIGS	37
3.2.1 <i>U-pipe, BHE4</i>	37
3.2.2 <i>U-pipe with spacers, BHE7</i>	39
3.3 SUMMARY OF PAPER I	40
3.4 HEAT TRANSFER ON THE GROUNDWATER SIDE	44
3.5 EFFECT OF DIFFERENT FLOW RATES	52
3.6 HEAT PUMP OPERATION	61
3.7 CONCLUSIONS	67
4 MEASUREMENTS ON A U-PIPE THERMOSYPHON	69
4.1 SPECIFIC OBJECTIVE	69

4.2	THE EXPERIMENTAL RIG, BHE12	69
4.3	SUMMARY OF PAPER II	70
4.4	OPERATION OF THE U-PIPE THERMOSYPHON	72
4.5	CONCLUSIONS	78
5	MEASUREMENTS ON PIPE-IN-PIPE BHEs	79
5.1	SPECIFIC OBJECTIVES	79
5.2	THE EXPERIMENTAL RIGS	79
5.2.1	<i>Pipe-in-pipe, BHE9</i>	79
5.2.2	<i>Insulated Pipe-in-pipe, BHE10</i>	81
5.3	SUMMARY OF PAPER III	84
5.4	OTHER ASPECTS OF BHE9 AND BHE10	89
5.5	HEAT PUMP OPERATION	95
5.5.1	<i>First heating season, 2010-2011</i>	96
5.5.2	<i>Second heating season, 2011-2012</i>	99
5.6	CONCLUSIONS	102
6	MEASUREMENTS ON A MULTI-CHAMBER BHE	104
6.1	SPECIFIC OBJECTIVES	104
6.2	THE EXPERIMENTAL RIG, BHE3	104
6.3	SUMMARY OF PAPER IV	105
6.4	THERMAL POWER DISTRIBUTION	109
6.5	HEAT PUMP OPERATION	112
6.6	CONCLUSIONS	115
7	MEASUREMENTS ON A MULTI-PIPE BHE	116
7.1	SPECIFIC OBJECTIVES	116
7.2	THE EXPERIMENTAL RIG, BHE11	116
7.3	SUMMARY OF PAPER V	118
7.4	FLOW REGIME IN MULTI-PIPE BHEs	125
7.5	HEAT PUMP OPERATION	127
7.6	CONCLUSIONS	129
REFERENCES		131
APPENDED PAPERS		139

Index of Figures

Figure 1. Illustration of the different types of coaxial BHE geometries	21
Figure 2. Mean fluid temperature variation with borehole resistance and specific heat extraction rates (calculated for one day of constant operation with $\lambda_{\text{rock}}=2.5 \text{ W/mK}$, $\alpha=1.25 \times 10^{-6} \text{ m}^2/\text{s}$, and $T_{\text{rock}}=8^\circ\text{C}$)	27
Figure 3. Residence time of BHE types tested in this thesis (100 m deep borehole)	31
Figure 4. Viscosity of ethanol concentrations at different operating temperatures	35
Figure 5. BHE4: U-pipe borehole heat exchanger	38
Figure 6. Sketch of the fiber loop in BHE4	38
Figure 7. Ground temperature profile around BHE7	39
Figure 8. BHE7: U-pipe with spacers	39
Figure 9. Connection of BHE7 to the heat pump evaporator	39
Figure 10. Fluid mean temperatures in each section during the whole first DTRT in BHE4	40
Figure 11. Instantaneous fluid temperatures during heat injection	41
Figure 12. Instantaneous fluid and groundwater temperatures during thermal recovery	42
Figure 13. Local ground thermal conductivities in U-pipe, BHE4	43
Figure 14. Local borehole resistances in U-pipe, BHE4	43
Figure 15. Standard deviation of measurements during undisturbed ground conditions (30 seconds integration and repetition time during two hours)	45
Figure 16. Thermal power and volumetric flow rate during the N ₂ injection DTRT	46
Figure 17. Average fluid temperature in each section during the N ₂ injection DTRT	46

Figure 18. Fluid temperatures before and during N ₂ injection	47
Figure 19. Fluid and groundwater temperatures previous to N ₂ injection	48
Figure 20. Fluid and groundwater temperatures one hour after starting N ₂ injection	48
Figure 21. Average power distribution in the BHE during the different DTRT phases	49
Figure 22. Average fluid to groundwater resistance along BHE4 with and without N ₂ injection	50
Figure 23. Comparison of local thermal resistances obtained in BHE4	50
Figure 24. Temperature difference and heat injection in section 2	51
Figure 25. Temperature difference and heat injection in section 4	51
Figure 26. Temperature difference and heat injection in section 5	52
Figure 27. Instantaneous secondary fluid temperatures during the first two hours of heat injection in BHE4	53
Figure 28. Flow rate and thermal power during heat injection experiments in BHE7	53
Figure 29. Fluid and groundwater temperatures during heat injection in BHE7 at four volumetric flow rates	54
Figure 30. Themal power distribution along the BHE7 up-going and down-going shanks at different flow rates	55
Figure 31. Local average specific injected power	56
Figure 32. Fluid to groundwater ΔT	56
Figure 33. Fluid to groundwater resistance	56
Figure 34. Fluid to groundwater thermal resistance vs. flow rate	57
Figure 35. Reynolds number at four different flows in U-pipe BHE	58
Figure 36. Heat transfer coefficient at four different flows in a U-pipe BHE	58

Figure 37. Fluid to inner pipe wall thermal resistances along the depth at different flows	59
Figure 38. Reynolds number along the pipe length of BHE4 allowing the viscosity to change for given secondary fluid temperatures (flow 0.3 l/s)	60
Figure 39. Comparison of pressure drop in U-pipe with and without fiber optic cable having the same secondary fluid (see section 3.2.1)	60
Figure 40. Temperatures in BHE7 at short intervals after heat pump start (at 0.4 l/s).	61
Figure 41. Secondary fluid and groundwater temperature profile at 0.36 l/s after elapsed residence time, including local fluid to groundwater thermal resistance	63
Figure 42. Secondary fluid and groundwater temperatures at 0.81 l/s after elapsed residence time, including local fluid to groundwater thermal resistance	63
Figure 43. Secondary fluid and groundwater temperature at 0.60 l/s, after elapsed residence time, including local fluid to groundwater thermal resistance	64
Figure 44. Secondary fluid and groundwater temperatures at 1.00 l/s, after elapsed residence time, including local fluid to groundwater thermal resistance	64
Figure 45. Comparison of secondary fluid temperature profiles after elapsed residence time during the first heat extraction experiment in U-pipe ($\Delta T \approx 3.5$ K)	65
Figure 46. Comparison of secondary fluid temperature profiles after elapsed residence time during the second heat extraction experiment in U-pipe ($\Delta T \approx 2.5$ K)	66
Figure 47. Installation and illustration of the U-pipe thermosyphon	70
Figure 48. Temperatures along the riser during heat pump operation. The heat pump starts at 15:40 and stops at 16:45	71
Figure 49. Temperatures along the riser during borehole recovery	71
Figure 50. Temperatures of the riser outer pipe wall at different depths in BHE12 before and after start of the heat pump on April 6 th	72

Figure 51. Riser pipe wall and groundwater temperature at 16.02	73
Figure 52. Energy flows at the different components of the heat pump system during the heat pump cycle between 15:40 and 16:45 on April 6 th 2009	74
Figure 53. Heat transfer coefficient along the depth in BHE12	75
Figure 54. Pipe to groundwater thermal resistance along BHE12	75
Figure 55. P-h diagram showing how the CO ₂ travels in BHE12 at four simulated cases	76
Figure 56. Comparison between calculated CO ₂ temperatures along the riser and measured temperatures in BHE12	76
Figure 57. Average calibrated temperatures and standard deviation along the fiber cable during a 25 hours measurement period (6 measurements per hour).	77
Figure 58. BHE9: Pipe-in-pipe with PE40x2.4 central pipe	80
Figure 59. Cross section of BHE9	80
Figure 60. Sketch of the fiber optic loop in BHE9	80
Figure 61. Undisturbed temperature measurement along all fibers in BHE9	81
Figure 62. Cross section of BHE10	81
Figure 63. BHE10: Pipe-in-pipe with insulated central pipe	82
Figure 64. Sketch of the heat pump system connected to BHE10	82
Figure 65. Double-ended fiber calibration in BHE10. Undisturbed ground conditions	83
Figure 66. Section division of BHE9 and BHE10	84
Figure 67. Evolution of temperatures during the DTRTs in BHE9	85
Figure 68. Evolution of temperatures during the DTRTs in BHE10	86
Figure 69. Comparison of fluid temperature profiles in BHE9 and BHE10	88

Figure 70. Thermal power distribution in BHE9 during DTRT1	89
Figure 71. Thermal power distribution in BHE9 during DTRT2	90
Figure 72. Thermal power distribution in BHE10	90
Figure 73. Reynolds number along the depth at two different flows in Pipe-in-pipe BHE	91
Figure 74. Convection heat transfer coefficient at two different flows in Pipe-in-pipe BHE	92
Figure 75. Thermal resistances in different central pipe polyethylene ($\lambda_{PE}=0.42$ W/mK) alternatives. Convection resistances calculated at 0.5 l/s using $v=1.14\times10^{-6}$ m ² /s, $\lambda=0.58$ W/mK, and $Pr=10.4$.	93
Figure 76. Pressure drop in Pipe-in-pipe BHE	94
Figure 77. Comparison of convection thermal resistances in a pipe-in-pipe BHE at different Reynolds numbers in the annulus. Calculated using $v=1.14\times10^{-6}$ m ² /s, $\lambda=0.58$ W/mK and $Pr=10.4$. Central pipe of type PE40x2.4mm.	95
Figure 78. Residence time through BHE10 at different volumetric flow rates	96
Figure 79. Inlet, outlet, and average borehole wall temperatures at 0.6 l/s	97
Figure 80. Development of the fluid profile in BHE10 at 0.6 l/s	98
Figure 81. Instantaneous fluid and borehole wall temperature profiles during heat pump operation at different volumetric flow rates in BHE10	98
Figure 82. Annulus to borehole wall thermal resistance during heat pump operation at three flow rates	99
Figure 83. Inlet and outlet temperatures during days with ambient temperatures between 0 and 12 °C (December 2011)	100
Figure 84. Inlet and outlet temperatures during days with ambient temperatures between -2 and 12°C (January 2012)	100
Figure 85. Inlet and outlet temperatures during days with ambient temperatures between -8 and 2°C (January 2012)	101

Figure 86. Inlet and outlet temperatures during days with ambient temperatures between -18 and 0°C (February 2012)	101
Figure 87. BHE3: Installation of the Multi-chamber BHE installation	104
Figure 88. Measured volumetric flow rate with two different meters during TRT1 and TRT2 in BHE3	106
Figure 89. Temperatures during TRT1 in BHE3 (secondary fluid going down through the central pipe)	107
Figure 90. Temperatures during TRT2 in BHE3 (secondary fluid coming up through the central pipe)	107
Figure 91. Comparison of pressure drop in U-pipe and Multi-chamber BHE	108
Figure 92. Net thermal power distribution in Multi-chamber BHE (BHE3) during TRT1	110
Figure 93. Net thermal power distribution in Multi-chamber BHE (BHE3) during TRT2	110
Figure 94. Comparison of two fluid mean temperature approaches during TRT1 in BHE3	111
Figure 95. Comparison of two fluid mean temperature approaches during TRT2 in BHE3	112
Figure 96. Measurements in BHE3 at 0.80 l/s during heat pump operation. Downward flow in central pipe.	113
Figure 97. Measurements in BHE3 at 0.80 l/s during heat pump operation. Upward flow in central pipe.	113
Figure 98. Comparison of the net thermal power absorbed as the fluid travels downwards in two different flow directions at a rate of 0.80 l/s	114
Figure 99. Comparison of the net power absorbed as the fluid travels upwards in two different flow directions at a rate of 0.80 l/s	114
Figure 100. Cross section of BHE11	116
Figure 101. Photo of BHE11	117

Figure 102. Installation of BHE11	117
Figure 103. Connection points to BHE11	118
Figure 104. Undisturbed temperature profile in BHE11	118
Figure 105. Section division of BHE11 during DTRT analysis	119
Figure 106. Temperature and thermal power evolution during all DTRTs in BHE11	119
Figure 107. Heat flow from section 1	120
Figure 108. Heat flow from section 4	121
Figure 109. Fluid temperature profiles at two different volumetric flow rates. Secondary fluid travels downwards through the external pipes	121
Figure 110. Local borehole resistance results obtained after analyzing all DTRTs	123-124
Figure 111. Heat transfer coefficient along the measured peripheral pipe in each section	125
Figure 112. Heat transfer coefficient at two different flows along BHE11	126
Figure 113. Reynolds number distribution at two different flows along BHE11	126
Figure 114. Secondary fluid temperatures at the inlet, bottom and outlet points of the multi-pipe BHE during a day of measurements at 0.13 l/s	128
Figure 115. Temperature profiles during heat pump start up at 0.20 l/s	128
Figure 116. Comparison of measured temperature profiles in BHE11 at different flow rates during heat pump operation (residence time has not elapsed at 0.13 l/s)	129

Index of tables

Table 3-1. Chronology of the bubble injection DTRT	44
Table 3-2. Standard deviation of the measured flow rates during heat injection in BHE7	54
Table 3-3. Characteristics of the heat extraction experiment with $\Delta T \approx 3.5$ K	63
Table 3-4. Characteristics of the heat extraction experiment with $\Delta T = 2.5$ K	64
Table 3-5. Heat extraction percentage along each half of the BHE7 tubes during the first heat extraction experiment ($\Delta T \approx 3.5$ K)	66
Table 3-6. Heat extraction percentage along each half of the BHE7 tubes during the second heat extraction experiment ($\Delta T \approx 2.5$ K)	66
Table 5-1. Global thermal resistance results from BHE9 and BHE10	87
Table 6-1. Effective ground and borehole resistance during TRT1 and TRT2	108
Table 6-2. Standard deviation of temperature measurements during TRTs in BHE3	109
Table 7-1. Chronology of the different parts of the heat injection test in BHE11	119
Table 7-2. Monitoring periods of Multi-pipe BHE	127

1 Introduction

1.1 General objective

The aim of this thesis is to suggest methods for reducing the temperature difference between the ground and the secondary fluid in borehole heat exchangers.

1.2 Context of the research

A Borehole Heat Exchanger (BHE) consists of one or several borehole(s) drilled into the ground allowing heat to be exchanged between the ground and a fluid circulating in the borehole(s).

Depending on whether there are one or several boreholes, the word “Single” or “Multiple” can be added, resulting in a simple classification subject to the amount of boreholes, “Single BHEs” or “Multiple BHEs”.

The fluid circulation normally takes place in an embedded collector pipe inside the borehole, but there are also open systems where the fluid is in direct contact with the surrounding soil or rock. BHEs are often connected to another heat exchanger at the ground surface level, commonly (but not always) the evaporator of a Ground Source Heat Pump (GSHP).

The most common single BHE is the U-pipe, where the secondary fluid travels down- and upwards through two equal tubes joined together at the bottom. There is also the coaxial type, classified depending on the geometry as pipe-in-pipe, multi-pipe, or multi-chamber (Figure 1).

Pipe-in-pipe BHEs consist of a central pipe inserted into a larger tube (external pipe), forming an annular flow channel between them, as shown in Figure 1(a). A Multi-pipe design, Figure 1(b), consists of a central pipe connected at the borehole bottom with several smaller external and independent flow channels. The multi-chamber BHE is similar to the multi-pipe case, except that the central pipe and the external channels (so called chambers) are all part of a common pipe structure, as shown in Figure 1(c).

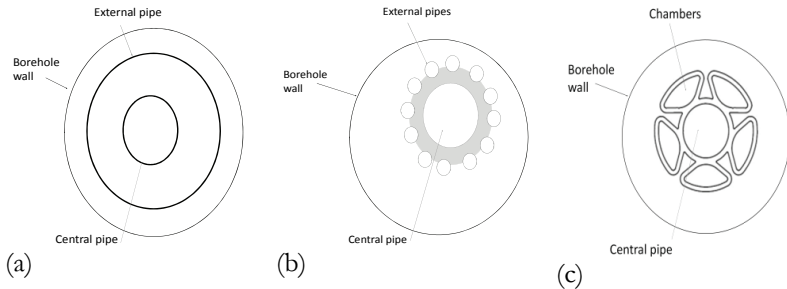


Figure 1. Illustration of the different types of coaxial BHE geometries

GSHPs are a well established technology for heating and cooling buildings. In 2010, over 100 000 GSHP units were sold in Europe, reaching a total of over one million installations (RHC, 2012). Worldwide, approximately 2.94 million ground source heat pump systems covered 49.0% of the world's used geothermal energy in 2010, accounting for 69.7% of the worldwide installed geothermal capacity (Lund et al, 2010). In Sweden, up to 12 TWh of cooling and heating are delivered yearly by this type of system (GEOTEC, 2012). About 30 000 units were sold during 2011 around the country, a number that has been relatively stable during the last years (SVEP, 2012). The low running costs have encouraged users to install GSHPs in spite of their relatively high installation cost. Statistics also show that the efficiency of these systems has substantially improved along the years.

Although the technology is well known, there still remain several technical aspects to be improved on which research should be addressed. Improving borehole heat exchangers was recently pointed out by (Spitler and Bernier, 2011) and by the European Platform for Renewable Heating and Cooling (RHC, 2012) as one of the focal research areas for the near future. It is known that a reduction of 1 K in the temperature difference between the ground and the evaporator of a GSHP can increase the heat pump Coefficient of Performance (COP) by 2 to 3%.

In order to find methods for increasing the COP by 6-9% and to increase the level of understanding of BHEs, this thesis mainly addresses the local thermal processes in several types of single BHEs.

Instead of conventional thermal response tests based on inlet and outlet fluid temperature measurements (limited to giving merely average and global information about the BHE performance), a new technique called Distributed Thermal Response Test (DTRT) is the main method used here, giving detailed information about the tested BHEs thanks to the application of Distributed Temperature Sensing (DTS).

1.3 Distributed temperature sensing in BHEs

DTS is based on Raman optical time domain reflectometry, consisting of the injection of laser light pulses through a length of optical fiber and the subsequent detection of a non-linear part of the reflected light that is re-emitted with a different frequency than the input signal, a backscattered signal that travels through the whole fiber. This frequency shifted light scattering is called Raman scattering, and the temperature is determined by analyzing it over a period of time (integration time) for a given cable section.

The re-emitted Raman scattered light has one part at lower frequencies (stokes) and another at higher frequencies (anti-stokes) than the original injected light. The low and high frequencies are related to the energy gap between them. The ratio between their intensities depends only on temperature, meaning that the temperature can be determined at a certain section as a function of the ratio between stokes and anti-stokes backscattered light.

The differential loss between anti-stokes and stokes that affects the temperature reading in proportion to the distance from the measurement instrument is adjusted. The loss is normally within the order of 0.3 decibels per kilometer with lasers operating at around 1064 nm (wavelength in fiber systems vary from 850 to 1300 nm). This loss, often called attenuation, limits the signal traveling distance and can also be induced by human installation errors.

The precision of a DTS measurement depends on the fiber index of refraction (ratio comparing the speed of light in a vacuum to the speed of light in a medium, normally of around 1.35 in fibers), the amount of information read by the data acquisition instrument per unit time, and on the size of the observed section along the fiber. Better accuracy is obtained when more photons are observed per unit time. However, the photon density decreases with increasing length of the measurement section, meaning that the amount of information read by the instrument in a certain period of time may also be smaller if the distance to the observed section is large.

With known travel time and velocity, it is possible to identify the source of the Raman scatter, i.e. the position where a signal comes from. This is carefully done accounting for the delay between the instant of light injection to observation of the backscatter arrival, subsequently trimming the signal in order to account for light dispersion within the fiber.

DTS instruments integrate the signals and determine an average temperature for different continuous sections. The length of these sections depends on the instrument specifications and the most powerful instrument in the market today has a sampling resolution of 12.5 cm. A section of the fiber located far away from the instrument needs a longer integration time because the amount of information coming back to the instrument decreases with the distance (the light signal becomes exponentially weaker as it travels through the fiber).

Different integration instruments have different so called spatial resolutions, the least width of a temperature change that it can detect. The best spatial resolution today goes down to 0.25 cm. A step temperature change having a width lower than the instruments spatial resolution results on a measured temperature affected by a factor approximately proportional to the ratio between the spot width and the spatial resolution.

The expected precisions for temperature, time, and space, must be compromised in order to achieve the desired measurement quality. Longer measurement time give better temperature resolution, larger spatial averaging gives better temperature resolution, and temperature resolution decreases with distance due to attenuation.

The intensity of the laser varies between different DTS instruments and the fiber characteristics change from manufacturer to manufacturer. In order to guarantee quality on distributed temperature measurements, a careful calibration process must be carried out. This normally requires the adjustment of an offset (Raman conversion coefficient correction) and a slope (differential loss correction).

Typically, the whole measuring process is carried out in single ended mode, the laser pulses are sent in one direction along the fiber. If a fiber is looped having two connectors to the instrument (one at each fiber end), a combined measurement commonly known as double-ended measurement can be made. In the latter case, sending the pulses from each end allows for signal compensation based on two measurements, giving simultaneous correction of differential losses and attenuations. The offset correction may still be necessary.

The measurements in this thesis have been done in single and double ended mode, depending on the installation. All installations use multi-mode fiber cables having an external diameter of 3.8 mm. Although the readings are given in terms of BHE/fiber lengths, the borehole deviations have been disregarded and the word “depth” has, for didactic reasons, been used along this thesis when referring to the length.

The calibration process in all experimental installations has consisted of placing two or more relatively long fiber sections into one or even two environments with a known temperature such as an ice bath. These reference sections are separated from each other by twice the borehole depth and are, at least, located before and after the fiber inside the bore-hole. The integration instrument has also been kept at constant room temperatures during calibration and measurements.

Besides the trade off made at each installation site regarding the spatial, time and temperature accuracy of the instrument, a systematic uncertainty when measuring inside BHEs might arise due to the unknown position of the fiber optic cable in the borehole/pipes, specially at laminar flow conditions. For turbulent flow, for instance, it is well known that the temperature profile is flat across the pipe outside the thermal boundary layer at the pipe wall.

This possible systematic uncertainty has been handled by estimating the laminar sub-layer at the pipe wall within which heat is transferred only by thermal conduction. The temperature difference between the pipe wall and the inner border of the boundary layer is calculated for each case. With known pipe dimensions, fluid thermo-physical properties, fluid velocity, and heat flux from or to the ground, it is possible to estimate the convection heat transfer coefficient and thereby the temperature difference between the pipe wall and the bulk fluid temperature, resulting in an indication of where across the pipe the temperature change takes place during laminar or turbulent flow.

On the groundwater side, the risk to fall into this type of systematic error depends on the radial temperature gradient between the collector pipes and the borehole wall, which depends on the heat extraction/injection rate, volumetric flow rate, type of heat exchanger, and the temperature levels. This is discussed in connection to specific tests where measurements on the groundwater side are evaluated.

For more details about generalities of the DTS technique and their use in BHEs, the reader is referred to (Selker et al, 2006), (Tyler et al, 2009), and (Acuña, 2010), among others.

2 Previous work

As this thesis is a experimental study on the thermal response of U-pipe and coaxial heat exchangers in groundwater filled boreholes, this chapter is dedicated to giving a theoretical background about the four different active parts that can be distinguished inside a heat exchanger installed in a ground-water filled borehole. These are the ground, the collector pipes, the groundwater filling the space between the borehole wall and the pipes, and a fluid circulating inside the collector pipes (the secondary fluid). Previous work concerning the study of the thermal processes in these borehole heat exchanger parts is surveyed in sections 2.1 through 2.4.

2.1 The ground thermal response

The thermal process in the ground has mainly been studied as a time dependent three dimensional heat conduction problem, rarely accounting for the effects of groundwater movement. The heat transfer from the borehole wall to the ground depends on the ground thermal conductivity, the thermal diffusivity, and the undisturbed ground temperature.

The different heat transfer forms with origin in the heat conduction equation are mainly linear partial differential equations, and their solutions can be superposed, as mathematically proven in (Claesson et al, 1985). The transient thermal response to thermal loads from the BHE is superposed on the natural stationary temperature distribution that previously existed in the ground. Analytical one-dimensional heat conduction models treating the heat transfer outside the borehole such as the Infinite Line (Ingersoll and Plass, 1948) and Cylinder Source (Carslaw and Jaeger, 1959) have been used for many years to study these problems, as well as the finite difference two dimensional g-function introduced by (Eskilson, 1987).

The Infinite Line Source (ILS) model assumes the thermal load to be a line source of constant heat rate and infinite length surrounded by an infinite homogeneous ground. The cylinder heat source model assumes the borehole as a cylinder surrounded by homogeneous ground and having constant heat flux across its periphery; and the g-function (mostly used for multiple BHE problems) gives a relation between the heat exchange with the ground and the temperature at the borehole wall. Another ap-

proach is the Finite Line Source Solution (FLS) which considers the finite length of the boreholes, also presented in (Eskilson, 1987) but further developed by (Zeng et al, 2002) and (Lamarche and Beauchamp, 2007).

None of the above mentioned models really consider the thermal capacity effects inside the borehole and, for a single borehole, their solutions (ILS, cylinder source, FLS, and g-function) meet after a few hours and are the same as long as the heat transfer is essentially one dimensional in the radial direction. The cylinder line source and the g-function are equal from the beginning. The same happens with ILS and FLS solutions. This is because the former two account for heat being exchanged at the borehole wall while the line source solutions assume that heat is exchanged from/to the center of the borehole.

The ILS model, which has been used at a local level throughout this thesis, evaluates the temperature response at radius r after time t of a step change in supplied heat, allowing that the temperature response of many heat steps at different times may need to be superposed. A thermal resistance R can be also added to the ILS model in order to represent the temperature difference between the secondary fluid and the borehole wall as suggested by (Mogensen, 1983).

The infinite line source approach is, for instance, commonly used for measuring the ground thermal conductivity and the thermal resistance R through Thermal Response Tests (TRT), where the ground thermal response to a few days of constant heat injection or heat extraction is analyzed in order to obtain this information. The cylindrical source model as well as numerical evaluation methods have also been used, even to calculate the thermal conductivity along the depth (Fujii et al, 2006). Many times the evaluation accounts for the above described superposition of the response to heat steps and/or use parameter estimation techniques such as suggested in (Shonder and Beck, 1999). The FLS method has also been used for TRT analyses by (Bandos et al, 2011).

The TRT method was first used by (Mogensen, 1983) and then by (Eskilson et al, 1987) and (Claesson and Hellström, 1988), and it is now extensively used worldwide in the academy and commercially after the work presented by (Gehlin, 2002), at Luleå University of Technology at the same time as it was developed at Oklahoma State University. IEA Annex 21 (<http://www.thermalresponsetest.org/>), at the moment on final reporting stage, has studied and collected a large amount of information about TRTs. The reliability of this method as compared to laboratory core tests was recently demonstrated by (Liebel, 2012).

The borehole thermal resistance R has traditionally been denoted R_b after (Claesson and Hellström, 1988) and (Hellström, 1991), representing today a well established parameter for characterizing BHEs. It is a thermal resistance per unit length of the borehole [K/(W/m)], and it is typically used assuming that the fluid temperatures of the downward and upward flow are the same. Experimentally, R_b is normally found during steady-flux conditions achieved with TRT tests, in order to avoid accounting for thermal capacitance effects in the borehole.

As the fluid temperatures obtained from a single BHE are influence by the surrounding ground but also by R_b , an example shown in Figure 2 presents the effect of the borehole resistance R_b on the secondary fluid mean temperature exiting from the BHE calculated using ILS. It is seen that the same fluid temperature can be obtained with different heat extraction rates by changing the BHE. The temperature difference between the highest and lowest fluid temperature becomes larger with increasing values of borehole resistance and heat rate in Watts per meter. A low R_b gives a low temperature difference between the fluid and the ground.

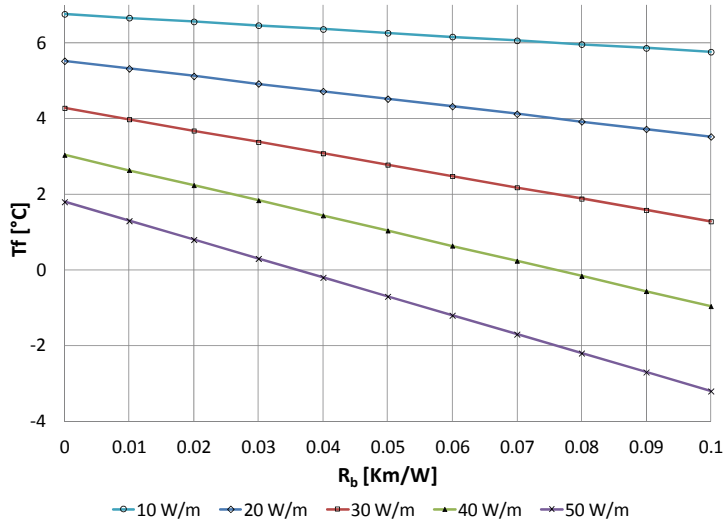


Figure 2. Mean fluid temperature variation with borehole resistance and specific heat extraction rates (calculated for one day of constant operation with $\lambda_{rock}=2.5$ W/mK, $\alpha=1.25 \times 10^{-6}$ m²/s, and $T_{rock}=8^\circ\text{C}$)

In commercial software such as those by (Hellström and Sanner, 1997), (Spitler, 2000), and (Kavanaugh and Rafferty, 1997), the calculation of the borehole resistance is done for steady-state conditions. Commercial software concentrate mostly on what happens in the surrounding ground and are mainly devoted to calculating the long term borehole wall tem-

peratures for multiple BHEs using spatial and temporal superposition. The theory behind the solutions is the above mentioned Eskilson's g-functions, which are based on the so called Superposition Borehole Model (SBM), explained in detail in (Eskilson, 1986).

For multiple BHEs, g-functions can also be generated with the FLS model, and the simulated solutions for variable heat load can also be superposed in time to describe the ground response of any BHE geometry. FLS generated g-functions are based on a constant heat flux at the borehole periphery as boundary condition and they seem to fit to some extent with the g-functions generated with SBM, besides a certain degree of overestimation (Fossa, 2011). Numerical solutions are more time consuming while analytical FLS calculations allow the rapid and flexible study of the thermal response of any field geometry. (Fossa et al, 2009) is an example on the use of the FLS approach.

The g-function concept has, sometimes with limitations (including U-pipe geometry normally modeled with a single cylinder having equivalent diameter, negative borehole wall temperatures for very short times, lack of thermal interaction between pipes, neglecting thermal capacity of the secondary working fluid, among others), been extended to shorter time steps by modeling the heat transfer from the fluid to the borehole wall through the inclusion of the thermal resistances and even capacitances inside the borehole. This has partially been studied in (Yavuzturk and Spitler, 1999), (Yavuzturk and Spitler, 2001), (Yavuzturk et al, 2009), (Beier and Smith, 2003), (Bandyopadhyay et al, 2008), (Lamarche and Beauchamp, 2007), (Javed and Claesson, 2011) and (Claesson and Javed, 2011). Including shorter time steps is important in order to better account for peak loads where the secondary fluid, the pipe, and the filling material inside the borehole, can perhaps dampen the temperature response of the ground. A large heat capacity is normally desirable in BHEs in order to avoid rapid temperature changes during short heat pump operation periods. More about what happens inside the borehole is documented in section 2.3.

Although water movement in the ground has not been studied as much as the heat conduction problem, it is important to be aware that it may influence the thermal processes in a BHE. Some studies about the influence of groundwater flow in the design of multiple BHEs are those by (Claesson and Hellström, 2000), (Chiasson et al, 2000), and (Bauer et al, 2012).

2.2 Groundwater-filled boreholes

Groundwater filled boreholes are common in North European countries. It has been shown that natural convection is induced by the temperature gradients around the BHE. Conductive heat transfer has been found to still be dominant, i.e. calculated borehole thermal resistances were only 1.2 to 1.3 times higher than experimental (Claesson and Hellström, 1988). The magnitude of the natural convection depends on the heat transfer rate and the temperature level (Kjellsson and Hellström, 1997).

(Witte and Van Gelder, 2006) studied the effect of natural convection by imposing so-called multi-level heating and cooling pulses. Similar approaches were later used by (Gustafsson and Gehlin, 2006), (Gustafsson and Gehlin, 2008), (Gustafsson et al, 2010), and (Gustafsson and Westerlund, 2010), who evidenced the presence of natural convection through multi-level-injection TRTs. The works from Gustafsson et al. found that heat transfer in the groundwater inside the borehole was about three times better with temperature induced natural groundwater movement as compared to stagnant water at temperature levels between 10 and 35°C. A suggestion to using different equivalent diameter approximations depending on the TRT circumstances was pointed out.

(Kharseh, 2011) and (Liebel, 2012) imposed forced convection conditions in the groundwater by N₂ injection at the borehole bottom and using a submersible pump, respectively. They found larger effects on the effective borehole resistance than those found in natural convection, as expected.

The alternative to groundwater-filled boreholes is a backfill material, or grout, commonly used in USA, central and southern Europe. These are used to prevent contaminants from migrating along the axis of the borehole. In some countries, grouting materials are used by law even when no risks for contaminant migration exist. Cement and bentonite based materials with additives are mainly used. It is normally preferred to use highly conductive grouting materials for enhancing the heat transfer from the borehole wall to the collector pipes.

A disadvantage of highly conductive grout is that it also increases the thermal shunt flow between the down-going and up-coming secondary fluid flows. Grouted BHEs may also be thermally unstable for a long time after installation, as shown by (Montero et al, 2012). Proposals are at the moment being studied for guaranteeing the proper use of these materials (Anbergen et al, 2012). Even groundwater movement in grouted BHEs can occur (Fujimoto et al, 2012). No expressions for calculating heat transfer specifically in the groundwater of groundwater-filled

boreholes have been presented, in contrast to the grouted case, which has been studied by several researchers (Paul, 1996), (Hellström, 1991), (Sharqawy et al, 2009).

If the thermal conductivity of the grout is lower than in the surrounding ground, a smaller diameter borehole may reduce the borehole resistance. With a large borehole diameter the collector pipes could be placed close to the borehole wall and apart from each other, making a better BHE, thereby reducing the thermal resistance R_b . Also, if the thermal capacitance of the grout is high, the short term performance of the heat exchanger may be improved. Results from five thermal response tests in U-pipe BHEs, where different grouting material were used, illustrate these effects (Bose et al, 2002). (Hellström, 1998) presented calculated thermal resistances using different borehole filling materials with three different U-pipe positions in the borehole.

A literature survey covering practical aspects of grouted boreholes from a Swedish perspective was recent presented by (Hjulström, 2012).

2.3 The collector pipes

The collector pipes are typically made of medium density polyethylene, a flexible material having a thermal conductivity of 0.42 W/mK, which is high for a plastic, and offering good mechanical properties for this application. There are also some few exceptions with pipes made of stainless steel, copper, PVC and other types of plastic.

Two general BHE types are known depending on the geometry: U-pipe (single, double, or triple; including the use of spacers for separating the shanks) and coaxial BHEs. The amount of pipes and their geometrical arrangement allows classifying them in several other categories accordingly as presented in section 1.2.

Each BHE type may demand specific flow rates for operation at optimum conditions, i.e. low borehole resistance, low thermal shunt flow between pipes, long enough fluid residence time, among others. Different fluid residence times are, as an example, shown in Figure 3, illustrating how long time a fluid plug takes to travel through the whole heat exchanger at different flow rates. Regarding the thermal resistances in BHEs, a literature survey covering all types of BHEs is presented in sections 2.3.1 and 2.3.2.

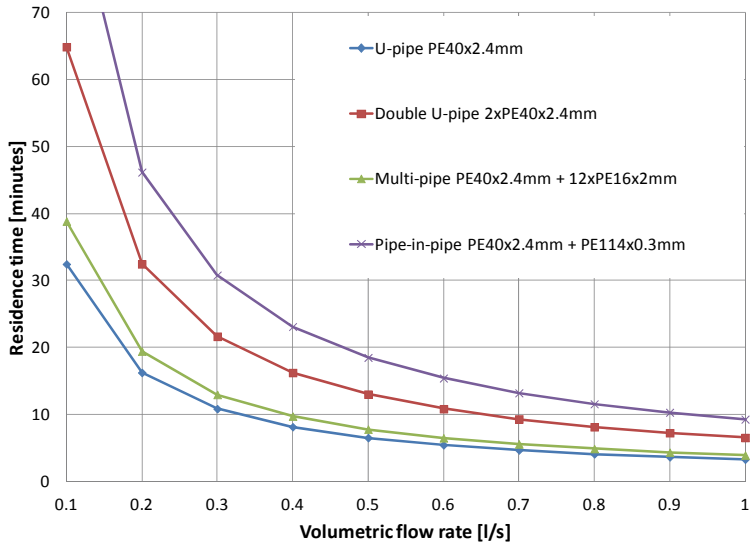


Figure 3. Residence time of BHE types tested in this thesis (100 m deep borehole)

2.3.1 U-pipe BHEs

U-pipe BHEs represent the most common method to exchange heat with the ground today, having standard dimensions of 40 mm outer diameter and 2.4 mm wall thickness. Their thermal performance is poor due to thermal shunt flow between pipes and undesirable pipe placement relative to the borehole wall.

Theoretical studies on U-pipe BHEs have dominated the single BHE research work published until now. (Claesson and Bennet, 1987) and (Claesson and Hellström, 2011), for example, computed the heat flows between the pipes (located at any position) and the outer rock. (Hellström, 1991), (Zeng et al, 2003) and (Diao et al, 2004) are other examples of extensive studies of U-pipe BHEs where mathematical expressions for calculating a borehole resistance for the case of uniform borehole wall temperature and uniform heat flux along the depth were developed. Also, (Claesson and Eskilson, 1988) show calculated borehole thermal resistances for laminar and turbulent flow in three different U-pipe configurations, including cases surrounded by frozen water. It is clear that laminar flow in the pipes should be avoided as it increases the thermal resistance between the fluid and inner pipe wall. The calculations for the unfrozen cases were done considering only conduction heat transfer.

Calculating borehole thermal resistances has, in many studies, been done based on the use of the arithmetic fluid mean temperature. (Marcotte and Pasquier, 2008) argued that this may lead to an overestimation of the borehole resistance and introduced an approximation where the circulating fluid temperature varies linearly along the flow path. (Lamarche et al, 2010) used 2D and 3D numerical simulations to evaluate different methods. Other articles including study of thermal resistance in U-pipe BHEs are (Du and Chen, 2011) and (Beier, 2011), (Bauer et al, 2011). (Zarella et al, 2011) improved and validated the work by (De Carli et al, 2010), a capacity resistance model that studies the behavior of BHEs in some borehole field configurations.

Almost all the above mentioned papers, except for (Eskilson et al, 1987), (Gehlin, 2002), (Bose et al, 2002), and (Witte and Van Gelder, 2006) use numerical and not measured results as a reference. Many times, just in and outlet temperatures are used for model validation. An experimental article providing data sets for U-pipe BHEs and for ground thermal conductivity estimates is (Beier et al, 2011), where a sand box with a large amount of temperature measurement points is used for laboratory controlled experiments.

2.3.2 Coaxial BHEs

The first multi-pipe BHE ideas were introduced by Ove Platell in Sweden, who wrote several publications (in Swedish) about this heat exchanger. (Platell, 2006) discussed the thermal advantages of this design that operates with laminar flow in the peripheral pipes. Tests of a first prototype achieved thermal resistances between 0.009 - 0.028 Km/W (Hellström and Kjellsson, 2000). It consisted of 62 thin peripheral pipes (diameter of 3.8 mm and thickness of 0.65 mm) arranged close to the borehole wall in a special laboratory installation. The diameter of the laboratory “borehole” was 104 mm.

(Oliver and Braud, 1981) presented an analytical solution of annular heat exchangers under steady state operation (using a constant temperature boundary condition 1 m away from the borehole wall), having limited practical application due to the purely transient process around the borehole in reality. Later, (Mei and Fischer, 1983) presented a study of a 50 m deep borehole with a polyvinylchloride (PVC) pipe-in-pipe BHE. The borehole had a diameter of 200 mm, and was backfilled with sand. Spacers were used in order to center the central pipe and temperature sensors were installed along the depth approximately every 7.5 meters inside and outside the annular channel as well as at the inlet and outlet. Although this borehole instrumentation was good, the measurements taken had certain limitation for validating the BHE model due to the high thermal resistance in the external PVC pipe, resulting in differences of up to 0.9

K from the measurements during continuous operation. During cyclic operation, predicted fluid temperatures at 16.8 m depth in the annulus matched very well with the measurements. Outside the outer PVC pipe, an asymptotic behavior of the temperatures showed that it almost does not feel the cyclic temperature behavior inside. On the other hand, it just decreases or increases slowly (during heat extraction or injection, respectively). Besides this experimental work, an analytical model presented in (Mei and Fischer, 1983) is compared to the measurements and allows discussing the effects of geometry variations, flow rate, among others, including the ground thermal response.

(Hellström, 1994) and (Hellström, 2002) described experiments where the secondary fluid travels in direct contact with the rock, with only a single central pipe. Turbulent operating conditions resulted in R_b of circa 0.01 Km/W, while drastically higher resistance values were found for laminar flow, R_b 0.12 Km/W, (the latter also due to the central pipe eccentricity). The same year, (Yavuzturk and Chiasson, 2002) showed that pipe-in-pipe BHEs have potential for a very low R_b .

Older work regarding coaxial BHEs from the early 1980s is presented in the EU project GROUNDHIT where a pipe-in-pipe prototype was suggested (Sanner et al, 2007). (EWS, 2006) also describes the GROUNDHIT design, which consisted of one PE 63x5.3 mm outer pipe with an inner channel with dimensions PE 40x3.7mm. Installation and assembling methods were tested and presented. However, the thermal resistances of this BHE were high due to material thermal properties, thermal shunt flow, and distance to borehole wall.

The effects of flow rate and of thermal short-circuiting (and methods to avoid it) are studied based on a numerical model in (Zanchini et al, 2010) but no experiments are done. These effects are studied further in (Zanchini, et al, 2010b), where an outer pipe made of stainless steel is driven into the ground without having any grouting. (Witte H. , 2012) presented the development of another coaxial BHE called GEOTHEX, consisting of a pipe-in-pipe design having an insulated central pipe with helical vanes on its outer part. This BHE still had a high borehole thermal resistance, but a rather good installation method. A similar pipe-in-pipe geometry consisting of a steel helix placed in the annular zone was studied in (Zarella et al, 2011). The helix is welded around a central steel pipe which contains an insulated polyethylene tube inside. The fluid circulated in direct contact with the ground. The BHE was studied extending the approach of (De Carli et al, 2010) and carrying out simple temperature measurements. This coaxial BHE had a good performance.

2.3.3 Thermosyphon BHE pipes

The secondary fluid circulating inside these U-pipe and coaxial BHEs is commonly pumped with an electrically driven pump. However, the circulation in thermosyphons is driven by fluid density differences.

(Sanner, 1991) pointed at the importance of using appropriate pipe materials that tolerate the pressure levels at which thermosyphons operate and that are suitable from the corrosion point of view (e.g. for long-term contact with groundwater).

(Kruse and Russmann, 2005) studied a design consisting of a counter-current liquid-vapor BHE consisting of a corrugated stainless steel heat pipe, a dozen of which have been installed on a commercial basis in Germany and Austria (Kruse and Peters, 2008). The number of known commercial heat pump installations using natural circulation was about 100 between 2001 and 2005, according to (Rieberer et al, 2005), a study that shows results from two 65 m deep self circulating BHEs, having a heat extraction rate of 58 W/m. Here, the probe head was identified as the bottleneck of these systems (they must guarantee a small pressure drop and good heat transfer at operating conditions).

Most work carried out until today correspond to solutions implying counter-current flow between the liquid and gas phases of the fluid, with the exception of (Ochsner, 2008), who presented a design consisting of a 40 mm flexible high-grade steel corrugated heat pipe system with the same working principle, but used as single or two tubes. The proposed two tube arrangement is in fact a coaxial design, where the liquid phase falls down through a central pipe and the liquid/vapor phase flows upwards through an annular channel, i.e. between the central pipe and the inner wall of the external pipe. Heat extraction rates of about 50 W/m are mentioned. The installation of this BHE is done with an unwinding device, similar to those used in common polyethylene pipe installations.

2.4 The secondary fluid

When connected to a ground source heat pump, the circulating fluid in BHEs is commonly called secondary fluid, given that the primary fluid (or refrigerant) is circulating inside the heat pump itself. Other names such as brines are also often used. However, brines originally refer to salt based solutions, which rarely is the case.

A secondary fluid normally varies from water to an antifreeze aqueous solution of ethanol, glycol, etc. or a salt. There are also natural circulation probes or thermosyphons using fluids as carbon dioxide, able to change phase at typical ground temperature levels.

2.4.1 Aqueous antifreeze solutions

Aqueous solutions of different additives, used instead of water, reduce the freezing point of the secondary fluid. Depending on the additive and its concentration, the thermophysical properties such as density, specific heat, viscosity, Prandtl number, etc., change; meaning that the choice of fluid has an important influence on the hydrodynamic and thermal performance of the system. A comprehensive study of the thermophysical properties of different secondary fluids is found in (Melinder, 2007). Ethanol plus water is the most common secondary fluid used in Sweden. As an example, Figure 4 shows how the ethanol concentration affects the kinematic viscosity of the fluid at different operating temperatures.

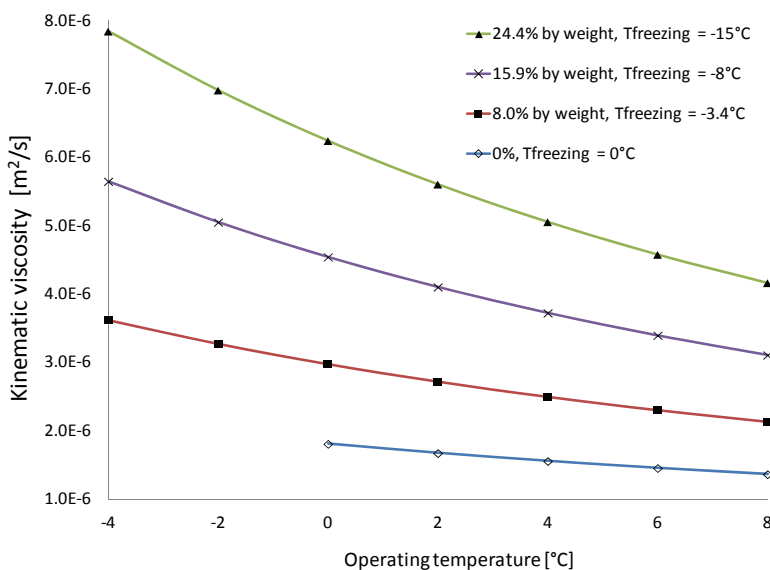


Figure 4. Viscosity of ethanol concentrations at different operating temperatures

Many other secondary fluids including salt solutions, their thermophysical properties, and their usage potential were largely studied in (Melinder, 2007) and the reader is referred to this document for details. An interesting report where potassium carbonate is compared to other secondary fluids is (Melinder et al, 1989).

2.4.2 Fluids for thermosyphons

Since phase change takes place inside the collector pipes, the condition for the secondary fluid in thermosyphon BHEs is its capacity to evaporate and condense at the temperature levels of a specific location. Carbon dioxide and propane are two examples of fluids that have been studied and used in this context.

Since most of processes in thermosyphon BHEs occur in saturation state, the pressure levels in the fluid loops are determined by the bore-hole (or rock) temperature levels. Normal rock temperatures in countries with heating demand imply, for example, CO₂ operating pressures of about 30-45 bar. The vapor density is high (approximately 7 times higher than the density of R-134a), resulting in a high volumetric refrigeration capacity (which leads to small volumetric flow rates and small pressure loss).

From the environmental point of view, CO₂ has zero ozone depletion potential, a GWP equal to 1, it is non-explosive, non-flammable, moderately toxic, and non-reactive. In case of leakage, no environmental effects are caused in the groundwater and, on the building side, since CO₂ is also odorless and colorless, the installation of CO₂ gas detectors is recommended in order to detect harmful gas concentrations.

The first investigations of CO₂ BHEs were done by (Rieberer et al, 2002), whose first tests showed undesired CO₂ superheat at the head of the borehole, a problem that was later solved. The temperature levels measured at different depths confirmed good operation of the system during the heat pump cycle. (Rieberer et al, 2004) presented details about mass flow rates, the refrigerant superheat temperature differences in the heat pump, different BHE probe heads (heat pump evaporator), and discussed the number of probes to be inserted in a single borehole. Later, (Rieberer, 2005) added results from a computer model showing simulated saturation temperatures in the probe heads at different filling concentrations.

(Kruse and Russmann, 2005) studied the minimum charge to guarantee a liquid film along the whole length of the BHE that they tested. The filling ratio was found to be directly related to the specific heat flux under which the thermosyphon worked. The requirement of higher filling rates to achieve higher heat fluxes became evident. Regarding visualization about what happens along the depth in pipes with natural circulation, (Kruse and Peters, 2008) presented measurements where temperatures varied between -1.5 °C and -3.0 °C along the pipe, while the inlet CO₂ temperature to the heat pump was -3.9 °C.

(Grab et al, 2011) and (Storch et al, 2011) demonstrated and showed a heat pipe operating with propane and presented visual observations on the wetted areas and the transition from start to boiling conditions, respectively. (Storch et al, 2012) showed other results on selected solid surfaces with similar systems.

3 Measurements on U-pipe BHEs

The general purpose of this chapter is to contribute to a better understanding of the operation and thermal response testing of U-pipe heat exchangers installed in groundwater filled boreholes. The specific objectives are presented in section 3.1.

3.1 Specific objectives

- i. Measurement of local ground thermal conductivity and local thermal resistances during a distributed thermal response test on a U-pipe BHE
- ii. Qualitative and quantitative comparison of the local thermal performance of U-pipe BHEs during forced and natural convection in the groundwater
- iii. Measure and observe the effect of varying the secondary fluid volumetric flow rate and the thermal power distribution vs. depth in U-pipe BHEs during heat pump operation and thermal response tests

3.2 The experimental rigs

The experiments presented in this chapter were carried out in BHE4 and BHE7. Details about these heat exchanger installations are given below (sections 3.2.1 and 3.2.2, respectively).

3.2.1 *U-pipe, BHE4*

The groundwater level in BHE4 measured from the top of the casing was 5.5 m. The borehole diameter is 140 mm and the total depth is 260 m. The secondary fluid is an aqueous solution of 12.6% ethanol by weight. The pipe is of type PE40x2.4mm.

Figure 5 shows two photos of BHE4. On the left-hand side, the different temperature measurement cables are pointed out. These are located

both inside and outside the pipes for measuring the secondary fluid and the groundwater temperatures. The picture on the right-hand side shows a 6 mm plastic pipe installed afterwards for injection of nitrogen (N_2) in the groundwater side at a depth of 85 m. This plastic pipe was connected to a pressurized nitrogen tank. A programmable relay connected to a solenoid valve in the outlet of the tank controls the gas flow.

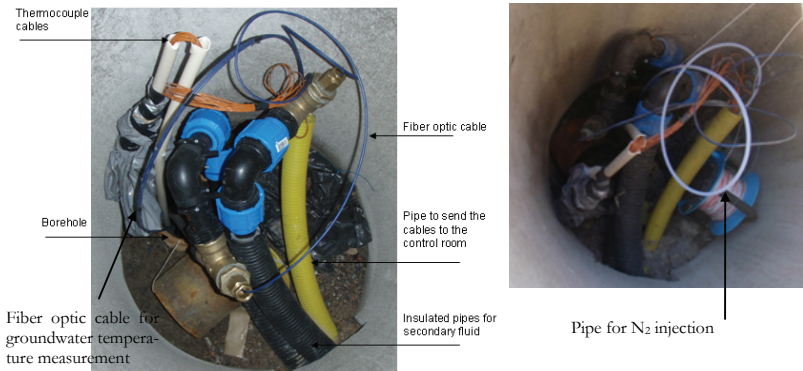


Figure 5. BHE4: U-pipe borehole heat exchanger

Figure 6 shows the fiber cable loop used in BHE4. This is connected in such a way the laser pulses passes from the measurement instrument (DTS) first through the secondary fluid path and then down and up on the groundwater side. There is a welding box where the fiber cables from the secondary fluid and groundwater side are spliced at the ground surface. There is about 15 m of extra cable between the top of the borehole and the welding box.

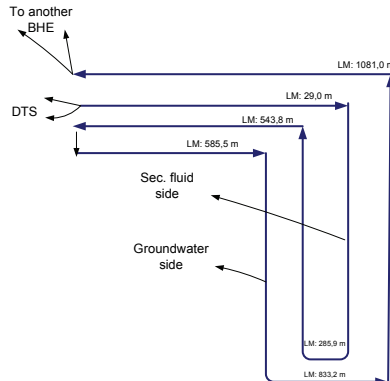


Figure 6. Sketch of the fiber loop in BHE4

During calibration, part of the extra cable at the ground surface was inserted into an ice-bath. The calibration was then done by matching the profiles measured with the laser travelling downwards and upwards in the secondary and groundwater side. Single-ended measurements are carried out. Section 1.7 in (Acuña, 2010) gives more details about the calibration method used.

3.2.2 U-pipe with spacers, BHE7

This U-pipe BHE is of type PE40x2.4mm and it uses spacers separating the pipe shanks with a center to center distance of 78 mm.

This borehole is denoted BHE7 in this thesis and it has a diameter of 140 mm. The total depth is 220.4 m. The secondary fluid is an aqueous solution of 12.6% ethanol by weight. The groundwater level measured from the top of the casing in this borehole was 5.5 m.

The set up and calibration of the fiber cable loop in BHE7 is exactly the same as in BHE4 (see Figure 6). In this case, the extra length of optical fiber at the ground surface was significantly longer. The measured temperature of the ground surrounding this BHE has a profile as shown in Figure 7. Figure 8 shows a photo of the top end of BHE7 as it was installed into the ground. The connections between the borehole and the heat pump evaporator are shown in Figure 9.

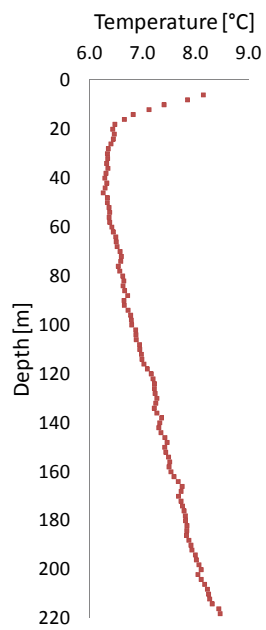


Figure 7. Ground temperature profile around BHE7

At the top of the borehole, before the manifold, BHE7 is instrumented with an inductive flow meter of the type Brunata HGS9-R6, two Pt500 temperature sensors and two thermocouples for measurement of the inlet and outlet fluid temperatures, and a STA-D flow regulation valve.



Figure 8. BHE7: U-pipe with spacers

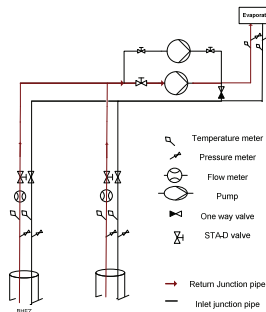


Figure 9. Connection of BHE7 to the heat pump evaporator

Note the bypass arrangement between the inlet and outlet manifolds, used in order to separately regulate the flow circulating through the collector pipes and through the heat pump evaporator.

3.3 Summary of paper I

The title of this paper is “Distributed thermal response test on a U-pipe borehole heat exchanger” and it describes a heat injection DTRT carried out in BHE4. A total of 9 kW was supplied to the BHE. Distributed temperature measurements along the secondary fluid path were taken during four continuous test phases: undisturbed ground conditions, fluid pre-circulation, constant heat injection, and borehole thermal recovery. The measured fluid mean temperatures in each section during all phases are presented in Figure 10.

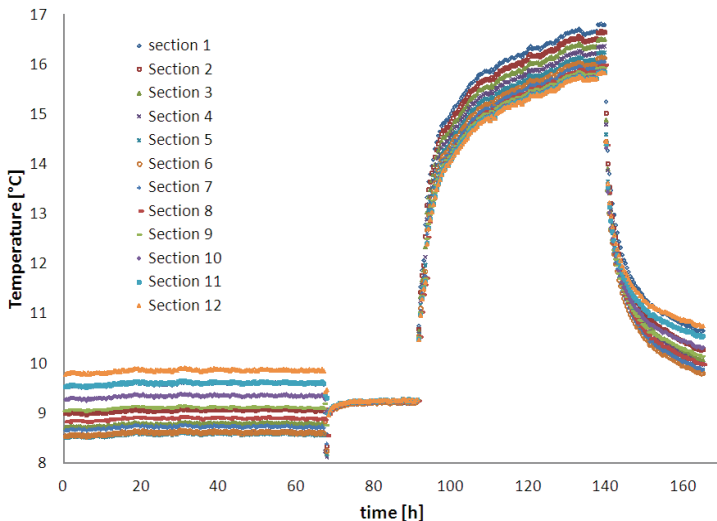


Figure 10. Fluid mean temperatures in each section during the whole first DTRT in BHE4

Figure 10 shows undisturbed ground temperatures during the first 65 hours, followed by 24 hours of fluid pre-circulation (without heat injection besides the circulation pump contribution) where the temperature along the whole borehole becomes almost constant. At the end of the pre-circulation, about two days of relatively constant heat injection into the borehole followed, concluded by about 20 hours of thermal recovery (without fluid circulation). During the latter phase, the temperatures at different depths along the borehole start going back to their initial values.

The fluid volumetric flow rate was 0.50 l/s. The borehole was divided into 12 consecutive 20 meter long sections, starting at 10 m depth, i.e. section 1 ranges from 10 to 30 meters and the last section 12 from 230 to 250 m. The section division is illustrated in the paper.

Some instantaneous vertical temperature profiles during the heat injection phase are presented in Figure 11 (legend in hours according to Figure 10), showing how the local secondary fluid temperature evolves in time. The profile at 93 hours has a lower temperature difference between inlet and outlet due to a lower supplied power during the first two hours of the test but, as time passes, the profiles are just displaced towards warmer temperatures. The profiles show in general the same shape before and during steady flux conditions.

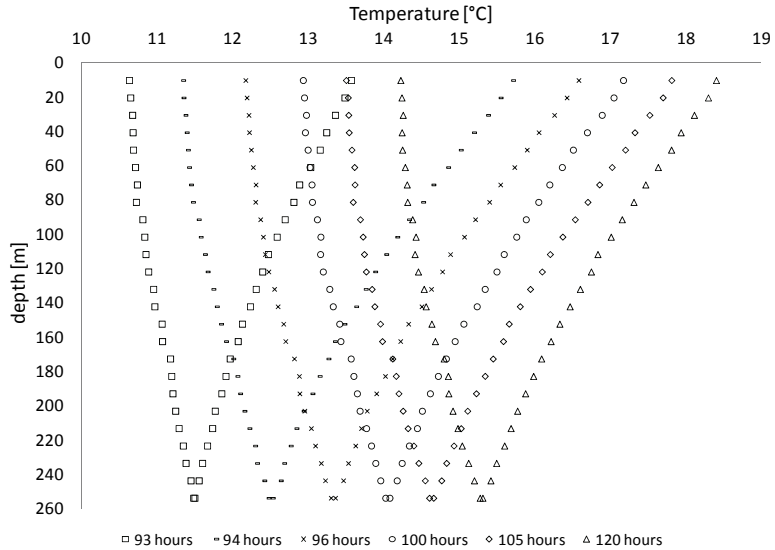


Figure 11. Instantaneous fluid temperatures during heat injection

During the thermal recovery phase, right after heat injection, the radial temperature gradients in the borehole become very small. This period is therefore used to determine the local ground thermal conductivity in all borehole sections accounting for the early activities in the borehole. The absence of a radial temperature gradient increases the accuracy of the calculation. Instantaneous temperature profiles during this phase are presented in Figure 12.

Figure 12 shows how fast the borehole recovers and demonstrating the absence of the radial temperature gradient during thermal recovery. The shape of the vertical profile is similar to the original undisturbed ground temperature profile having a minimum between 90 and 110 m depth. Relatively seen, a slower recovery occurs along the first 100 m, which indicates a slightly lower thermal conductivity there.

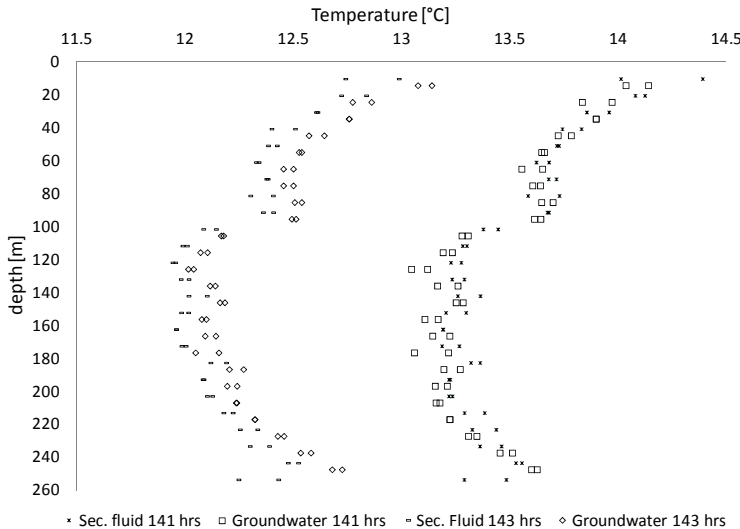


Figure 12. Instantaneous fluid and groundwater temperatures during thermal recovery

A jump to colder temperatures between 90 and 100 m is observed, and the faster thermal recovery of the sections between 100-200 m may indicate that colder groundwater enters and circulates through the borehole in these sections, and/or the presence of a rock section having larger thermal conductivities. A groundwater flow was not identified in the characterization of this borehole although a small anomaly was found at about 190 m depth (between sections 8 and 10, barely visible in Figure 12). Also, it is known that BHE4 deviated considerably after 110 m while drilling, as compared to its upper 100 meters (Acuña, 2008).

The resulting local thermal conductivities are presented in Figure 13. The rock thermal conductivity values range between 2.60 and 3.62 W/Km and the rock is considered homogeneous, although slightly higher values are found along the lower half of the borehole (except section 9). The propagated error in thermal conductivity varies in the borehole between 12 and 15%.

The determination of the ground thermal conductivity in all sections is followed by the determination of the local borehole thermal resistance in each section during the heat injection period using the previously calculated thermal conductivity as an input. In these calculations, the temperature response is again calculated using the line source model by superposing the temperature response of all small heating steps. The squared error between calculated and measured values is now minimized by adjusting R_b . The resulting local borehole resistances are presented in Figure 14, varying within a range of 0.054 to 0.078 Km/W.

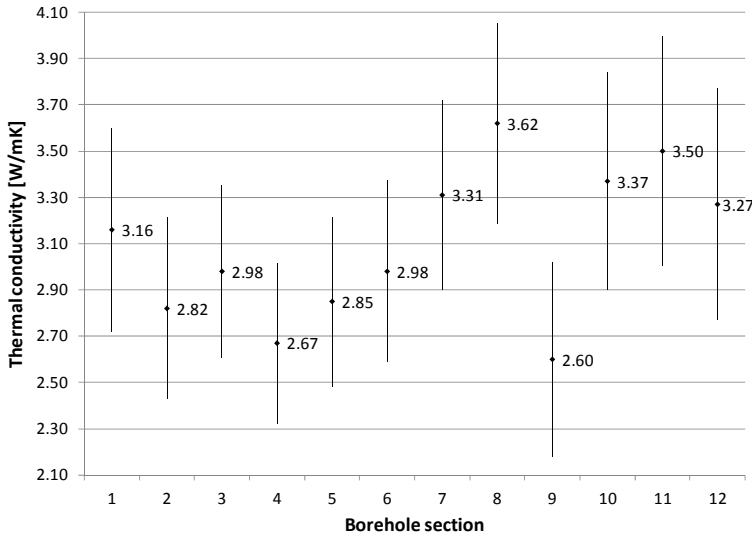


Figure 13. Local ground thermal conductivities in U-pipe, BHE4

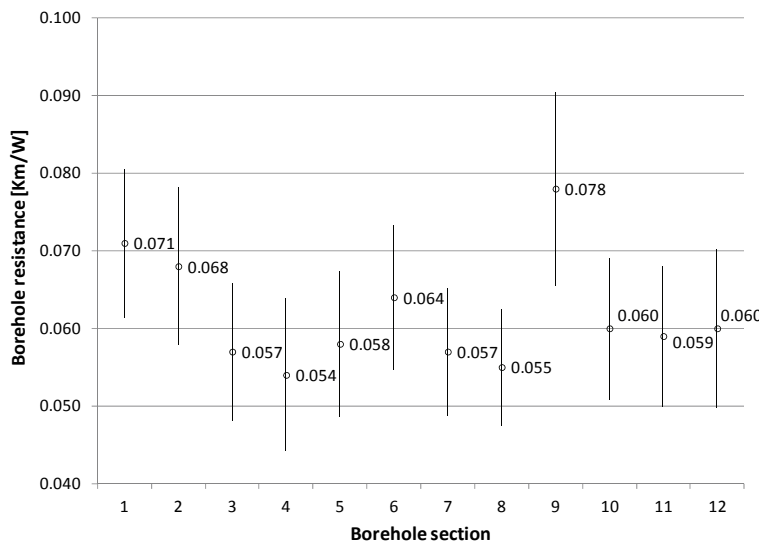


Figure 14. Local borehole resistances in U-pipe, BHE4

The variations in R_b may indicate changes of the pipes position along the borehole, but also the presence of an anomaly in section nine reflects in a higher local borehole resistance. However, the propagated error in the borehole resistance calculation varies between 13 and 17%. This relatively high error is mostly due to the large error in the thermal conductivity calculation, which is an input for the R_b estimate.

The average λ_{mck} and R_b obtained in the analyses were 3.10 W/mK and 0.063 Km/W. These were compared with those from a conventional TRT analysis based on the measured arithmetic mean between in and outlet temperatures, i.e. the effective ground thermal conductivity and the effective borehole resistance, 3.08 W/mK and 0.079 Km/W, respectively, showing good conformity regarding thermal conductivity, but resulting in a deviation of circa +28 % in the borehole thermal resistance. This is mainly caused by the overestimation of the fluid mean temperature during the conventional TRT analysis.

3.4 Heat transfer on the groundwater side

The measurements in section 0 confirmed, at the local level, that lower borehole thermal resistances are obtained (due to natural convection) during heat injection TRTs in groundwater-filled boreholes, as compared to a case when heat is transferred by conduction only. The present section gives some new insights of what happens in the groundwater with and without imposing groundwater movement (i.e. under natural and forced convection conditions) in U-pipe BHEs.

Radial temperature gradients outside the U-pipe tubes were measured to be low, allowing for the measurement of local fluid to groundwater thermal resistances. These have been quantified during a set of DTRTs on BHE4 at similar heat injection and volumetric flow rate conditions as those presented in paper I. In this new case, forced convection has been imposed on the groundwater side by injecting N₂ at 85 m depth using the test rig with the thin plastic pipe (see Figure 5).

After letting the borehole rest to reach essentially the initial undisturbed conditions, the fiber calibration for the temperature measurements in the groundwater and the fluid was re-checked with 30 second (integration time) continuous measurements during 2 hours, resulting in the same values for the uncertainty in the random errors ±0.05 to 0.07 K. These are standard deviations as shown in Figure 15. The chronology of this new DTRT in the BHE is presented in Table 3-1.

Table 3-1. Chronology of the bubble injection DTRT

DTRT phase	Test time [h]	Start date and time
Phase 1: Pre-circulation	0 to 71.7	2012-04-27 15:01
Phase 2: heat injection without N ₂ injection	71.7 to 170.3	2012-04-30 14:48
Phase 3: heat and N ₂ injection	170.3 to 192.9	2012-05-04 17:07
Phase 4: heat injection without N ₂ injection	192.9 to 275	2012-05-05 16:10

As presented in Table 3-1, the test lasted 275 hours and it included about 3 days of pre-circulation (phase 1) followed by circa 200 hours of constant heat injection. The latter is divided in three phases: heat without N₂ injection during about 3 days (phase 2), heat and N₂ injection during almost one day (phase 3), and once again heat injection without N₂ for about 85 hours (phase 4). The heat injection part of the test is shown graphically in Figure 16 in terms of the injected power and the volumetric flow rate, showing that the injected thermal power was 7.97 ± 0.17 kW and the volumetric flow rate 0.44 ± 0.02 l/s. More information about this test can be found in (Calzada, 2012).

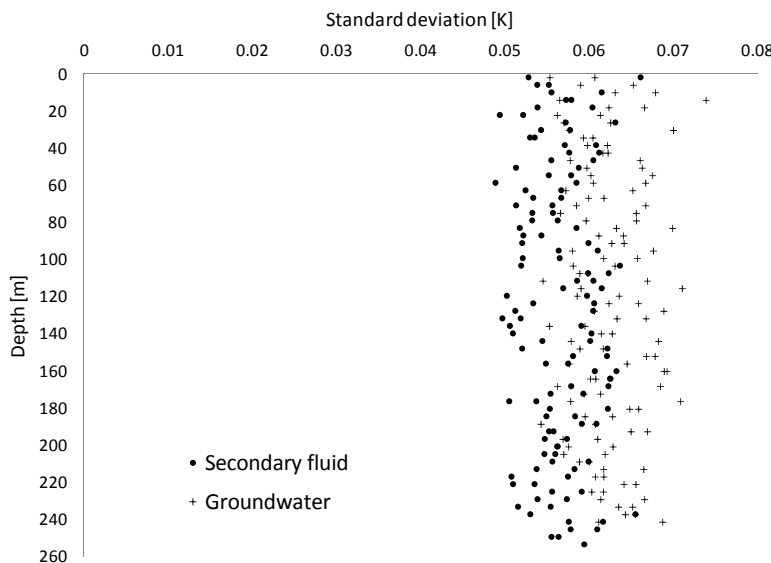


Figure 15. Standard deviation of measurements during undisturbed ground conditions (30 seconds integration and repetition time during two hours)

Following the same DTRT methodology as presented in paper I (section 0), local average fluid temperatures at each section during this new test are presented in Figure 17, where the temperature drop at about 170 hours corresponds to the beginning of the N₂ injection phase.

The nitrogen flow rate was measured to be about 10 g/min. The N₂ bubbles that formed inside the groundwater during the air injection phase were observed with a submersible camera, allowing experimental determination of the bubble flow velocity. The camera was located at the groundwater level and the time between the activation of the N₂ injection and the observation of the first bubbles was measured to about 4:15 minutes. Similar tests but stopping the N₂ injection and waiting for the

last bubble to arrive to the surface confirmed the time to be 4:00 (21.2 m/min). The latter time was considered to be more accurate because it probably took some seconds for the N₂ injection to start after opening the gas cylinder valve at the ground level (due to pressure stabilization). Since the N₂ bubbles accelerate as they travel upwards, a third experiment was done by placing the camera at 16.5 meters below the ground-water level, resulting in a travel time of 3:30 minutes (19.6 m/min).

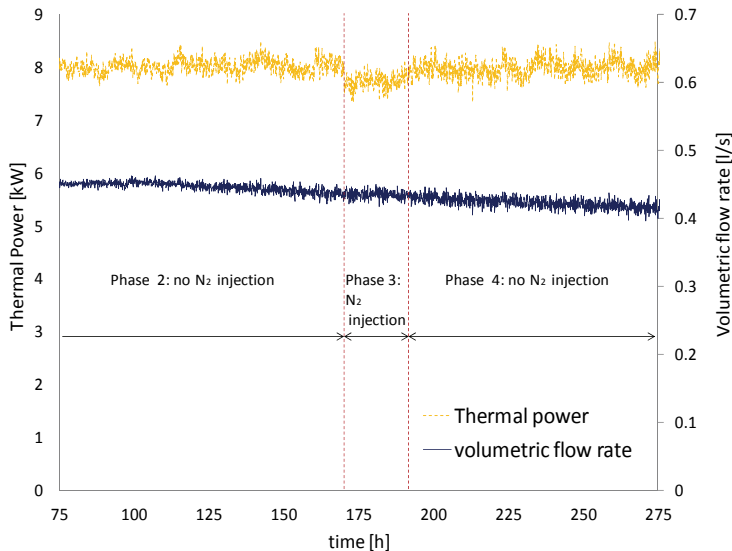


Figure 16. Thermal power and volumetric flow rate during the N₂ injection DTRT

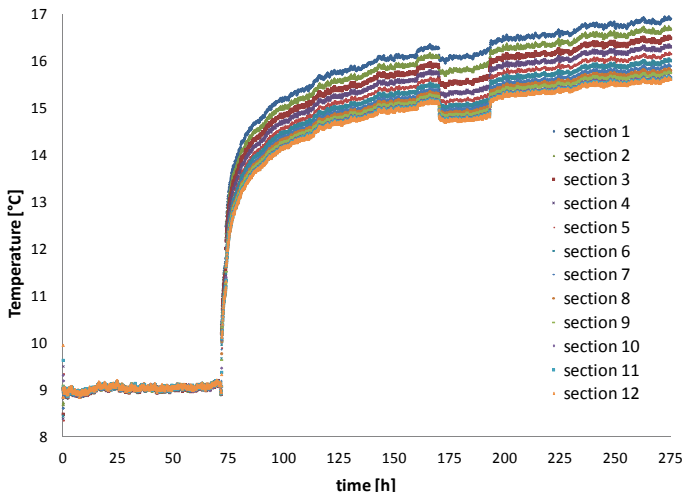


Figure 17. Average fluid temperature in each section during the N₂ injection DTRT

The results of this DTRT were first evaluated qualitatively. Instantaneous fluid temperatures before and during the N₂ injection period have been compared in Figure 18 (the exact moment that these profiles represent is better contextualized with the information in Table 3-1). When observing this figure, it is important to remember that the N₂ is injected at 85 m depth and that the flow rate and the injected power are kept constant.

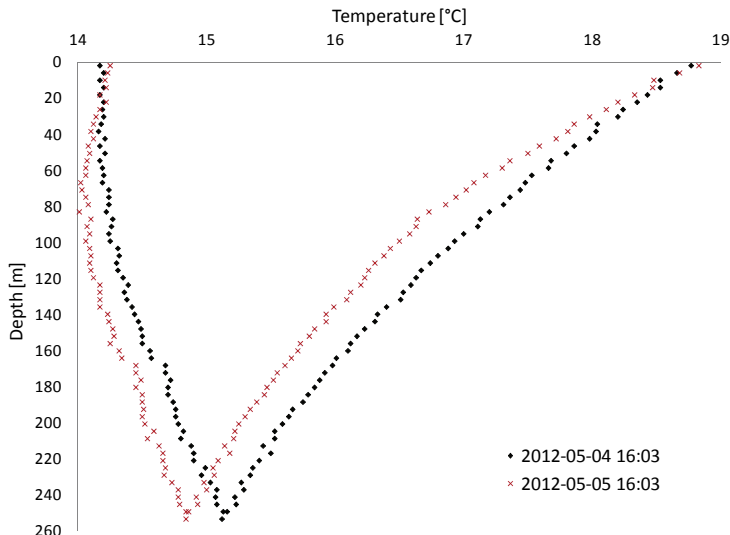


Figure 18. Fluid temperatures before and during N₂ injection

The change in temperature profile when N₂ is injected into the borehole (2012-05-05) illustrates that the convection enhances the heat transfer in such a way that the fluid travelling downwards is able to release even more heat than in the case with natural convection (2012-05-04), resulting in a higher degree of thermal shunt flow between the U-pipe shanks. The fact that the temperatures are displaced some tenths of degrees to the left (towards colder temperature levels) indicates that the temperature difference between the fluid and the borehole wall and/or the undisturbed ground decreased, i.e. the borehole resistance is lowered (as also shown in Figure 17).

Instantaneous groundwater temperatures show the effect of the forced convection process in the groundwater. Figure 19 and Figure 20 present the instants before and during N₂ injection, respectively. From Figure 19, it could be said that no strong evidence of natural convection can be qualitatively inferred from these profiles. This pattern is preserved during the whole steady-flux period. Only the magnitude of the local thermal resistances found in paper I (at similar conditions) quantitatively

proves that a natural convection process occurs outside the pipes when no forced groundwater movement is imposed. On the other hand, Figure 20 shows how groundwater temperatures are homogenized in the borehole above the N₂ injection point.

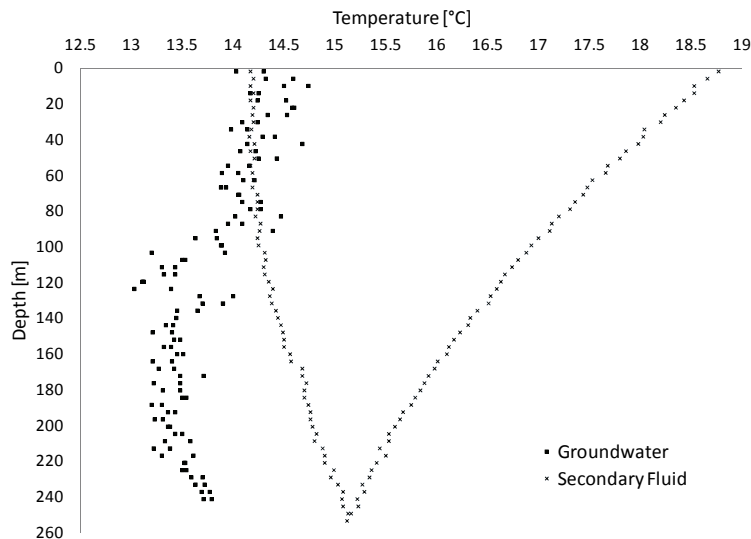


Figure 19. Fluid and groundwater temperatures previous to N₂ injection

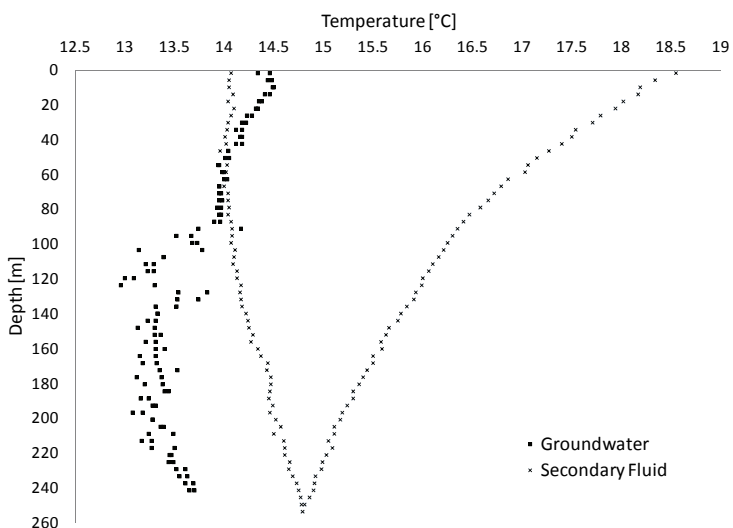


Figure 20. Fluid and groundwater temperatures one hour after starting N₂ injection

Although not fully visible in Figure 19 and Figure 20, the temperature difference between the groundwater and the secondary fluid decreases

along the whole depth while injecting N_2 . The reduction is 0.3 to 0.4 K in the upper four sections and 0.1 to 0.2 K in sections 5 to 12. Also, it is found that a re-distribution of the heat input occurs. The heat transfer increases in the upper four sections (above the injection point) and decreases in the lower parts of the borehole, as shown in Figure 21.

A simple calculation of the thermal resistance between the secondary fluid and the groundwater (R_{fgw}) has been done. For each section, the difference between the mean fluid temperature and the groundwater temperature is divided by the heat transfer rate per meter at each time instant during all heat injection phases. The average of these results is presented in Figure 22.

R_{fgw} is decreased by about 30% in the upper four sections due to the forced convection in the groundwater (phase 3), as compared to the non-injection cases (phase 2 and 4) when only natural convection occurs. The improvement is measured to increase as the bubbles travel upwards. The results from all non- N_2 -injection tests (shown in Figure 22) that were carried out in BHE4 are compared in Figure 23, together with local calculations of groundwater to borehole wall resistances (R_{gw-bw}) from the DTRT in paper I. R_{gw-bw} is based on measured groundwater temperatures along each section, used as input in the line-source model instead of the secondary fluid temperatures. R_b values found in paper I are also included in Figure 23.

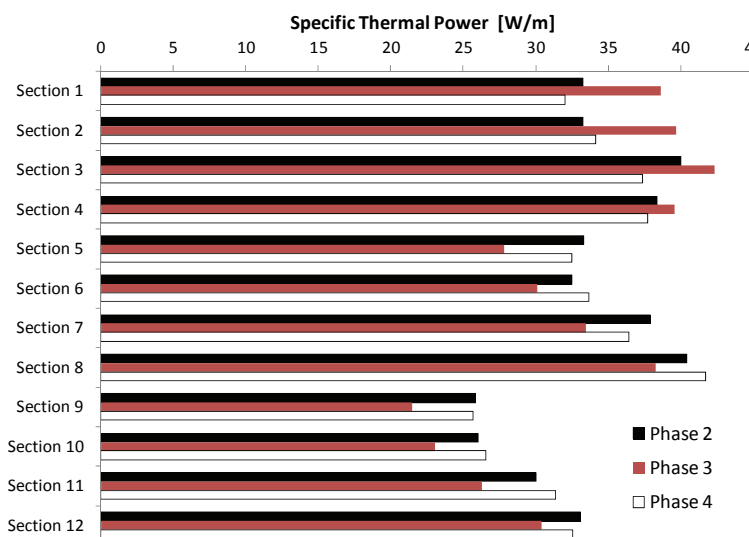


Figure 21. Average power distribution in the BHE during the different DTRT phases

A nearly constant difference of about 0.055 Km/W between R_b and R_{gw-bw} is found along the depth, meaning that the contribution of the thermal resistance in the groundwater to R_b is the largest.

It is almost certain that the radial position of the fiber optic cable changes along the depth. The low and large values of R_{gw-bw} and R_{fgw} , respectively, may thus imply the lack of a large radial groundwater temperature gradient around the U-pipes along the whole borehole. The position of the fiber optic cable will of course affect this conclusion, but this possible mixing effect occurring outside the pipes are confirmed with the measured groundwater temperatures presented in Figure 19, showing temperature scatter of about 0.5K in the groundwater.

At these temperature levels, it is concluded that R_{fgw} were found to vary locally and that the variations have almost the same trend vs. depth as for R_b . Sections where the power was low gave high R_{fgw} , and vice versa. R_{fgw} ranged from about 0.048 to 0.072 Km/W, being in average 0.055 Km/W for an average heat injection of 30 W/m.

Regarding the reduction of R_{fgw} during forced convection, the effect is seen in Figure 18 and Figure 22, being in average 0.036 Km/W. These local results depend directly on the temperature and power redistribution taking place in the different test phases.

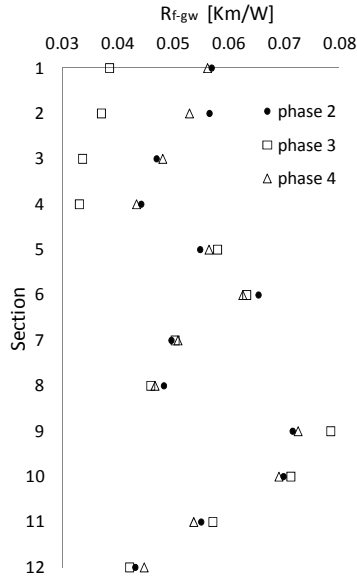


Figure 22. Average fluid to groundwater resistance along BHE4 with and without N_2 injection

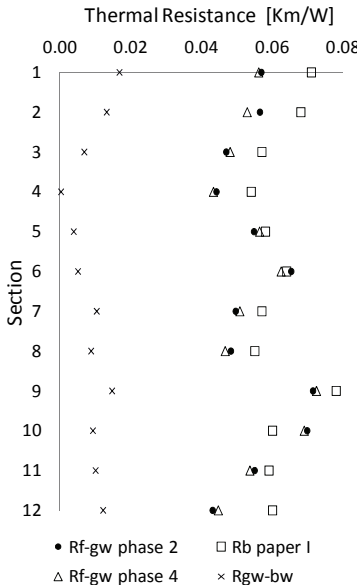


Figure 23. Comparison of local thermal resistances obtained in BHE4

Figure 24, Figure 25 and Figure 26 show the evolution in time of the temperature difference between the secondary fluid and groundwater and the thermal power at borehole sections 2, 4 and 5.

The behavior of section 2 is typical for the region above the N₂ injection point where the temperature differences decrease while the specific thermal power increases. In section 4, although no clear variation in the injected power is observed, the temperature difference is reduced by about 0.5 K, explaining the reduction in thermal resistance. Section 5 is representative of all sections under the N₂ injection point where both the temperature differences and the injected power decrease.

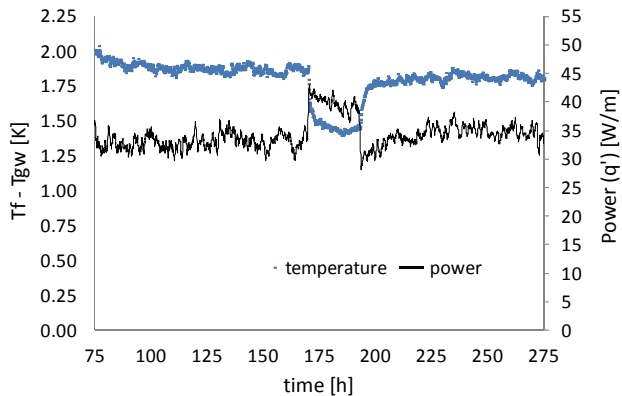


Figure 24. Temperature difference and heat injection in section 2

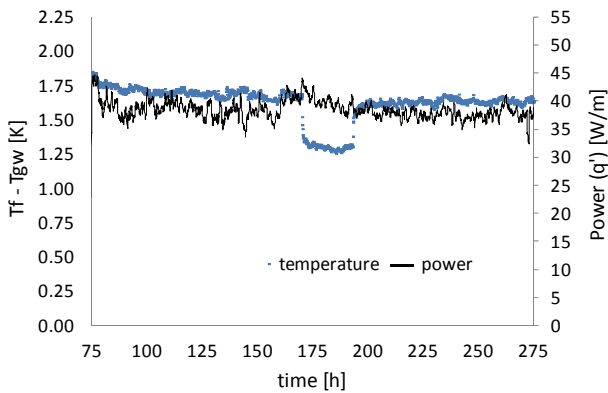


Figure 25. Temperature difference and heat injection in section 4

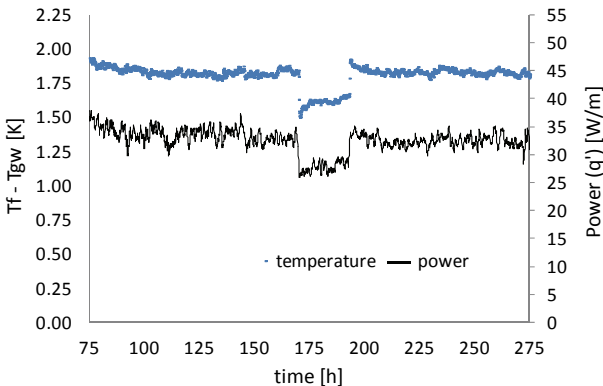


Figure 26. Temperature difference and heat injection in section 5

3.5 Effect of different flow rates

A varying volumetric flow rate of the secondary fluid may have an effect on the thermal resistances inside the borehole, the thermal shunt flow between the U-pipe shanks, the fluid residence time, and the pressure drop. These are intimately related to, but also dependent of the borehole depth.

Operating cycles of the same duration (or lower) than the fluid residence time may happen relatively often at real BHE installations and the secondary fluid flow rate may change depending on operation cases. The fluid residence time and the thermal capacity effects, as introduced in section 2.3, would influence the rate at which temperature profiles will develop inside the borehole. For example, instantaneous profiles measured during the first two hours of the DTRT presented in paper I, and having a volumetric flow rate of 0.5 l/s, differ according to Figure 27 (legend in hours according to Figure 10).

During these first two hours, the total supplied power was 6.5 kW. During secondary fluid pre-circulation (no heat injection), the fluid temperature quickly adopts a rather vertical shape at (9.19°C), a temperature slightly higher than the undisturbed ground temperature average (9.10°C), being the difference attributed to the circulation pump work.

The heat injection starts at 91.5 hours and, after this instant, Figure 27 shows that the injected power is redistributed along the borehole and the two U-pipe shanks progressively become more active in the heat exchange process to the ground.

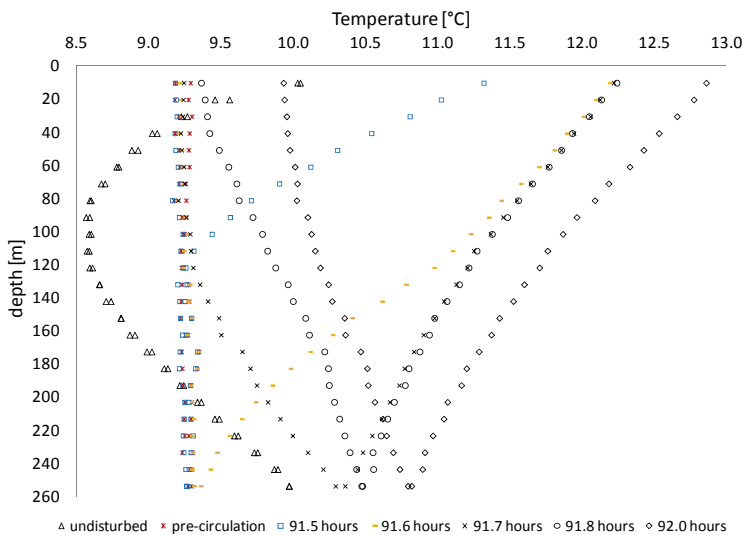


Figure 27. Instantaneous secondary fluid temperatures during the first two hours of heat injection in BHE4

Regarding the effect of the volumetric flow rate on the shape of the temperature profiles, on the thermal shunt, and on thermal resistances inside U-pipe BHEs, heat injection experiments have been carried out in BHE7 (see section 3.2.2 for details about this installation).

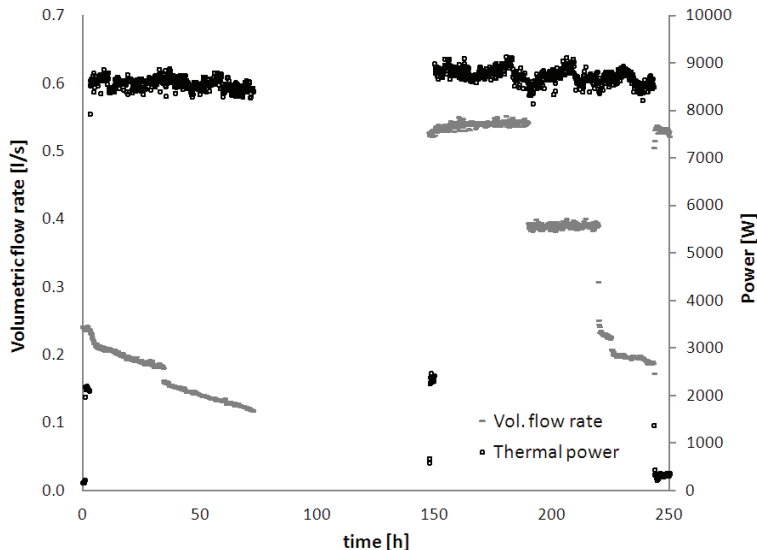


Figure 28. Flow rate and thermal power during heat injection experiments in BHE7

A power of 8722 ± 162 W was injected during several hours, as shown in Figure 28. The flow rate was intentionally varied between 0.20 and 0.54 l/s, as tabulated chronologically in Table 3-2. During the first 70 hours approximately, it was difficult to sustain stable low flow rates.

Table 3-2. Standard deviation of the measured flow rates during heat injection in BHE7

Date and time	Interval [h]	Flow rate [l/s]	Standard deviation [l/s]
2011/08/15, 15:27:23 – 2011/08/17, 10:15:21	147.5 to 189.7	0.538	± 0.010
2011/08/17, 10:25:23 – 2011/08/18, 16:10:55	189.8 to 219.5	0.389	± 0.009
2011/08/18, 21:51:58 – 2011/08/19, 15:55:20	225.2 to 243.2	0.195	± 0.022

During these experiments, the temperatures were measured along the secondary fluid paths and in the groundwater. Instantaneous temperature profiles at different flow rates are presented in Figure 29, including one picked up from the early part of the test at a flow of 0.14 l/s.

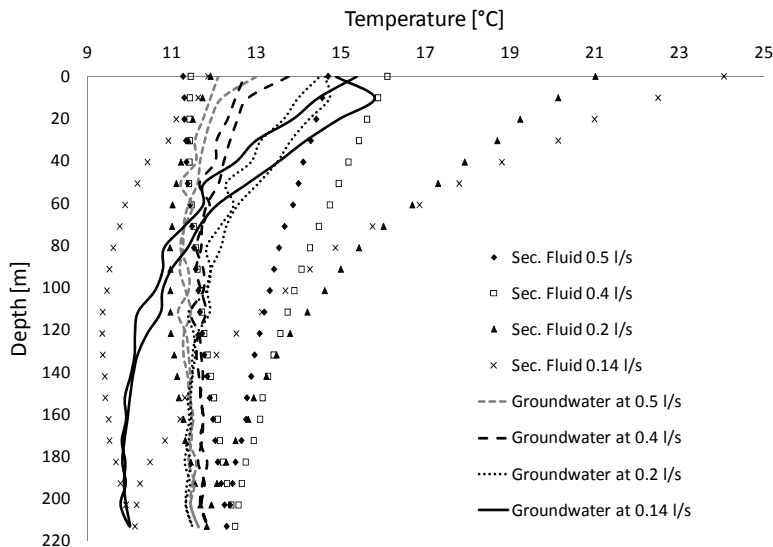


Figure 29. Fluid and groundwater temperatures during heat injection in BHE7 at four volumetric flow rates

Figure 29 shows that changing the volumetric flow rate has effects both on the secondary fluid and in the groundwater. A decrease in the flow rate causes an increase in temperature difference between down- and up-

going flows which, since the depth is a fixed parameter, imposes significant changes on the vertical temperature profiles. The temperature difference between the down- and up-coming flows causes an internal heat transfer between the two pipes, a thermal shunt flow, as part of the heat passes from the warmer to the colder pipe, and part of it flows from both pipes to the ground.

The average specific supplied power during these tests was 40.6 W/m (8722 W divided by the active borehole depth of this borehole, 214.9 m). However, the distribution of injected heat is different for each of the four measured cases. Figure 30 shows how the thermal power along both U-pipe legs for the four cases presented in Figure 29. Although the uncertainties of these measurements, caused by the varying temperature difference from point to point in Figure 29, it is seen that almost no heat is injected into the ground from the up-going pipe at the lowest flows. The temperature change through this shank tends to be insignificant and even negative.

Comparing Figure 29 to Figure 7, higher injection rates are expected in the upper parts of the borehole at all flow rates due to larger temperature differences between the secondary fluid and the undisturbed ground.

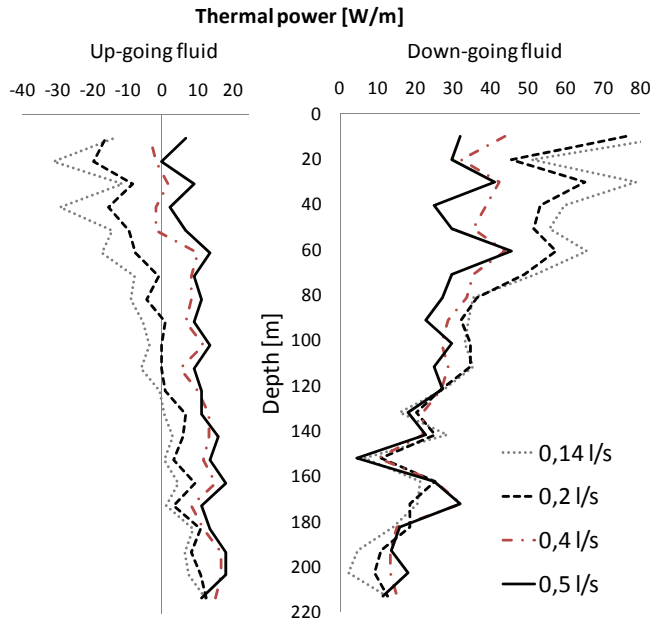


Figure 30. Themal power distribution along the BHE7 up-going and down-going shanks at different flow rates

For these four flow rates, the total power injected per meter borehole (sum of those presented in Figure 30 at each section) at a local level is presented in Figure 31, showing that the injected power at the lower borehole sections tends to decrease with decreasing volume flow rate. For the upper borehole sections it has a tendency to increase to some extent with decreasing flow rate. The power during the steady-flux conditions achieved during these DTRTs does not present an even distribution along the borehole depth. Higher flow rates would yield a more even power injection along the borehole.

In a similar way as in section 3.4, local fluid to groundwater thermal resistances ($R_{f\text{-}gw}$) have been calculated with the measured data shown in Figure 29 and Figure 30. The local fluid to groundwater temperature differences are presented in Figure 32. These are divided by the thermal powers from Figure 31, resulting in local $R_{f\text{-}gw}$ values shown in Figure 33.

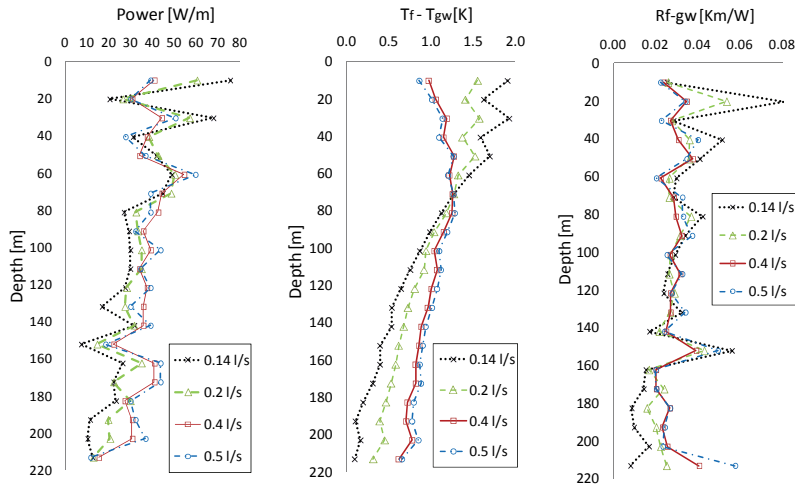


Figure 31. Local average specific injected power

Figure 32. Fluid to groundwater ΔT

Figure 33. Fluid to groundwater resistance

The fluid to groundwater temperature differences and the power injection profiles have the same shape for all flow rates. Their ratio results in nearly constant fluid to groundwater thermal resistances along the borehole depth, being in average equal to about 0.03 Km/W. The average at all flows is presented in Figure 34 as a function of the volumetric flow rate.

The fluid-to-inner pipe wall thermal resistance is expected to increase with decreasing flow rate and make a difference among the cases presented in Figure 34. Any change is hardly noticeable from these meas-

urements. However, it is known that the latter resistance is a very small fraction of the total borehole resistance.

The fluid to groundwater thermal resistances found in BHE4 (Figure 23) were about 60% higher than those found in BHE7 at a similar volumetric flow rate, possibly due to the use of spacers. Future work will be dedicated to study these differences further.

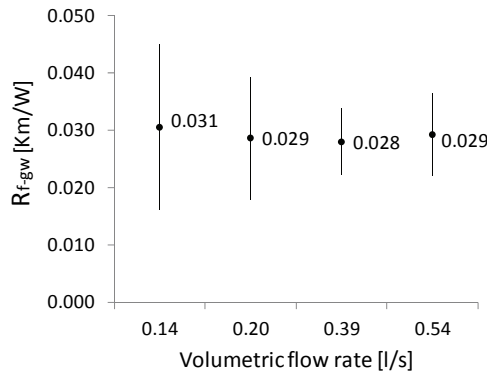


Figure 34. Fluid to groundwater thermal resistance vs. flow rate

The secondary fluid temperature from Figure 29 were also used to calculate, at each measured point, temperature dependent thermophysical fluid properties from (Melinder, 2007) and then visualize how the Reynolds numbers and the heat transfer coefficients vary inside the U-pipe shanks.

The Reynolds numbers are shown in Figure 35. The inlet and outlet differ from each other and the distributions become more asymmetric with decreasing flow rates. At the lowest flow, Reynolds numbers indicate laminar conditions (possibly explaining the somewhat higher R_{f-gw} shown at the upper part of the borehole in Figure 33), but even increase somewhat due to the thermal shunt flow. These Reynolds numbers are used as inputs in the Gnielinski correlation for the Nusselt number (Incropera et al, 2007) in order to obtain calculated heat transfer coefficients along the depth, shown in Figure 36.

The calculated heat transfer coefficients vary from about 200 to 1500 W/m²K depending on the flow rate. As seen, the differences in the heat transfer coefficients are significant going from 0.2 to 0.5 l/s, although all represent turbulent conditions. The jump at 0.14 l/s (at about 100 m depth) is due to the limit set by the correlations for Nusselt numbers between turbulent and laminar flow.

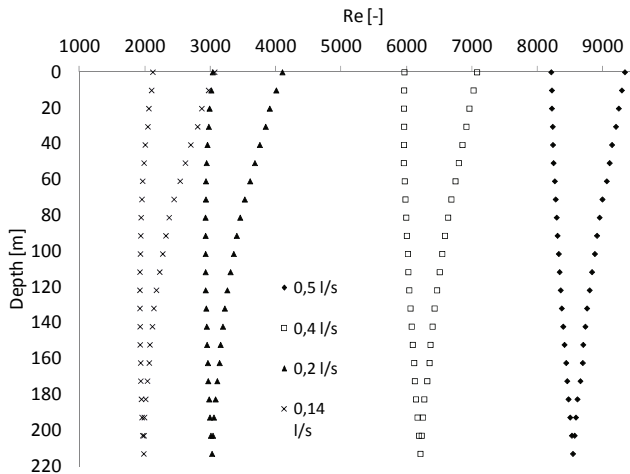


Figure 35. Reynolds number at four different flows in U-pipe BHE

These heat transfer coefficient profiles imply critical thermal resistances between the fluid and the inner pipe wall varying between 0.006 and 0.05 Km/W (depending on the flow rate and where along the U-pipe it is measured), as shown in Figure 37. The higher resistance corresponds to the low flow rate. In reality, due to transition effects, there is no guarantee that these profiles (at 0.14 l/s) are as shown in these figures. A fuzzy transition area has thus been marked on Figure 36 and Figure 37 in order to show that, in at least in this region, the used correlations may not give correct values.

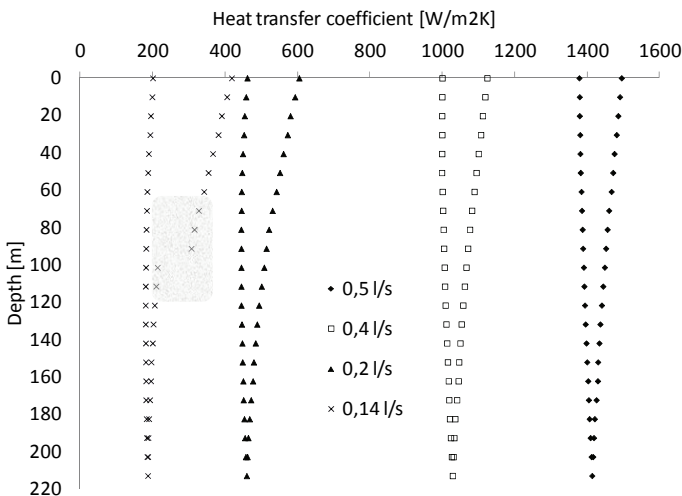


Figure 36. Heat transfer coefficient at four different flows in a U-pipe BHE

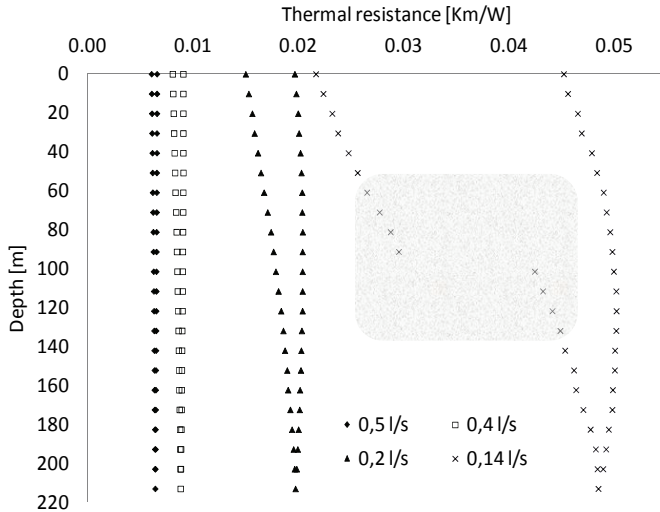


Figure 37. Fluid to inner pipe wall thermal resistances along the depth at different flows

Even more alarming heat transfer coefficients and fluid to pipe thermal resistances may be observed during heat pump operation given the lower temperature levels while extracting heat. The viscosity increases with decreasing temperature and with the concentration of the antifreeze additive, as pointed out in Figure 4. A large viscosity gives low Reynolds numbers, higher risk for laminar conditions (i.e. low Nusselt number and low heat transfer coefficient), and (not least) larger pressure drop.

In order to illustrate how flow regime can change during heat extraction as a function of the viscosity, the Reynolds number has been quantified for a given temperature profile along BHE4 using three fluids: water + ethanol 24% by weight, water + ethanol 12% by weight, and water. Figure 38 shows the result of these estimations.

Besides for the thermal implications discussed in relation to Figure 36 and Figure 37, Figure 38 implies that larger or lower ethanol concentrations would result in larger or lower pressure drops, respectively, for the same flow rate.

In order to have a feeling about the pressure drop aspect, measurements and calculations were carried out at three different flow rates (0.42, 0.50, 0.69 l/s) in BHE4. An instrument of the type TESTO 526-2 was connected between pressure taps located at the collector inlet and outlet. The operating temperatures during the measurements were between 6 and 8°C and the effect of bends and accessories have not been considered.

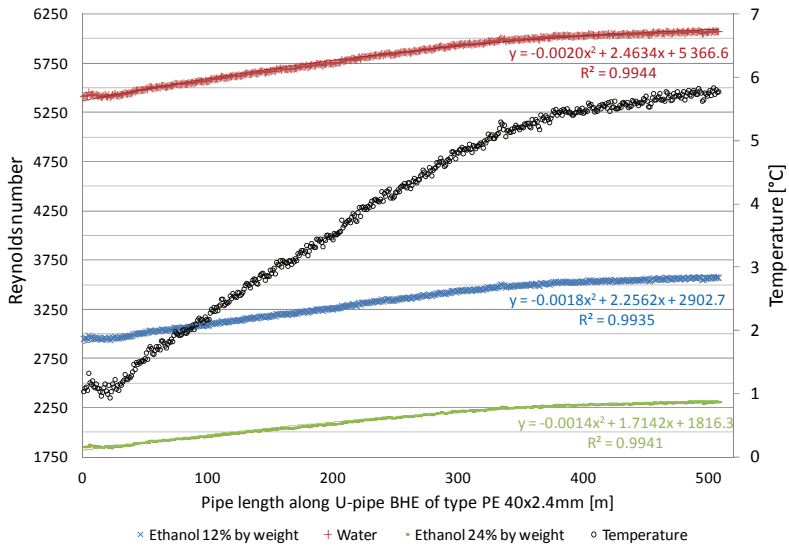


Figure 38. Reynolds number along the pipe length of BHE4 allowing the viscosity to change for given secondary fluid temperatures (flow 0.3 l/s)

The result for the experimental and calculated pressure drop was 61.4 and 56.4 kPa at 0.42 l/s, 87.3 and 78.2 kPa at 0.50 l/s, and 149.6 and 129.5 kPa at 0.69 l/s, respectively. As expected, the pressure drop increases with increasing flow rate. The difference between the measurement and calculations is partially attributed to the presence of the fiber optic cable installed inside the BHE4 pipes. Figure 39 compares the pressure drop per meter collector pipe for BHE4 and another U-pipe not having optical fiber cable at the three flow rates, evidencing the effect of the fiber cable inside the U-pipe shanks on the pressure drop.

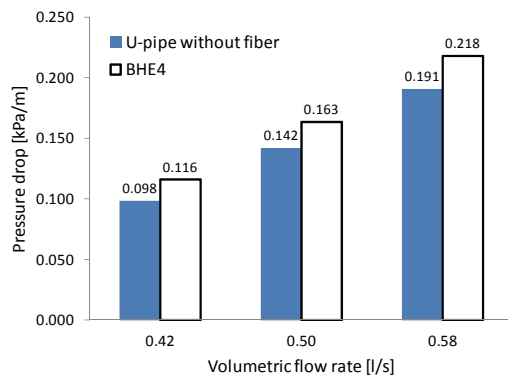


Figure 39. Comparison of pressure drop in U-pipe with and without fiber optic cable having the same secondary fluid (see section 3.2.1)

3.6 Heat pump operation

Experiments during heat pump operation were done in BHE7 during the winter 2009-2010. Figure 40 shows temperature profiles in this BHE at different instants after the start of a heat pump ON period. The secondary fluid flow rate was 0.4 l/s, and the effect of the fluid residence time on the temperature distribution in the borehole is clearly seen.

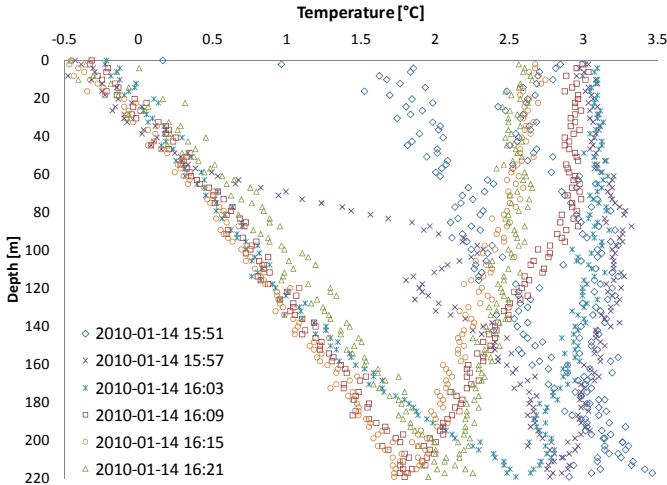


Figure 40. Temperatures in BHE7 at short intervals after heat pump start (at 0.4 l/s).

Typical heat pump cycles could be rather short even during winter months. The heat pump operation starts at 15:51 and, at the beginning of the heat extraction period, a temperature difference is only observed at the top of the down-going pipe, i.e. a part of the power is extracted into the secondary fluid in this part of the BHE. Seen from the heat pump, the power supply is coming from the stored heat in the secondary fluid. With time, stored heat in the groundwater will flow into the secondary fluid.

As time passes, the power extraction into the secondary fluid is slowly re-distributed deeper along the borehole depending on the volumetric flow rate of the secondary fluid. At 0.4 l/s (which is the case in Figure 40), the residence time is about 20 minutes, meaning that the first temperature profile at which the whole secondary fluid volume inside the BHE is active occurs at 16:15. Besides the effect of the residence time, it was shown in the previous section that changing the volumetric flow rate for a given total thermal power rate can drastically affect the temperatures and heat transfer coefficients along the depth. Moreover, depending on how long time the heat pump operates and how the U-pipe shanks are placed inside the borehole, different parts of the ground

might be successively activated. In heat pump OFF periods, heat from the surrounding ground flows into the borehole.

In this section, the temperature and power distribution are determined by imposing a constant temperature difference between the inlet and outlet of the BHE while having different flow rates, during heat pump operation. Keeping a constant temperature difference is achieved by adjusting the valves and pumps shown in Figure 9. An advantage of such a manifold connection is that it allows changing the fluid flow rates in the BHE without affecting the pressure drop over the evaporator. Since the temperature difference is kept constant, an increase in flow rate implies a proportional increase in the power. The measurements show how the temperature and heat distribution inside U-pipe BHEs are affected by the volumetric flow rate.

Two cases corresponding to temperature differences of about 3.5 K and 2.5 K respectively are studied through a selection of representative heat pump cycles. The short term development of the fluid temperature profile at all flow rates are similar to those shown in Figure 40 (but at different time scales) and only temperature profiles after the residence time has elapsed are thus considered from now on.

Table 3-3 and Table 3-4 present the general characteristics of each measurement for the 3.5 K and 2.5 K study cases, including average Reynolds numbers and power rates. Figure 41 and Figure 42 show groundwater and secondary fluid temperatures for the $\Delta T \approx 3.5$ K case. Figure 43 and Figure 44 correspond to the cases with $\Delta T \approx 2.5$ K. Instantaneous local fluid-to-groundwater thermal resistances R_{fgw} are included in these figures as an attempt to quantify the instantaneous performance at the tested conditions. These are calculated in the same way as in sections 3.4 and 3.5 but, in this case, only as an average of the upper and lower half of the borehole.

It is observed that the thermal resistances are lowered by about 30% when the fluid flow increases in both study cases. The Reynolds numbers have been approximately doubled and their average indicates turbulent conditions in all study cases, meaning that the inner fluid to pipe resistance should be very low and that the variation in total resistance only occurs on the groundwater side.

The large difference between the resistances at low and high volumetric flow rates is attributed to the drastic change in power between these cases. At the low flow rates, the heat extraction was about 12.5 W/m whilst they were approximately doubled (about 25.0 W/m) when running at higher flows.

Table 3-3. Characteristics of the heat extraction experiment with $\Delta T \approx 3.5$ K

Flow [l/s]	Power [kW]	Specific power [W/m]	Reynolds number
0.36	5.7	12.9	2780
0.81	11.4	25.8	6003

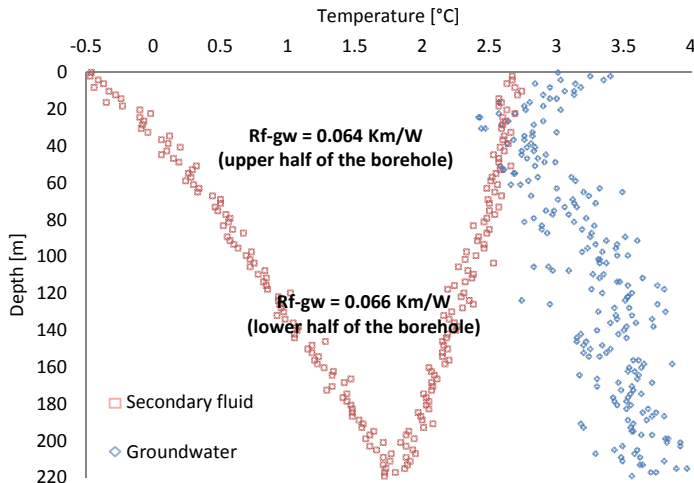


Figure 41. Secondary fluid and groundwater temperature profile at 0.36 l/s after elapsed residence time, including local fluid to groundwater thermal resistance

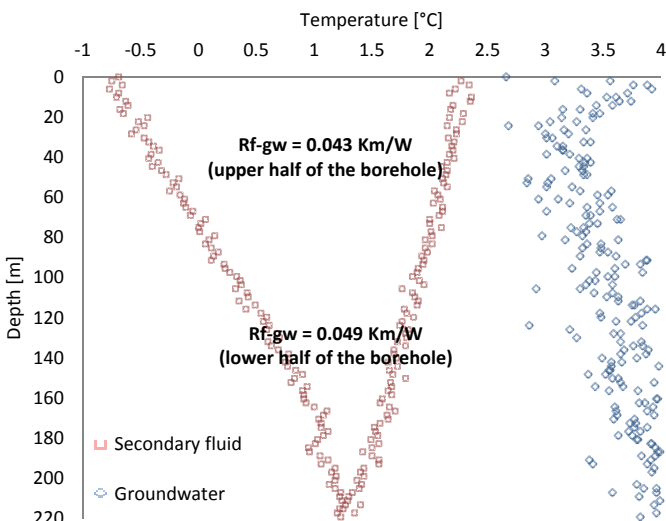


Figure 42. Secondary fluid and groundwater temperatures at 0.81 l/s after elapsed residence time, including local fluid to groundwater thermal resistance

Table 3-4. Characteristics of the heat extraction experiment with $\Delta T=2.5$ K

Flow [l/s]	Power [kW]	Specific power [W/m]	Reynolds number
0.60	5.5	12.4	4557
1.00	10.6	24.0	7575

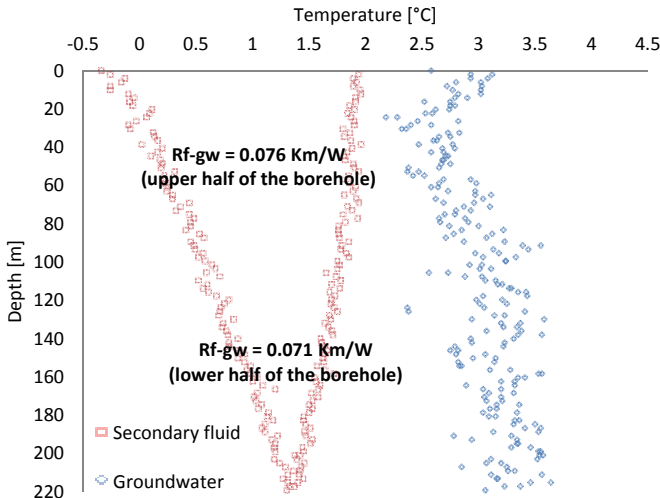


Figure 43. Secondary fluid and groundwater temperature at 0.60 l/s, after elapsed residence time, including local fluid to groundwater thermal resistance

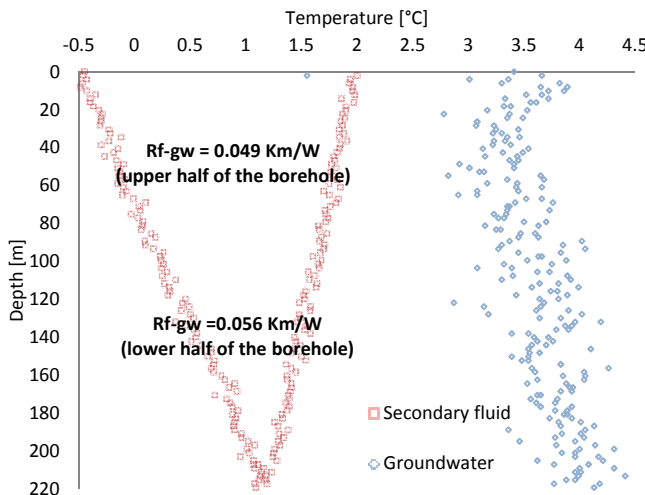


Figure 44. Secondary fluid and groundwater temperatures at 1.00 l/s, after elapsed residence time, including local fluid to groundwater thermal resistance

The instantaneous thermal resistances found during heat extraction are slightly higher than those found during heat injection (see sections 3.4 and 3.5). The latter varied in average between 0.030 to 0.055 Km/W.

In the heat injection cases, groundwater temperatures varied between 11 and 14°C while being between 2.5 and 4°C in the heat extraction cases. It is well known that the borehole resistance can increase to a large extent (by about 50%) at temperatures close to the water density maximum (Gustafsson, 2010). The difference between the heat extraction and the heat injection cases is therefore attributed to the temperature levels in the groundwater for each of these measurements.

The temperatures in the groundwater during the heat extraction cases show a scatter of about 1 K for measurements taken at the same depth. This scatter is larger than found during heat injection (about 0.5 K). It can be pointed out that at the higher flow rates during the heat extraction tests, larger radial temperature gradients inside the borehole were measured (observe the increased temperature difference between the groundwater and the fluid). Apart from these differences, the secondary fluid temperature profiles are similar in all heat extraction cases, as presented in Figure 45 and Figure 46.

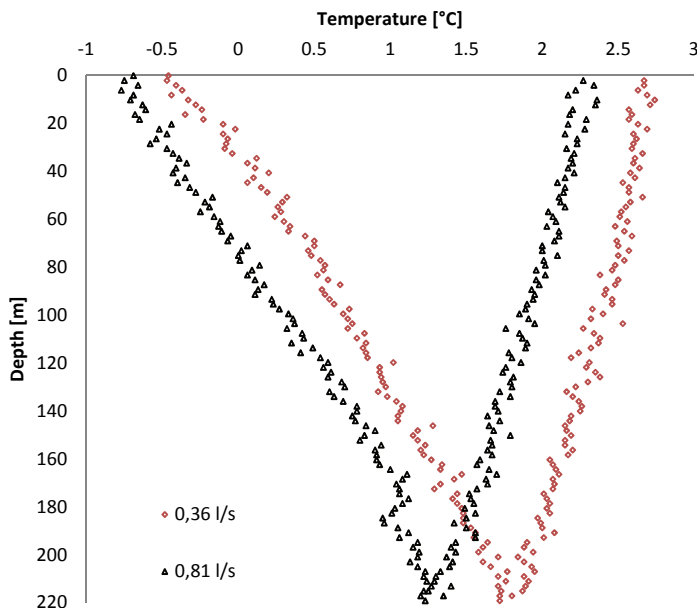


Figure 45. Comparison of secondary fluid temperature profiles after elapsed residence time during the first heat extraction experiment in U-pipe ($\Delta T \approx 3.5$ K)

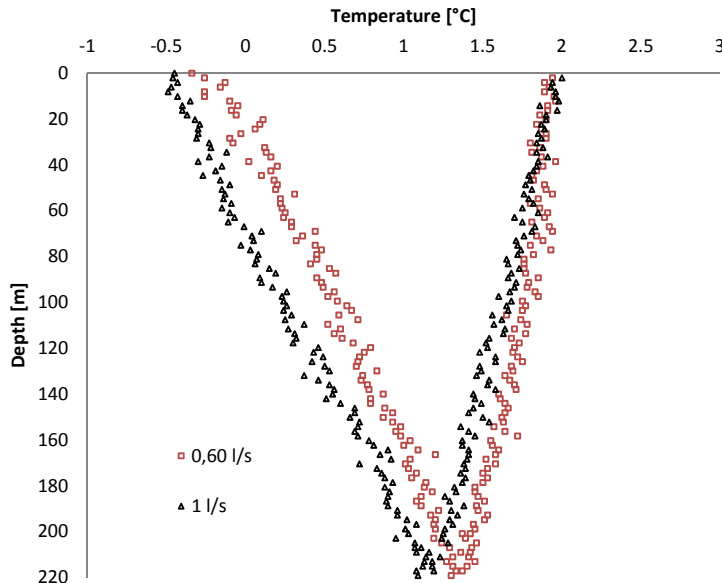


Figure 46. Comparison of secondary fluid temperature profiles after elapsed residence time during the second heat extraction experiment in U-pipe ($\Delta T \approx 2.5$ K)

Percentagewise, the power distribution is nearly the same along the borehole depth in both cases. The power extracted along each half of each U-pipe tube is presented in Table 3-5 and Table 3-6, relative to the total extraction rate.

Table 3-5. Heat extraction percentage along each half of the BHE7 tubes during the first heat extraction experiment ($\Delta T \approx 3.5$ K)

Flow [l/s]	0-110 m [%]	110-220 m [%]	220-110 m [%]	110-0 m [%]
0.36	39.6	30.0	21.1	9.3
0.81	37.8	27.0	21.6	13.5

Table 3-6. Heat extraction percentage along each half of the BHE7 tubes during the second heat extraction experiment ($\Delta T \approx 2.5$ K)

Flow [l/s]	0-110 m [%]	110-220 m [%]	220-110 m [%]	110-0 m [%]
0.60	37.7	34.2	21.1	7.0
1.00	33.5	29.4	19.6	17.6

3.7 Conclusions

- i. Slightly varying local ground thermal conductivities along a borehole have been measured during thermal recovery after a heat injection Distributed Thermal Response Test (DTRT). The average of all measured local thermal conductivities showed good agreement with the result found in a conventional TRT. Although the borehole is considered to be homogeneous, larger local thermal conductivities were to some extent found in the lower parts of the borehole, which recovered faster than the upper 100 meters. The slight increase in thermal conductivity starts at the same depth as the borehole deviation increased.

The local borehole thermal resistance was found to be lower than the effective resistance due to the overestimation of the fluid temperature during the conventional TRT analysis.

- ii. Forced convection in the groundwater achieved by injecting nitrogen bubbles reduces the local thermal resistance by about 30%. The specific power increases while the fluid to groundwater temperature difference decreases. The temperatures inside the groundwater are homogenized and no radial gradient was identified while injecting the N₂. The fluid to groundwater thermal resistance (R_{fgw}) during forced convection was measured to be 0.036 Km/W. This result applies for borehole sections located above the N₂ bubble injection point. Under this point, natural convection conditions were measured to be the same as during standard DTRT conditions (about 30% larger resistances).

At groundwater temperature levels between 11 and 14°C during DTRTs, R_{fgw} values were measured to vary locally. The variations with depth had the same trend as those for local R_b . Sections where the local power was low gave high R_{fgw} , and vice versa, and ranged from about 0.048 to 0.072 Km/W with an average of 0.055 Km/W. The average heat injection was 30 W/m. For a heat injection of about 40 W/m, R_{fgw} was measured in average equal to 0.03 Km/W in a different U-pipe BHE having spacers.

Local fluid-to-groundwater thermal resistances during heat pump operation were found to be slightly higher than those measured during heat injection, attributed to the temperature levels in the groundwater being close to the water density maximum, between 2.5 to 4°C.

- iii. In U-pipe BHEs, the heat exchange at the upper part of the down-going pipe slightly increases at lower flow rates. The opposite is noted along the neighbouring up-coming pipe, caused by the constant thermal shunt flow becoming a larger part of the total power.

If the volumetric flow rate is changed while keeping constant heat injection, the heat exchange between the ground and the secondary fluid varies significantly along the pipe length. On the other hand, if the inlet-to-outlet temperature difference is kept constant while the total power is allowed to vary, a change in the flow rate does not affect the power distribution along the pipe length as long as the thermal shunt influence is low.

Regardless of the relative power allocation along the pipes, the power in the tested U-pipe BHEs is, during heat pump operation and thermal response test periods, rather evenly distributed along the depth as long as the volumetric flow rate is high and no forced convection is imposed on the groundwater side. At very low flows, more heat is exchanged at the top of the U-pipe BHE.

4 Measurements on a U-pipe Thermosyphon

4.1 Specific objective

The aim of this work was to acquire a better understanding of the operation of a U-pipe thermosyphon heat exchanger installed in a groundwater filled borehole. The operation of this BHE is studied during heat extraction from the ground through observation and interpretation of distributed temperature measurements at the riser outer pipe wall and in the groundwater.

4.2 The experimental rig, BHE12

The experiments presented in this chapter were carried out in BHE12, a borehole where the groundwater level was measured to be 7 m from the top of the steel casing. The borehole diameter is 115 mm and the total depth is 70 m. The collector pipes are 65 meter long. The secondary fluid is CO₂.

BHE12 consists of a 22 mm insulated down-comer copper pipe brazed at the bottom to a 28 mm riser tube, also of copper. The bottom part, where the down-comer and the riser are brazed, is shown in Figure 47(a). Figure 47(b) shows how the whole pipe was rolled out in a yard during installation of the BHE.

A fiber optic cable is attached to the outside of the riser along the depth. The cable is tightly taped every thirty centimeters. The tape pieces can be seen in Figure 47(b). The optical fiber cable bends at the borehole bottom and returns upwards freely hanging along the groundwater side of the BHE. Figure 47(c) is an illustration of how BHE12 looks like along the depth. The total measured length along the fiber optic loop is 207 m and the measurements are done in single-ended mode using 5 minutes integration time and 2 meter spatial sampling along the cable.

During installation, CO₂ was filled into the collector pipes in such a way that the liquid level when the heat pump is not operating was visible at the top of the BHE. CO₂ circulation was achieved and overcharging the system did not result to be harmful (as compared to the case of too low filling where the risk for dry out in the riser increases).

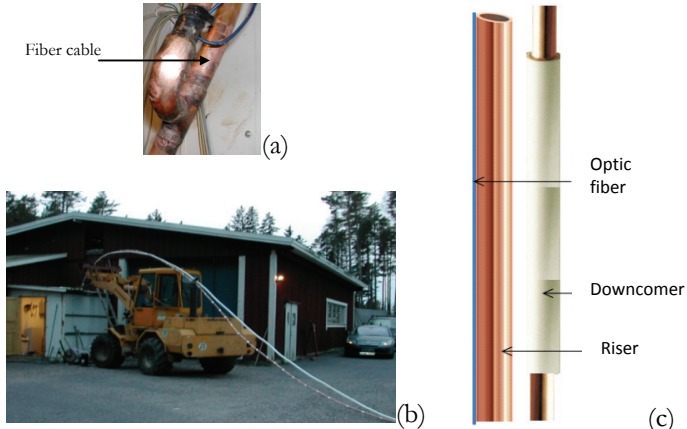


Figure 47. Installation and illustration of the U-pipe thermosyphon

4.3 Summary of paper II

The title of this paper is “Distributed temperature measurements on a U-pipe thermosyphon borehole heat exchanger with CO₂”. The paper concentrates mainly on describing the experiences with BHE12.

As implied in Figure 47, liquid CO₂ flows downwards through a 22 mm insulated copper pipe due to gravity, turns upwards in a copper 28 mm riser and starts to evaporate at some point forming a mixture of vapor and liquid. The temperatures close to the riser pipe wall while extracting heat from the ground were measured to vary within a very narrow range of less than 1 K, indicating that evaporation occurred in the riser.

Higher saturation pressure and saturation temperature at deeper locations in the BHE should be expected due to the liquid column. CO₂ working at high pressures and having somewhat lower density allows for a small change in saturation temperature with depth, compared to other refrigerants (as for example R134a) where a similar change in pressure would imply much larger differences in saturation temperature.

In this case, if the down-comer is filled with liquid, the saturation temperature at the inlet of the riser should be about 6 K higher than at the

outlet. However, this difference between top and bottom is not evident when observing the measurements in BHE12, where a slight decrease in temperature with depth is observed.

Figure 48 shows the evolution of the temperature profiles during a heat extraction period measured with the fiber sections attached to the outer riser pipe wall. The difference between the curves at 15:32 and 15:42 illustrates the rapid change that occurs after start up (which occurs at 15:40). Subsequently, the decrease in temperature levels due to heat extraction from the borehole is evident as time passes. The thermal recovery after the same heat extraction period is shown in Figure 49.

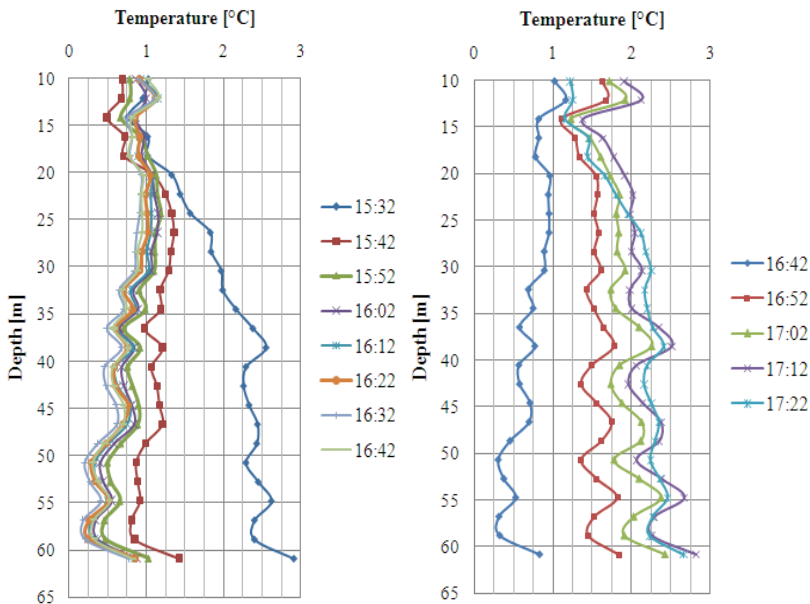


Figure 48. Temperatures along the riser during heat pump operation. The heat pump starts at 15:40 and stops at 16:45

Figure 49. Temperatures along the riser during borehole recovery

In paper II, the operation of this BHE was demonstrated and the shape of these temperature profiles resulted on the suggestion of two hypotheses about how this system operates:

1st hypothesis: Some evaporation may start to take place at the down-comer, resulting in an extra pressure drop that will be reflected in the temperature levels.

2nd hypothesis: Depending on how ideal the down-comer insulation is, the liquid may be sub-cooled at the bottom.

A discussion about which of these hypotheses is better supported by the measurements is discussed in the next section (4.4).

4.4 Operation of the U-pipe thermosyphon

The borehole was frozen about 10 days prior to the experiments (March 27th 2009) analyzed in paper II and it was therefore allowed to rest until liquid groundwater conditions around the pipes were achieved.

On April 6th, the conditions were considered proper for monitoring the system operation and the measurements presented in paper II correspond to this date. The borehole heat exchanger was inactive until early morning, when the system was put in operation. Figure 50 shows temperatures at different depths measured during this day.

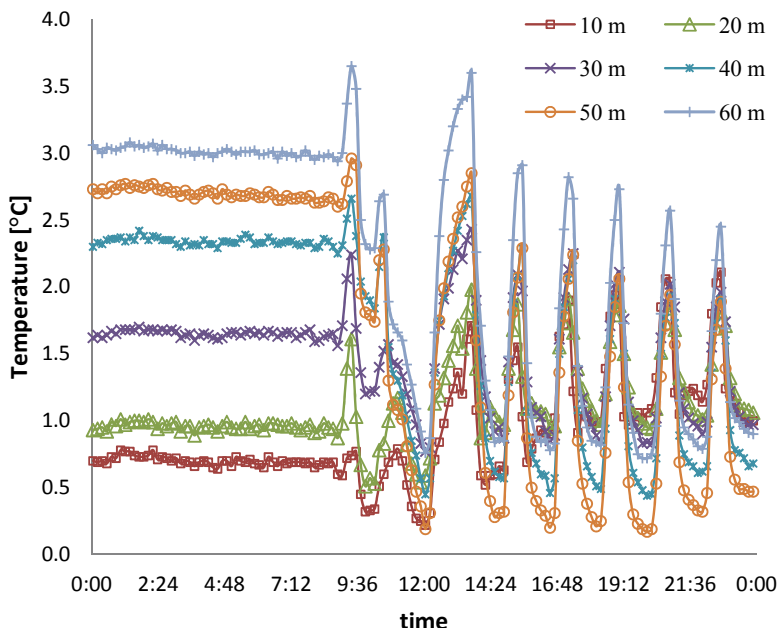


Figure 50. Temperatures of the riser outer pipe wall at different depths in BHE12 before and after start of the heat pump on April 6th

The first nine hours in Figure 50 show how the temperatures inside the borehole had stabilized before the heat pump was started. About six complete heat pump cycles are then observed during the rest of the day.

The heat pump ON period studied in particular in paper II was about 65 minutes, starting at 15:40. The temperatures along the outer pipe wall of the riser when extracting heat during the ON period were between 0.2 to 1.2 °C. An instant at 16:02 is shown in Figure 51, now together with the measured groundwater temperatures.

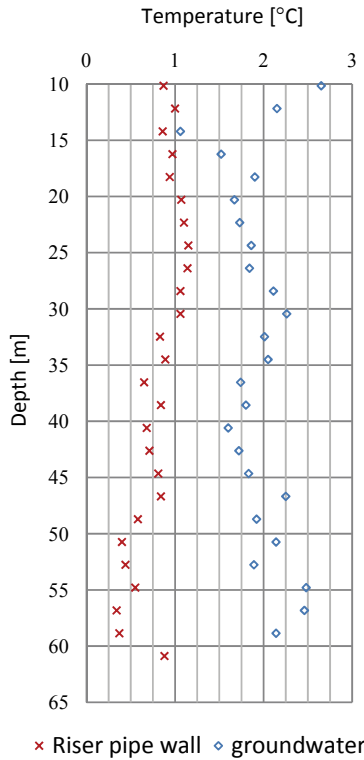


Figure 51. Riser pipe wall and groundwater temperature at 16.02

In general, the measured radial temperature difference between the riser pipe wall and the groundwater are about 1 K, except for the section between 27 and 14 m where the differences are slightly lower.

The electricity consumption and the heat flow at the heat pump condenser side were also monitored during this day and these values are shown in Figure 52 for the same operation cycle studied above. An average heating COP of 2.6 is inferred from Figure 52. The heat absorbed at the evaporator side is obtained as the difference between condenser heat and compressor power. In average, 70 W/m are extracted from BHE12.

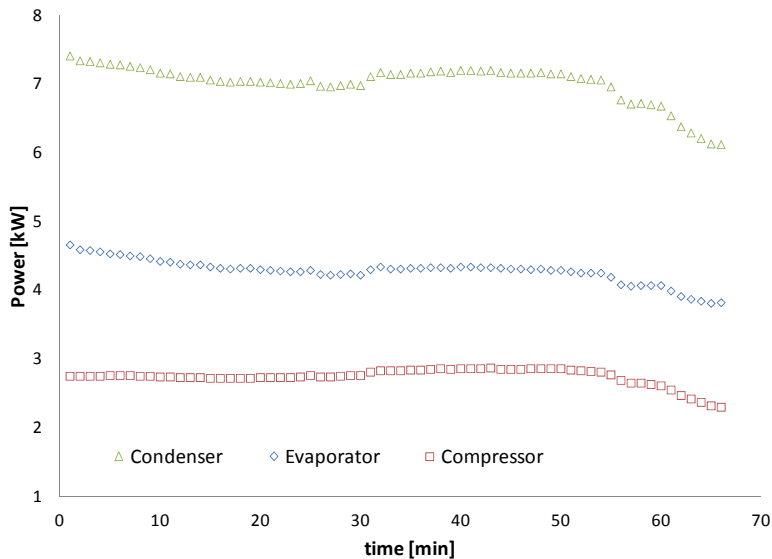


Figure 52. Energy flows at the different components of the heat pump system during the heat pump cycle between 15:40 and 16:45 on April 6th 2009

With the data shown in Figure 51, estimations of the heat transfer coefficient between the riser and the groundwater as well as of the pipe-to-groundwater thermal resistance have been done, assuming constant heat extraction along the borehole depth.

The heat transfer coefficient is found dividing the average heat extraction rate (≈ 70 W/m) with the product of the measured the pipe to groundwater temperature difference and the surface contact area.

The pipe to groundwater thermal resistance is obtained by dividing the temperature difference with the extracted heat in each two meter section.

The result is shown in Figure 53 and Figure 54. The estimated heat transfer coefficients resulted to be 827 W/m²K in average (the value at 14 m resulted to be too high due to the small temperature difference measured at this depth). The corresponding average pipe-to-groundwater thermal resistances were 0.018 Km/W in average.

The higher heat transfer coefficients (lower thermal resistances) found between 30 and 10 m depth may mean that better heat transfer conditions along the riser possibly occur in this section, perhaps due to CO₂ evaporating conditions.

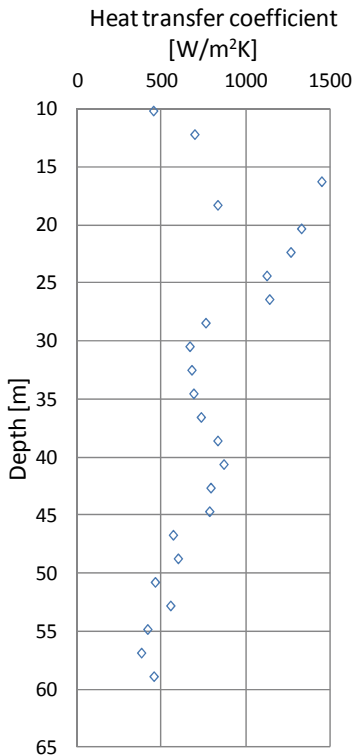


Figure 53. Heat transfer coefficient along the depth in BHE12

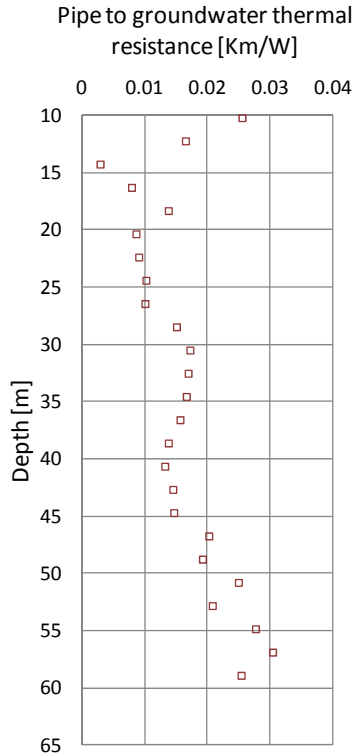


Figure 54. Pipe to groundwater thermal resistance along BHE12

This supports the 2nd hypothesis presented in section 4.3 stating that the fluid is sub-cooled at the bottom of the down-comer, bends and travels upwards in liquid phase, and starts evaporating at some point along the riser.

This hypothesis was strengthened with a thermodynamic model that accounts for the different contributions to the total pressure drop along this BHE and iterates with the mass flow rate until pressure balance is achieved, which indicated that the CO₂ is sub-cooled at the bottom of the down-comer pipe and along the lower 35 m of the riser. The simulations use the homogeneous model for calculating fluid properties and pressure drop.

The model assumes that the velocity of the gas and liquid are equal. A Pressure vs. Enthalpy (P-h) diagram is presented in Figure 55 showing the result of the iterative process and the operation of the U-pipe thermosyphon at some flow rates including the case at 0.55 kg/s where pressure balance is calculated to be achieved. The model itself is outside the

scope of this thesis but it helps understanding the measured data in a more complete way. Details are found in (Risorto, 2012).

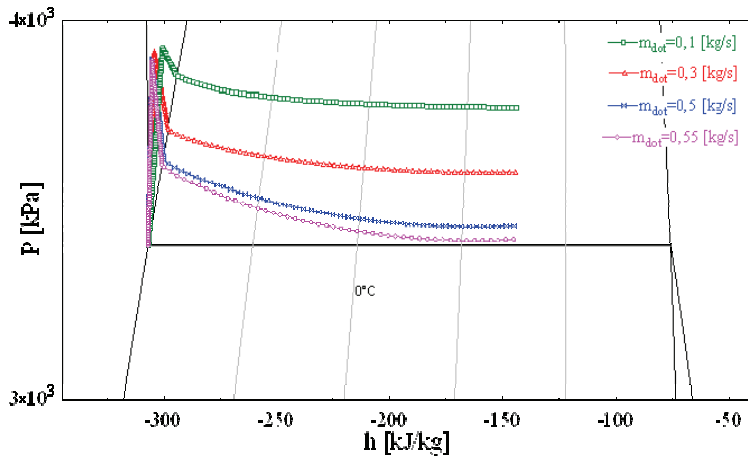


Figure 55. P-h diagram showing how the CO_2 travels in BHE12 at four simulated cases

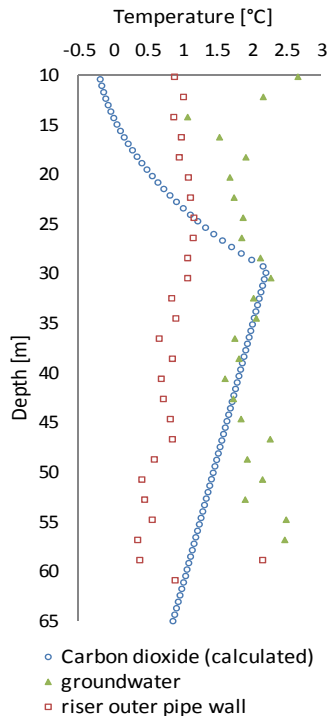


Figure 56. Comparison between calculated CO_2 temperatures along the riser and measured temperatures in BHE12

A comparison of the measured temperatures with the calculated CO₂ temperature profile in the riser is presented in Figure 56, showing an increase of the CO₂ temperature along the riser until about 30 m depth where saturation conditions are achieved. From this depth, the saturation temperature decreases as evaporation occurs at lower pressure levels.

Last, in order to corroborate the absoluteness and quality of the measured temperatures, the results from the fiber calibration (done after the installation had been running for some time) are shown in Figure 57. Control measurements were carried out for more than 24 hours, between March 27th 13:30 and March 28th 14:30, with an integration time of 5 minutes and 10 minute intervals. Before these measurements, the calibration was done such that the temperature of two reference sections of the fiber (before and after the cable enter into the borehole) indicated 0°C as they were inserted into an ice-bath. The standard deviation during the measured period is shown in the secondary vertical axis, being ±0.04 to 0.12 K depending on where along the cable the temperatures are measured. The two reference sections of the cable inside the ice-bath keep a temperature of 0.00 ± 0.04 °C during the whole control period after calibration. More scattered values are measured between 40 and 160 m (i.e. inside the borehole) due to the fact that BHE12 was operating at the same time as these measurements were taken.

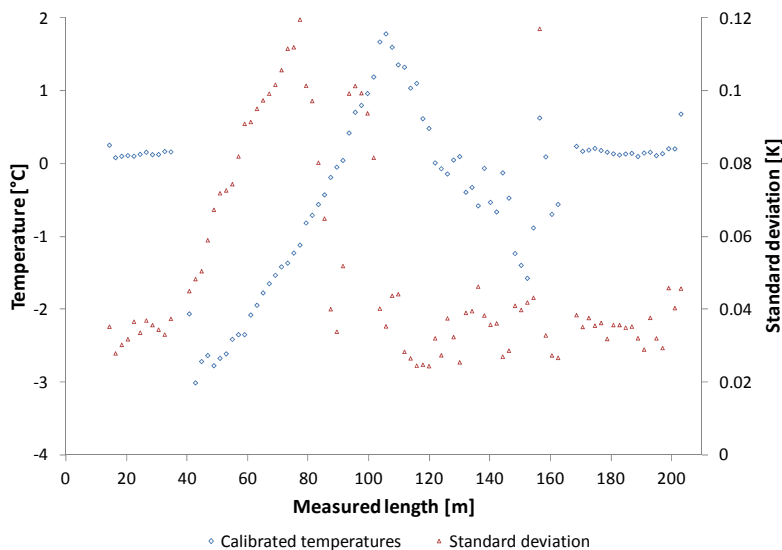


Figure 57. Average calibrated temperatures and standard deviation along the fiber cable during a 25 hours measurement period (6 measurements per hour).

4.5 Conclusions

The successful operation of a U-pipe thermosyphon BHE working with CO₂ consisting of a 22 mm insulated pipe brazed together at the bottom with a 28 mm riser pipe has been demonstrated.

Continuous temperature measurements along the outer wall of the riser indicate that phase change conditions occur inside this pipe. The fluid seems to be sub-cooled at the bottom of the down-comer pipe as a consequence of the increasing pressure and the pipe insulation. At an average heat extraction rate from the borehole of 70 W/m, lower thermal resistances are measured in the upper part of the riser, indicating that evaporating conditions are probably reached in this section. The total temperature change from bottom to top of the riser is about 0.6 °C, mainly occurring in the lower part of this pipe.

5 Measurements on Pipe-in-pipe BHEs

The general purpose of this chapter is to experimentally test two pipe-in-pipe borehole heat exchangers and to contribute to a better understanding of their function. The specific objectives are presented in section 5.1.

5.1 Specific objectives

- i. Measurement of effective and local thermal resistances inside two pipe-in-pipe BHEs having a flexible external pipe at different volumetric flow rates
- ii. Implementation of a method to measure the borehole wall temperature in BHEs
- iii. Experimental evaluation of insulating the central pipe
- iv. Assessment of the performance of a pipe-in-pipe BHE during heat pump operation

5.2 The experimental rigs

The experiments presented in this chapter were carried out in two heat exchangers denoted as BHE9 and BHE10. The former has a non-insulated central pipe while the latter uses insulation along the upper part of central pipe. Details about the heat exchanger installations are given below.

5.2.1 Pipe-in-pipe, BHE9

The groundwater level measured from the top of the casing in this borehole was 3 m. The borehole diameter is 115 mm and the total depth is 190 m. The secondary fluid is water. Figure 58 shows pictures taken during and after the installation of this heat exchanger, illustrating the position of each BHE part and the location of optical fiber cables for temperature measurements.

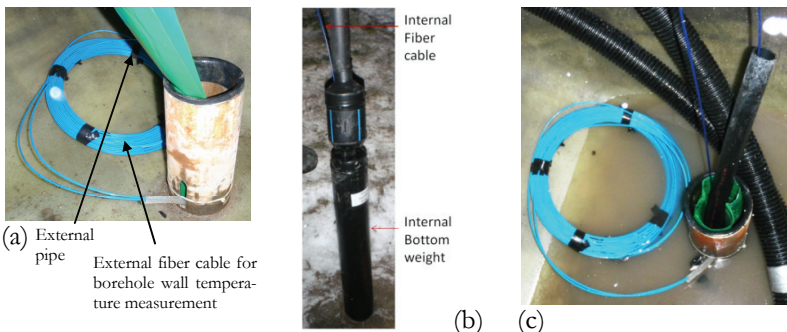


Figure 58. BHE9: Pipe-in-pipe with PE40x2.4 central pipe

A flexible external pipe consisting of a 0.4 mm thick plastic hose was sent into the borehole, Figure 58(a). It is sent down with the help of a bottom weight. The outer diameter of this pipe is 114 mm, 1 mm smaller than the borehole.

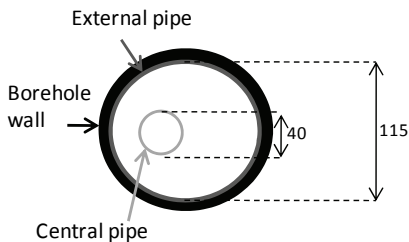


Figure 59. Cross section of BHE9

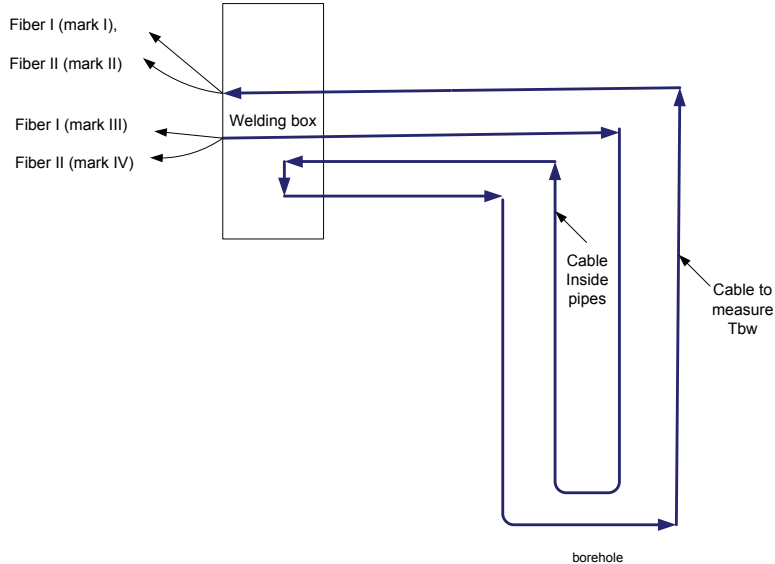


Figure 60. Sketch of the fiber optic loop in BHE9

Subsequently, the external pipe is filled with water, practically sealing the borehole from the surrounding rock and groundwater. The duration of the water filling process depends on the borehole dimensions and the flow rate.

The shape that the external pipe acquires once installed and filled with water is shown in a video available in the electronic version of Paper III. Local specific underground conditions (e.g. rock fissures or groundwater flow) require some extra considerations that may demand extra time.

The installation of the external pipe is followed by the insertion of the central pipe, also with a bottom weight, Figure 58(b). The cross section of the BHE after installation looks approximately as shown in Figure 59. The central pipe is of type PE40x2.4mm.

The optical fiber cable goes down through the inner pipe and then up through the annular channel. At the top, it is looped downwards passing down and up between the rock and the external pipe, to measure the borehole wall temperature, Figure 58(a). This fiber set up is shown in Figure 60.

Single ended measurements and offset corrections based on an ice-bath are done with two instrument channels in this heat exchanger. The measurements on the fluid and the borehole wall side are carried out with different channels with 5 minutes time delay between them. Figure 61 shows measurements with both channels at undisturbed conditions.

5.2.2 Insulated Pipe-in-pipe, BHE 10

The groundwater level from the top of the casing was 3 m before starting the installation. The borehole diameter is 115 mm, the depth is 190 m, and the secondary fluid is water. The installation procedure is the same as in BHE. The central pipe in this case is insulated down to a depth of 84 m.

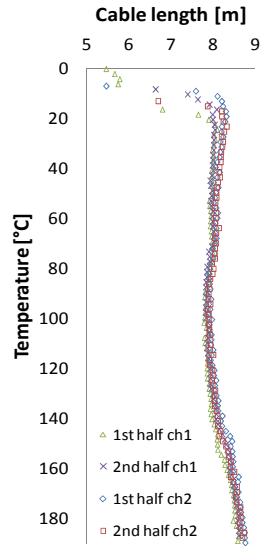


Figure 61. Undisturbed temperature measurement along all fibers in BHE9

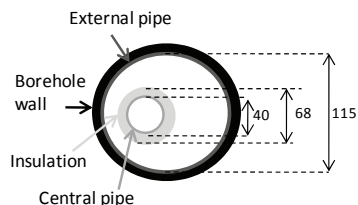


Figure 62. Cross section of BHE10

The external diameter of the insulation is 68 mm. A cross section of BHE10 is shown in Figure 62.

Figure 63 shows pictures during and after the installation of BHE10, illustrating the position of each BHE part and the location of the fiber optic cables. Figure 63(a) shows the bottom of the external pipe and the bending of the fiber optic cable that is used for measuring the borehole wall. Figure 63(b) shows the insulated central pipe as it is inserted, and Figure 63(c) shows a photo of the finished installation.

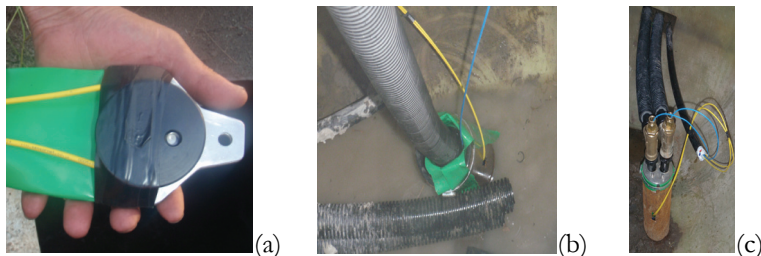


Figure 63. BHE10: Pipe-in-pipe with insulated central pipe

Measurements during heat pump operation while extracting heat from the ground with this BHE are also presented later in this thesis (section 5.5). The system and instrumentation set up between BHE10 and the heat pump is sketched in Figure 64, showing that a flow meter and temperature sensors are installed at the in- and outlet of the pipes. Although not shown here, it is important to mention that in this installation, the circulation pump actually sucks from the groundwater level, operating as a semi-open system. Also, the heat pump has variable speed control.

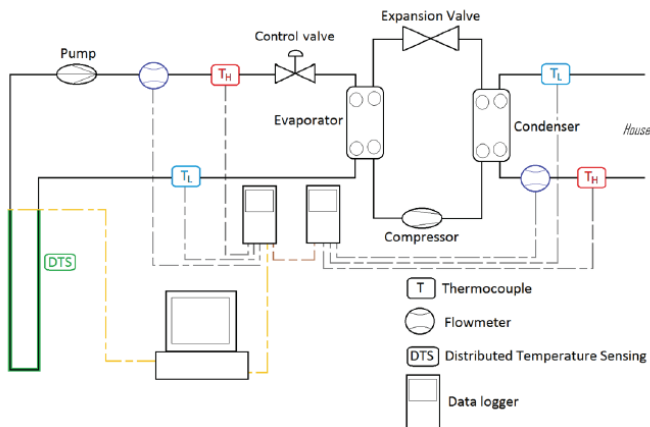


Figure 64. Sketch of the heat pump system connected to BHE10

The set up of the fiber optic cables is exactly as for BHE9 but, in this case, measurements were carried out in double-ended mode instead of single ended (the signal is sent in both directions from DTS instrument, allowing the simultaneous correction of slope and attenuations – see section 1.3).

A measurement during the equipment calibration is shown in Figure 65, including an offset correction based on the insertion of four cable sections into a common ice-bath.

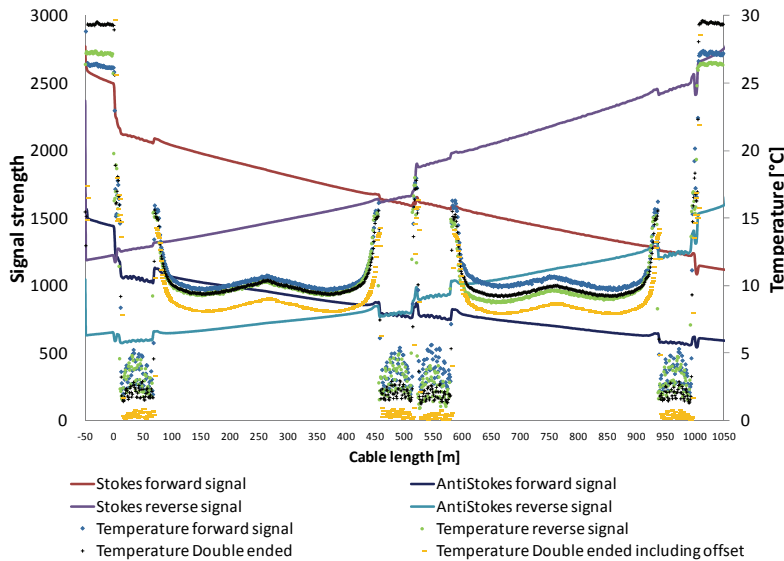


Figure 65. Double-ended fiber calibration in BHE10. Undisturbed ground conditions

The calibration measurements presented in Figure 65 were done during undisturbed ground temperature conditions. The symmetry of the measurement is due to the cable looping, i.e. the cable goes down and upwards through the different parts of the BHE in a similar manner as done in BHE9, explained in section 5.2.1.

The four cable sections inserted into the ice-bath are clearly seen, evidencing the adjustment for absolute temperature values along the whole cable length. This adjustment allowed for absolute readings with an uncertainty of about ± 0.1 K. The unknown position of the cable inside the BHEs can also contribute to the systematic error of the measurements, especially at low volumetric flow rates. In the heat injection tests on BHE9 and BHE10 presented here, it was strived to work high Reynolds numbers in order to have turbulent flow and reduce the influence of the unknown cable positions. Rather flat radial temperature profiles are ex-

pected inside the BHE at turbulent conditions. However, the conditions in the annulus are more vulnerable to this effect.

Regarding the random error, the standard deviation of all points along the borehole during undisturbed ground conditions in BHE9 and BHE10 is about ± 0.05 K.

5.3 Summary of paper III

The title of this paper is “Distributed thermal response tests on pipe-in-pipe borehole heat exchangers” and it describes the evaluation of three heat injection DTRTs carried out on two coaxial pipe-in-pipe BHEs (BHE9 and BHE10) at different flow rates.

The DTRTs were analyzed both globally and locally. For the global analysis, temperatures at 17 m depth were considered as the inlet and outlet points. This depth is chosen in order to avoid the upper segment where part of the water column inside the tube is above the groundwater level and where the BHE9 geometry is somewhat different.

For the local analyses, both BHEs have been divided in two sections: Section 1 from 17 to 77 m depth, and section 2 between 97 and 157, as illustrated in Figure 66. Both sections are 60 m long. The insulation in BHE10 reaches a depth of 84 m and the intention of this length division was to compare with the un-insulated case in BHE9.

In BHE9, two continuous heat injection DTRTs with different volumetric flow rates (DTRT1 with 0.58 l/s and DTRT2 with 0.50 l/s) were carried out. The temperature measurements were integrated during 2.5 minute periods with a repetition interval of 5 minutes and a spatial averaging along the fiber cable of 10 m. The flow rate was also logged every 5 minutes.

In BHE10, the integration time and time intervals were both 2 minutes and the integration length 1 meter. The flow rate was slightly lower than in BHE9 (0.43 l/s).

Figure 67 and Figure 68 show the fluid and borehole wall temperature evolution during the tests.

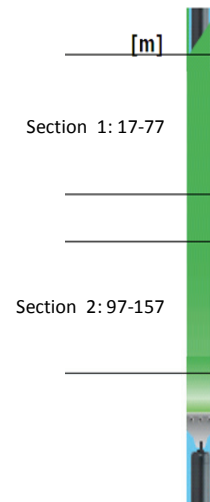


Figure 66. Section division of BHE9 and BHE10

In this BHE geometry, only the secondary fluid flowing through the annular channel has thermal contact with the borehole wall. The central pipe does not influence the total heat flux going to the ground. Also, it is considered important to distinguish between how this BHE affects the surrounding ground from how it would influence a heat pump above the ground surface. It is thus suggested in paper III that for studying the local problem (seen from the ground perspective), the borehole resistance in pipe-in-pipe BHEs should be calculated as an annulus-to-borehole wall resistance, not accounting for the fluid in the central pipe. On the other hand, for a global perspective representing what the heat pump would feel, requires the consideration of the central pipe temperature.

In order to illustrate this, the fluid temperature in Figure 67 and Figure 68 is presented using different definitions: the arithmetic mean temperature (i.e. average between in- and outlet) usually used in thermal response tests, the average of the local temperatures at along the depth (true mean), and also the average of the local temperatures in the annular channel. Figure 67 and Figure 68 also show the volumetric flow rate during both tests. The circulating fluid was water and it was fed through the central pipe, returning upwards through the annular space in both BHEs.

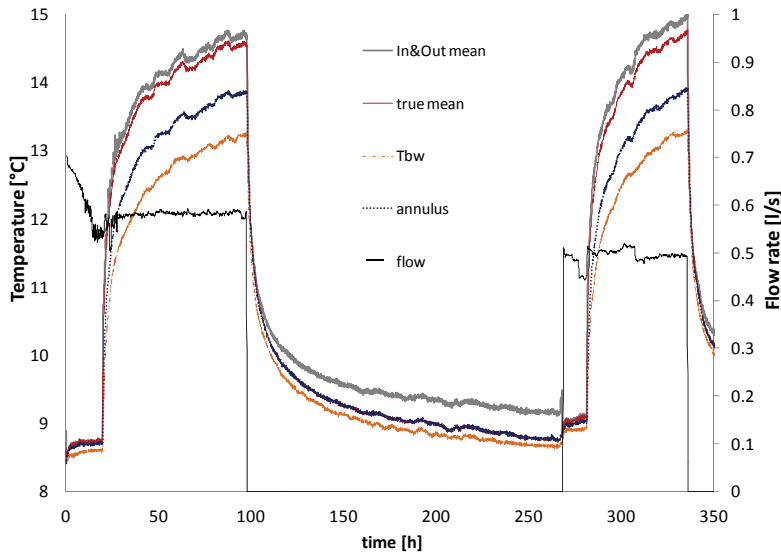


Figure 67. Evolution of temperatures during the DTRTs in BHE9

From these DTRTs, the ground thermal conductivity is first found during the thermal recovery phase between DTRT 1 and DTRT 2 in BHE9, as the value that minimizes the squared error between calculated (using the line source model) and measured fluid temperatures. The ground

thermal conductivities are then used as inputs for the determination of the borehole resistances by adjusting the resistance value during the heat injection steady flux period of each DTRT, also with the line source model.

This is done separately in section 1 and section 2, but also on a global basis such as done during a conventional thermal response tests. The undisturbed ground temperature used in the global calculation is the average of the profile shown in Figure 61, whereas average ground temperatures along section 1 and section 2 are used as input in the local calculations.

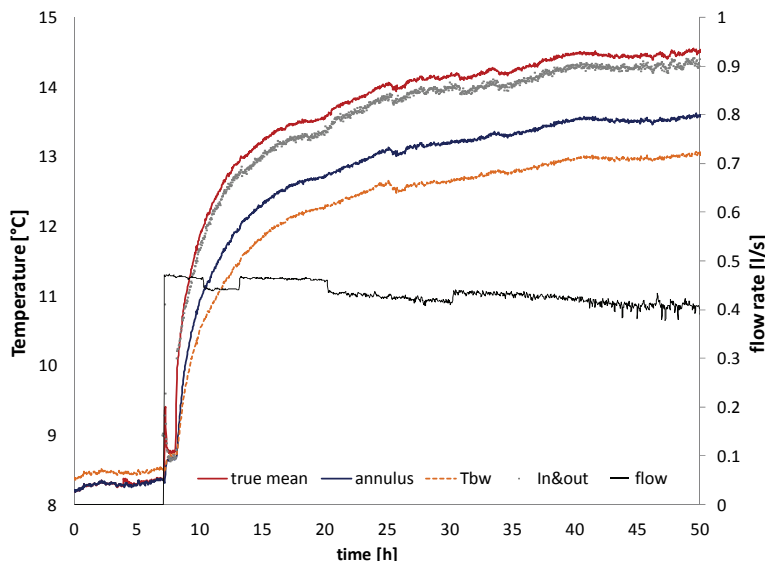


Figure 68. Evolution of temperatures during the DTRTs in BHE10

The resulting effective ground thermal conductivity from the thermal recovery phase was equal to 3.28 W/mK. The thermal conductivity of the ground can also be determined from the thermal response during the heat injection periods, but with slightly lower accuracy. The thermal conductivities obtained in this way were 3.53 W/mK and 3.21 W/mK in DTRT1 and DTRT2 (BHE9), and 3.25 W/mK in BHE10, respectively.

The effective thermal conductivity from the thermal recovery period has been used in the calculation of the following global resistances: the effective borehole resistance (R_b^*) calculated using the arithmetic mean of the inlet and outlet temperatures at 17 m depth, the effective borehole resistance calculated using the true mean fluid temperature (R_b^{**}), and effec-

tive annulus-to-borehole wall resistance calculated using the average temperature along the annulus, $R_{an\text{-}bw}$.

These are calculated during a steady flux period of each heat injection phase and the result is presented in Table 5-1.

Table 5-1. Global thermal resistance results from BHE9 and BHE10

	BHE9 DTRT1 0.58 l/s	BHE9 DTRT2 0.50 l/s	BHE10 0.43 l/s
R_b^* (arithmetic mean) [Km/W]	0.027	0.035	0.029
R_b^{*t} (true mean) [Km/W]	0.024	0.029	0.030
$R_{an\text{-}bw}$ (annulus temperature) [Km/W]	0.005	0.007	0.009

As expected, the thermal resistances in BHE9 increased with decreasing flow rate. R_b^* increases between DTRT1 to DTRT2 from 0.027 to 0.035 Km/W, R_b^{*t} from 0.024 to 0.029 Km/W, and $R_{an\text{-}bw}$ from 0.005 to 0.007 Km/W, evidencing the influence of the flow rate on the thermal performance. As seen, large improvements in performance are expected if the tested pipe-in-pipe BHEs are used instead of typical U-pipes.

The two pipe-in-pipe borehole heat exchangers show similar thermal performance, but the contrast between the arithmetic and true mean temperature definitions indicates that these BHEs operate differently, mainly due to the use of the insulation and the slightly lower flow in BHE10 which is clearly visible in Figure 69 where instantaneous profiles for all tested conditions are compared.

BHE9 shows a rather symmetric temperature distribution between down- and up-going fluid, while in BHE10 the temperature drop on the way down is about one fourth of the total temperature change. The total temperature drop downwards is similar for all cases but the derivative of the temperature curves is rather different. The lower half of the heat exchangers shows similar temperature profiles. At the upper part, the effect of the insulation in BHE10 is not clear (possibly due to deterioration by groundwater intrusion into the insulation pores), but an indication of its presence is palpable.

When the fluid in BHE10 flows through the upper half of the annular channel, it continues to exchange heat at a high rate in BHE10, while the thermal shunt becomes obvious in BHE9. The instantaneous thermal

power per meter in section 1 and section 2, shown in Figure 69, clearly show that the thermal shunt in BHE10 is significantly lower than in BHE9.

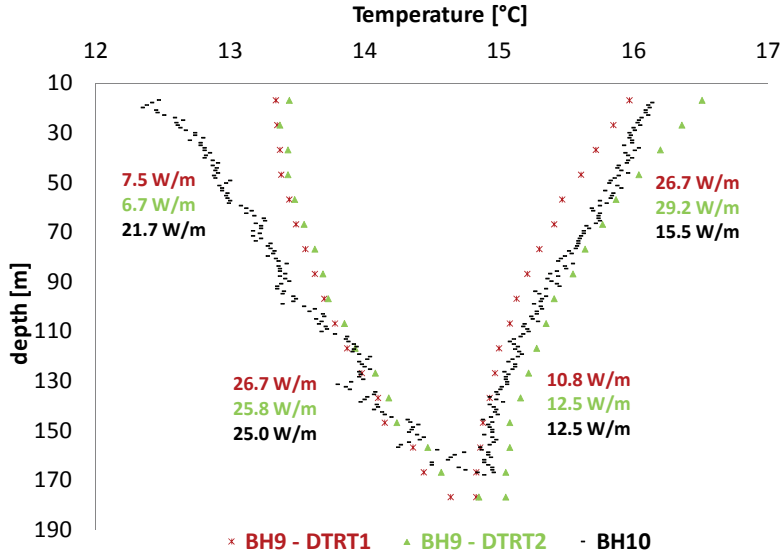


Figure 69. Comparison of fluid temperature profiles in BHE9 and BHE10

As mentioned above, the global results for the effective thermal conductivity and R_b^* are useful when understanding what the heat pump system sees. However, the observation of local temperatures as shown in Figure 69 gives a better idea of what the surrounding ground (and not the heat pump) feels during BHE operation, being dependent only on R_{an-bw} .

At the local level, the ground thermal conductivity measured during thermal recovery was 3.39 W/mK and 2.92 W/mK for section 1 and section 2, respectively. The local thermal resistances, however, are strongly dependent on the fluid temperature approach used in the calculation, and accounting for the fluid temperature in the central pipe (T_ϕ) leads to incorrect results. T_ϕ should not be considered for local borehole resistance calculation in pipe-in-pipe BHEs. T_ϕ can change, but the local heat transfer to the ground will not change if the temperature in the annulus does not change, for a given borehole wall temperature. It is therefore suggested in paper III to use R_{an-bw} for local analyses of pipe-in-pipe BHEs.

All the above mentioned results have been confirmed with direct calculations based on the measurement of the borehole wall temperature. As described in section 5.2, a fiber optic cable was pushed against the bore-

hole wall during installation, allowing for the measurement of this temperature vs. depth. The R_{an-bw} based on this temperature was about 0.015 Km/W, slightly larger than those measured with the line source model (around 0.010 Km/W).

5.4 Other aspects of BHE9 and BHE10

This section shows some more details about power distribution and flow regimes along the central and annular flow channels in BHE9 and BHE10, including a brief discussion about pressure drop and pipe dimensions in this type of heat exchanger.

Regarding the power distribution during heat injection DTRTs, paper III shows that the total heat flow injected in the tests was about 6 kW. The power distribution along the depth during each test is presented in Figure 70, Figure 71, and Figure 72. The values are calculated from the mass flow and the temperature change of the fluid as it passes each of the measurement sections, both through the central pipe and through the annulus. As summarized in Figure 69, differences are observed between BHE9 and BHE10.

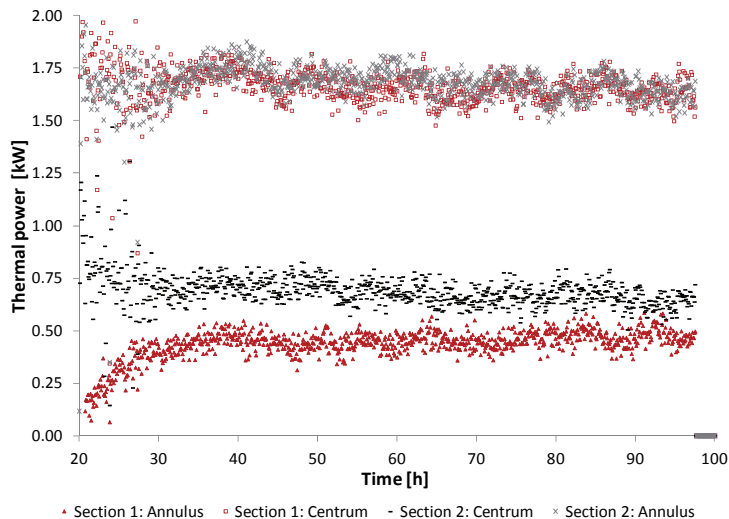


Figure 70. Thermal power distribution in BHE9 during DTRT1

The heat lost in section 1 from the central pipe in BHE10 is about 1 kW while 1.75 kW in BHE9, evidencing the influence of the insulation of the central pipe in BHE10. The heat lost from the central channel in section

2 is as high in BHE9 as in BHE10. The same applies to the annular channel in section 2 of both BHEs. This annular region is characterized by having high heat transfer rates in both BHEs (about 26 W/m). Major differences are observed in section 1 when looking at the annular channels. In BHE9, the heat transfer rate is low (around 7 W/m) while being high (about 22 W/m) in BHE10.

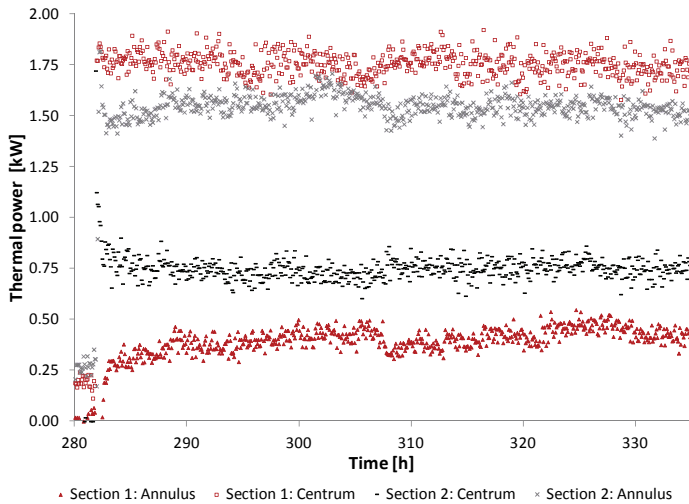


Figure 71. Thermal power distribution in BHE9 during DTRT2

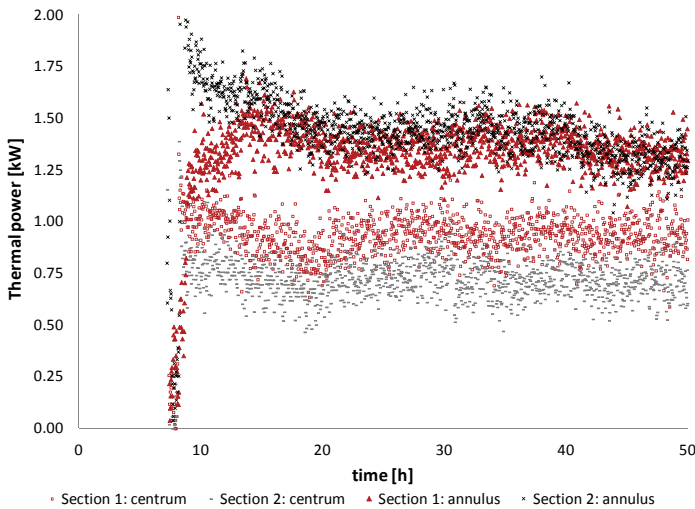


Figure 72. Thermal power distribution in BHE10

The heat transferred to the surrounding ground in section 1 and 2 was almost equal and the total power injection (sum of heat lost from the central channel plus heat lost from the annular channel) to the ground is found to be rather evenly distributed along the depth during the whole duration of the DTRTs.

Regarding the flow regimes, the effect of changing the volumetric flow rate along the depth is evaluated as the vertical profiles from the heat injection tests in BHE9 are compared, DTRT1 (at 0.58 l/s) and DTRT2 (at 0.50 l/s). The effect of the volumetric flow rate in BHE10 is evaluated during heat pump operation in section 5.5. The flows have been chosen to be the same or close to typical secondary fluid flows in heat pump systems, giving a total temperature change of about 3 K.

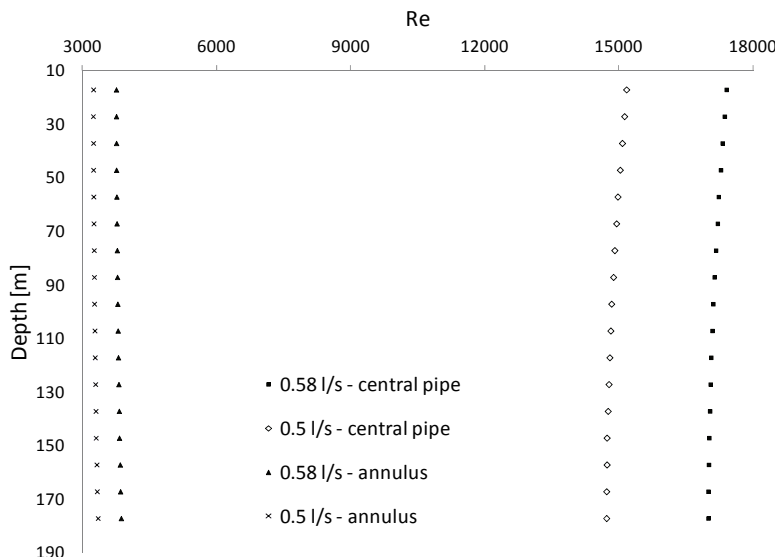


Figure 73. Reynolds number along the depth at two different flows in Pipe-in-pipe BHE

Calculated local Reynolds numbers and local heat transfer coefficients are presented in Figure 73 and Figure 74, respectively. It should be kept in mind that the magnitudes presented in these figures only apply for the heat injection case, and that the figures indicate the flow regime and the fluid to wall thermal resistances along the BHE under these conditions.

Figure 73 shows that the flow regimes are drastically different in the central and annular channel of this BHE. In the central pipe, the conditions are unarguably turbulent and, although heat transfer in this part of the heat exchanger is not desirable, convection heat transfer coefficients are

as high as in U-pipe BHEs. At the tested flow rates, the conditions in the annular pipe are close to become laminar ($Re \approx 3000$) due to the low fluid velocities. In general, the values are still turbulent thanks to the use of water having a low viscosity.

The Nusselt numbers along the annulus are about 27.5 and 32.5 for the 0.50 and 0.58 l/s case, respectively. The Dittus-Boelter and the Gnielinski correlations have been used for the calculation in the central pipe and the annulus, respectively. The resulting heat transfer coefficients are shown in Figure 74.

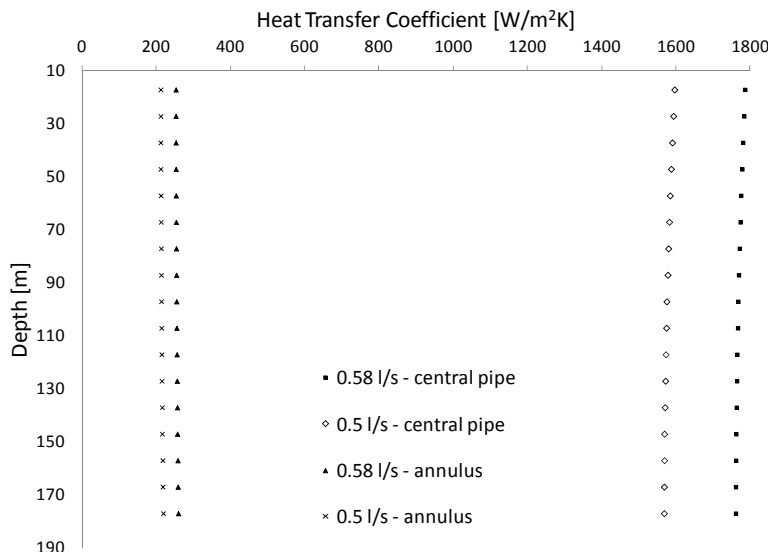


Figure 74. Convection heat transfer coefficient at two different flows in Pipe-in-pipe BHE

The heat transfer coefficients do not vary noticeably with the borehole depth. However, since the flow is near laminar conditions, the risk of falling in a regime with very low Nusselt numbers is high.

The situation will obviously change for different pipe-in-pipe dimensions. As an example, a short comparison between how different central pipe dimensions influence these pipe-in-pipe designs (having a flexible external pipe covering the whole volume of the borehole) is shown in Figure 75 in terms of the different convection and conduction thermal resistances, for a flow rate of 0.5 l/s. The pipe types chosen for this analysis are standard commercial pipes of the same pressure class PN8. Other configurations may give even better results.

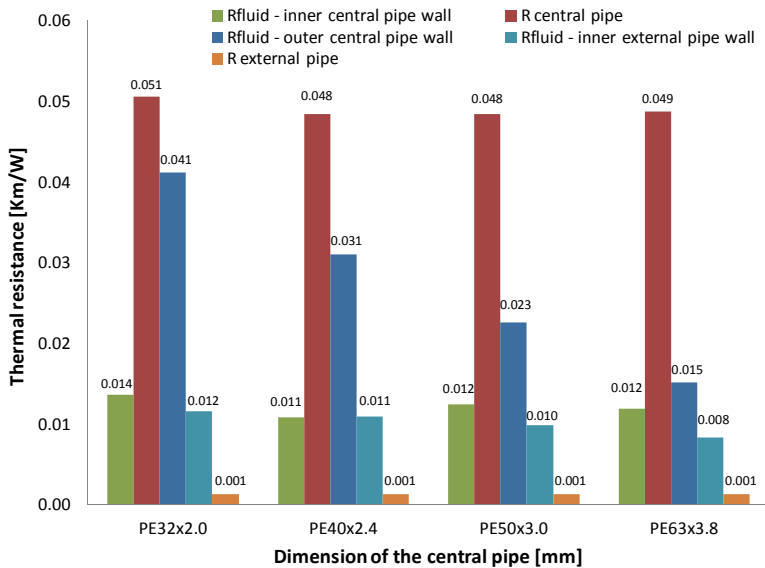


Figure 75. Thermal resistances in different central pipe polyethylene ($\lambda_{PE}=0.42$ W/mK) alternatives. Convection resistances calculated at 0.5 l/s using $v= 1.14 \times 10^{-6}$ m²/s, $\lambda=0.58$ W/mK, and $Pr=10.4$.

The resistances of the central pipe itself and the fluid-to-inner central pipe wall almost do not vary. The fluid-to-outer central pipe wall resistance decreases with increasing pipe dimensions, giving a feeling of how the insulation between the fluid in the central pipe and the annulus could be affected. The conduction thermal resistance through the external pipe is negligible.

Even more important, it is observed that the convective thermal resistance between the annulus and the inner external pipe wall can be reduced by increasing the size of the central pipe. This theoretical resistance between the fluid in the annulus and the inner wall of the external pipe is similar in magnitude to the measured R_{an-bw} in section 5.3. Higher mass flow rates will result in even lower values of the convection resistances, but also in larger pressure drops.

The pressure drop in a pipe-in-pipe BHE such as BHE10 is presented in Figure 76. The calculation is done using water properties at 5°C at typical flow rates in heat pump installations, 0.40 to 0.60 l/s, giving Reynolds numbers of about 9000 and 14000 inside the central pipe.

Along the PE40x2.4 central pipe, the result is similar to previously presented for U-pipes. When using water as secondary fluid as it is the case

in these pipe-in-pipe tests, the Reynolds number becomes significantly higher as compared to antifreeze aqueous solutions.

Along the annular channel, the flow becomes laminar at the lowest flow rate and is close $Re=2300$ at 0.50 l/s. The pressure drop per meter along the annulus is significantly lower than in U-pipe BHEs. It becomes significantly lower when using insulation and/or increasing the central pipe radius.

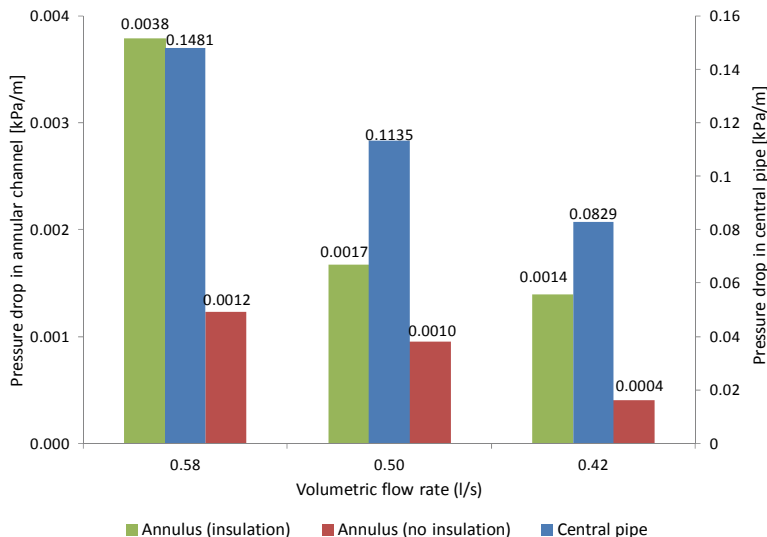


Figure 76. Pressure drop in Pipe-in-pipe BHE

Using a central pipe of type PE40x2.4mm, a closer comparison of the convection thermal resistances is done in Figure 77 for this configuration. Results at 0.30, 0.40, 0.50 and 0.60 l/s are presented. Instead of flow rate, Reynolds numbers in the annulus are shown in the horizontal axis (the conditions inside the central pipe are almost unchanged). The lowest flow gives a Reynolds number of 2177 in the annular channel at the given conditions.

All convective thermal resistances in Figure 77 are low as long as the flow regime is turbulent. The difference between the cases $Re = 2903$ and $Re=2177$ (0.40 and. 0.30 l/s, respectively) is significant. That the fluid-to-outer-central pipe wall resistance increases is actually positive, since it decreases the heat flow between the annulus and the central pipe. The eccentricity of the central pipe has not been considered here.

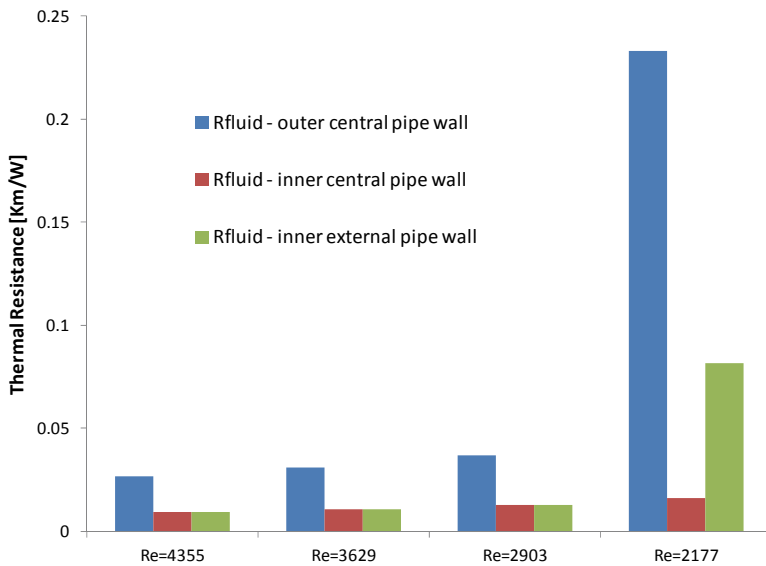


Figure 77. Comparison of convection thermal resistances in a pipe-in-pipe BHE at different Reynolds numbers in the annulus. Calculated using $\nu=1.14 \times 10^{-6} \text{ m}^2/\text{s}$, $\lambda=0.58 \text{ W/mK}$ and $\text{Pr}=10.4$. Central pipe of type PE40x2.4mm.

5.5 Heat Pump Operation

It has been demonstrated in this chapter that pipe-in-pipe borehole heat exchangers have a significantly lower borehole resistance than U-pipe BHEs, at least when using an external pipe having direct contact with the borehole wall, as is the case for BHE9 and BHE10. These heat exchangers have thus the advantage of lowering the temperature difference between the ground and the heat pump evaporator by some degrees, allowing for lower concentration of the anti-freeze additive and perhaps even the use of plain water.

Measurements during heat pump operation using BHE10 with the heat pump system presented in Figure 64 are evaluated here. Since the fluid residence time in BHE10 is relatively high when compared to the other heat exchangers studied in this thesis, Figure 78 shows how the residence time changes with the flow rate in the complete loop as well as in each BHE part. As expected, the longest fraction of the residence time occurs along the lower part of the annular channel given the space occupied by the thermal insulation in the upper part.

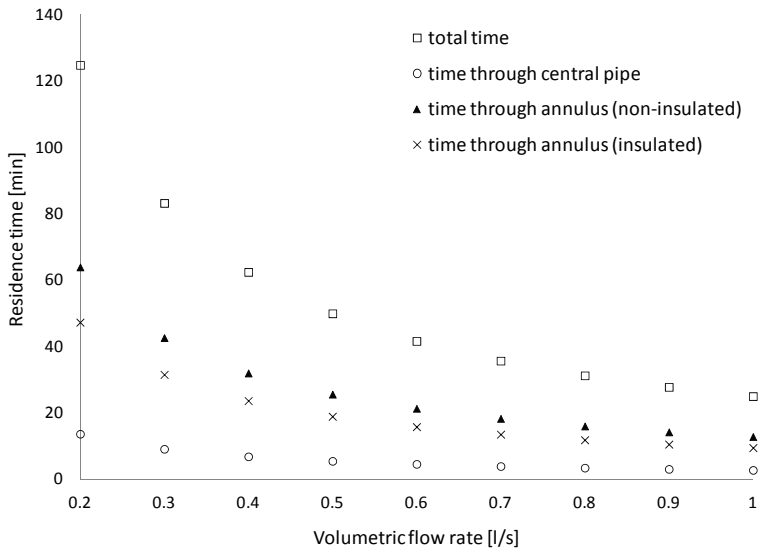


Figure 78. Residence time through BHE10 at different volumetric flow rates

Two continuous winter seasons, winter 2010-2011 and winter 2011-2012, have been followed during operation of a heat pump using water as the secondary fluid. These were the first two operation seasons of this heat pump system. During the first monitored season, the secondary fluid flow rate was intentionally set to 0.4, 0.5 and 0.6 l/s during several days in order to visualize and quantify the power distribution along this BHE, as described in section 5.5.1. During the second monitoring season, winter 2011-2012, a constant flow rate of 0.6 l/s was used, and monitoring was only intended to follow up the fluid temperatures relative to the freezing point of water.

5.5.1 First heating season, 2010-2011

The winter 2010-2011 was the first operating season of this BHE system. The vertical temperature profiles were measured as the heat pump was operating in heat extraction mode. The duration of the heat pump ON periods varied from a few minutes to a few hours depending on the heating demand.

Considering the residence time in Figure 78, the heat pump ON periods were many times not long enough to allow a proper visualization and comparison between flow rates. Luckily, some cycles were sufficiently long. Figure 79 shows, as an example, the monitoring period at 0.6 l/s, and presents the inlet, outlet, and average measured borehole wall temperature ($T_{bw\ mean}$). Figure 80 shows the development of the temperature

profile as the heat pump operates. As described for the U-pipe in Figure 40, a dynamic re-distribution of the heat extraction vs. depth takes place.

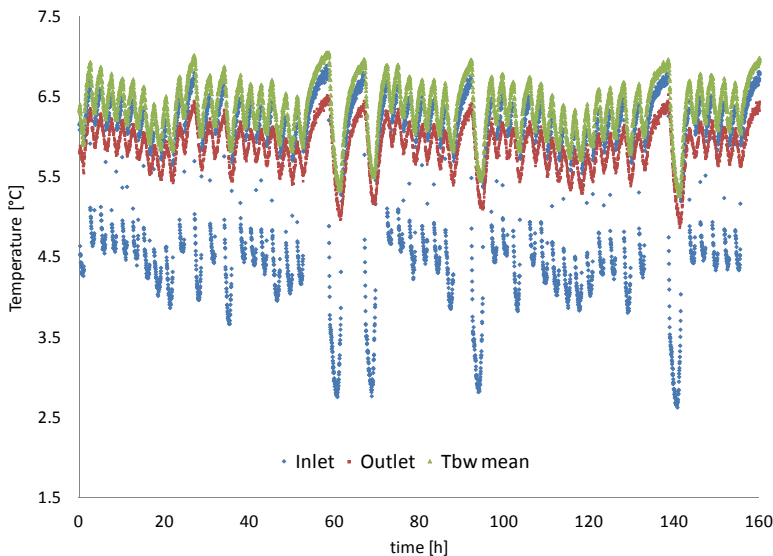


Figure 79. Inlet, outlet, and average borehole wall temperatures at 0.6 l/s

The borehole wall temperature was measured with the external fiber optic cable at the same time as the local fluid temperatures. The distributed measurements were taken with 2 minutes integration and repetition time, and with 4 meter integration length.

In order to compare what happens at different flow rates, Figure 81 shows instantaneous temperature profiles selected from the three monitoring periods with 0.40, 0.50, and 0.60 l/s, after the residence time had elapsed. The power absorbed in the heat pump evaporator was similar for all cases and thus, as expected, the inlet to outlet temperature difference is decreased as the volumetric flow rate is increased.

As seen in Figure 81, the outlet temperatures were always almost the same, about 6.1 °C, being a few tenths of a degree lower than the average borehole wall temperature, regardless of the flow rate, demonstrating the low borehole resistance of this BHE.

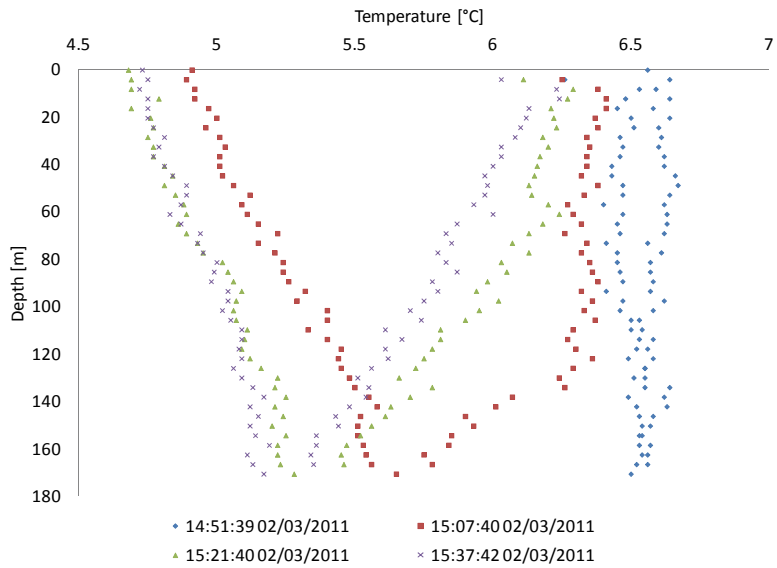


Figure 80. Development of the fluid profile in BHE10 at 0.6 l/s

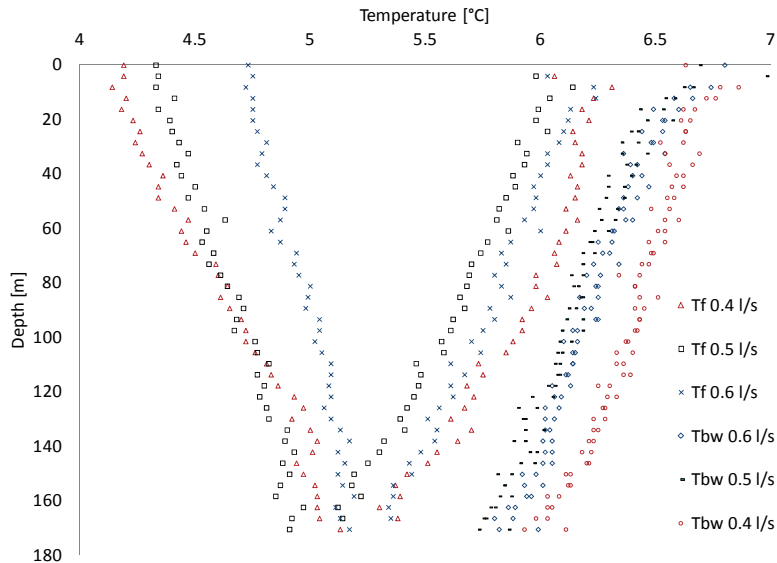


Figure 81. Instantaneous fluid and borehole wall temperature profiles during heat pump operation at different volumetric flow rates in BHE10

Instantaneous local annulus-to-borehole wall thermal resistances have been calculated for these three cases as presented in Figure 82, and found to be in average about 0.025 Km/W. The values are almost the same independently of the flow rate (slightly lower at 0.60 l/s). They are about twice as high as those found during heat injection, which were calculated during steady flux conditions. In addition, the water temperatures are in this case significantly lower than during the heat injection tests.

As the flow rate was decreased from 0.60 to 0.40 l/s and the inlet to outlet temperature difference changed, the inlet temperature became about 0.5°C lower, which is estimated to decrease the heat pump COP by about 1.5%.

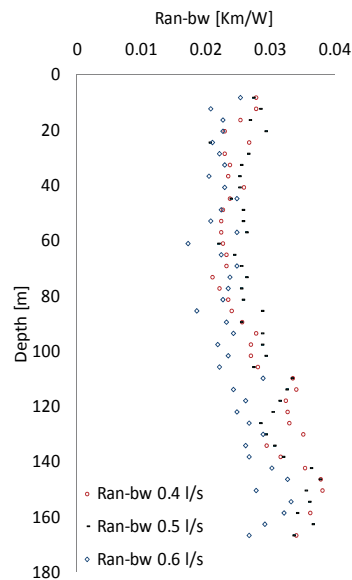


Figure 82. Annulus to borehole wall thermal resistance during heat pump operation at three flow rates

5.5.2 Second heating season, 2011-2012

Between November 2011 and March 2012, the inlet and outlet temperature levels in BHE10 were monitored and logged as well as the ambient temperature.

This is the second heating season with this BHE in operation. A measurement campaign of 120 days was carried out starting on November 4th 2011 (day “0”) and ending on March 6th 2012 (day “120”). The following graphs (Figure 83 through Figure 86) show a selected number of heat pump operation periods having different ambient temperatures and covering the whole winter duration. The idea with this monitoring is to evaluate the risk of the secondary fluid temperatures (water) to reach freezing conditions.

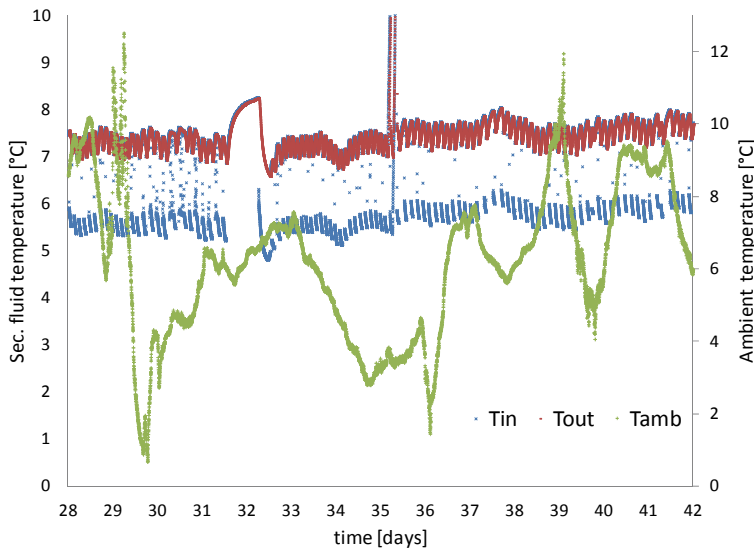


Figure 83. Inlet and outlet temperatures during days with ambient temperatures between 0 and 12 $^{\circ}\text{C}$ (December 2011)

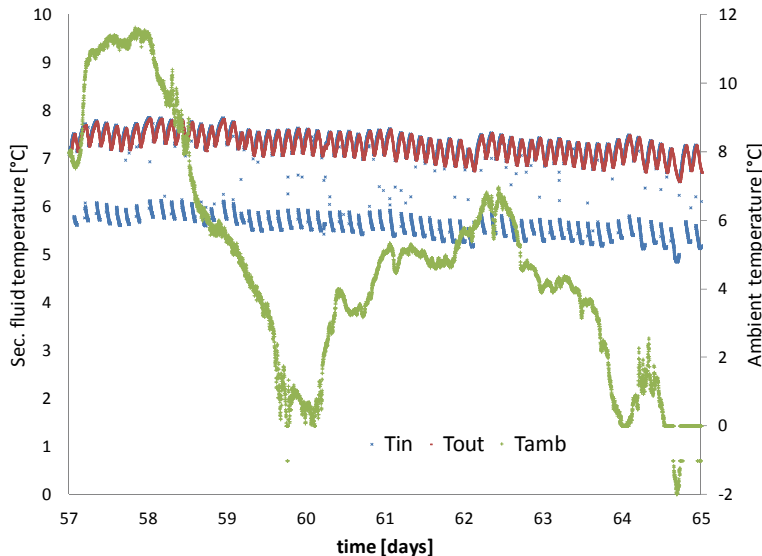


Figure 84. Inlet and outlet temperatures during days with ambient temperatures between -2 and 12°C (January 2012)

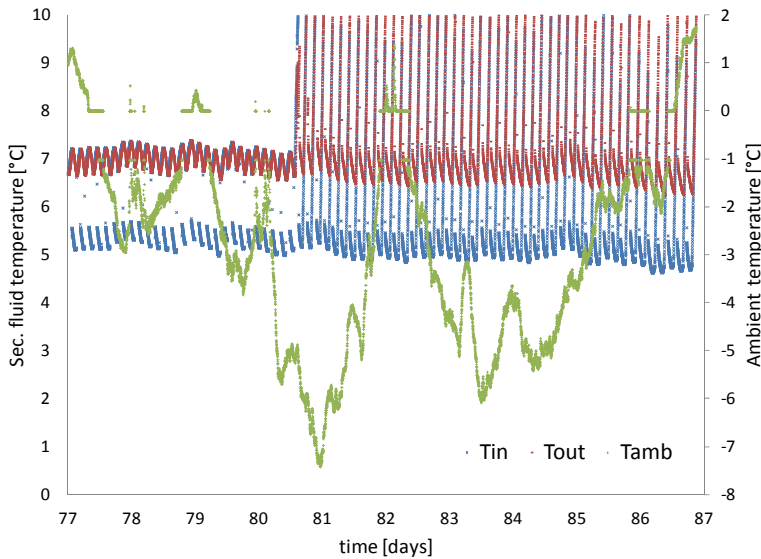


Figure 85. Inlet and outlet temperatures during days with ambient temperatures between -8 and 2°C (January 2012)

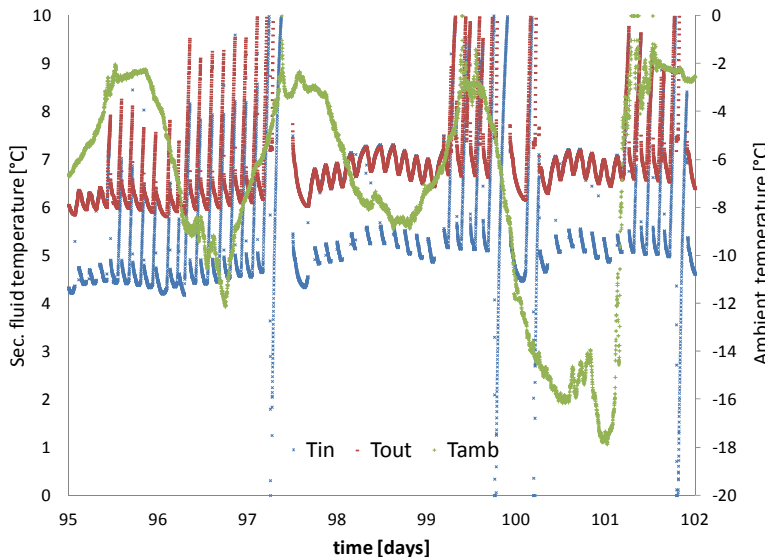


Figure 86. Inlet and outlet temperatures during days with ambient temperatures between -18 and 0°C (February 2012)

It is observed in Figure 83 to Figure 86 that the secondary fluid temperatures range between 4 and 8°C, independent of the ambient tempera-

tures, ranging from -18°C to +12°C. The absolute fluid temperatures decreased about 1°C from the beginning to the end of the winter season.

The cyclic fluctuations in inlet and outlet temperature in Figure 83 to Figure 86 indicate the ON/OFF periods of the heat pump. The heat pump ON and OFF periods were about 2 and 1.5 hours long, respectively.

During some periods, the circulation pump is left ON even when the heat pump is not operating. Such periods can be easily identified in the figures by observing the temperatures during thermal recovery after each heat pump cycle.

5.6 Conclusions

- i. Two pipe-in-pipe borehole heat exchangers of a new design having a flexible external pipe attached to the borehole wall have been tested. The effective borehole thermal resistance was measured to vary between 0.027 and 0.035 Km/W depending on the volumetric flow rate.

The thermal resistance between the annulus and the borehole wall has been suggested to be used when referring to local borehole resistance in pipe-in-pipe BHEs, since the fluid in the annular channel is the only part of the BHE being in direct thermal contact with the borehole wall. This local resistance was found to be between 0.005 and 0.025 depending on the temperature levels and the measurement method.

- ii. Installing an optical fiber cable between the flexible external pipe has been demonstrated as a method for measuring the borehole wall temperature in borehole heat exchangers.
- iii. The central pipe does not influence the total heat flux going to the ground in pipe-in-pipe BHEs. An insulation of the central pipe induces a change of the shape of the temperature profiles vs. depth. The axial temperature gradient in the annulus becomes larger than in the case with non-insulated central pipe, as more heat is exchanged between the fluid in the annulus and the surrounding ground. The heat loss from the central to the annular pipe in the upper section of the tested BHEs was about 16 W/m and 29 W/m with and without insulation, respectively.

When the secondary fluid circulated upwards through the annular channel, the power was found to be evenly distributed along

the depth at typical volumetric flow rates giving a total average temperature difference of about 3 K (and with a difference between borehole wall temperature and out-coming water often being less than 1 K). Reynolds numbers range from about 18000 in the central pipe to 3000 in the annular channel.

- iv. A pipe-in-pipe BHE having a low borehole resistance (effective and local resistance of about 0.030 and 0.015 Km/W, respectively) and using water as secondary fluid has been studied at different volumetric flow rates during two continuous Swedish winter seasons. No freezing problems were encountered thanks to a sufficiently long borehole and the use of a pipe-in-pipe BHE with a low borehole resistance.

6 Measurements on a Multi-chamber BHE

6.1 Specific objectives

- i. Measure the thermal performance of a multi-chamber BHE during thermal response tests with opposite secondary fluid flow directions
- ii. Suggestion of improvements to the tested multi-chamber design

6.2 The experimental rig, BHE3

The experiments presented in this chapter were carried out in BHE3, a Multi-chamber borehole heat exchanger made of Polyethylene installed in a groundwater-filled borehole and having the cross section shown in Figure 1c. The borehole diameter is 140 mm and the depth is 250 m. The groundwater level before the installation was 13 m, measured from the top of the steel casing. The secondary fluid is an aqueous solution of 16% ethanol by weight.

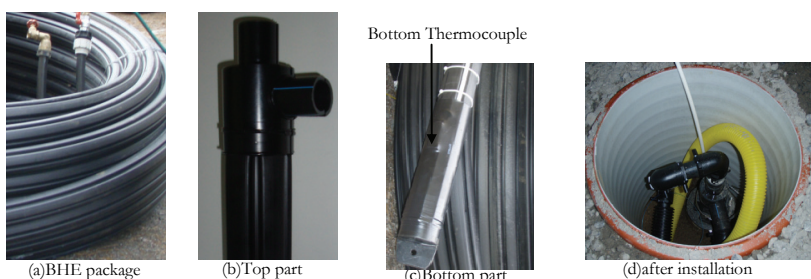


Figure 87. BHE3: Installation of the Multi-chamber BHE installation

Figure 87 shows some photos during the installation of BHE3: (a) the pipe package as it was delivered, (b) the top part of the heat exchanger, (c) the bottom part, and (d) BHE3 after the installation is finished. The installation of this heat exchanger is time consuming in groundwater-filled boreholes given the large buoyancy force caused by the large volume occupied by the collector, in spite of filling it with water before installation.

BHE3 is instrumented with an inductive flow meter of the type Brunata HGS9-R6, two Pt500 temperature sensors as well as two thermocouples for measurement of the inlet and outlet fluid temperatures into the bore-hole, a STA-D flow regulation valve, and an extra thermocouple at the borehole bottom. The thermocouples are T type stainless steel sheathed.

The inlet and outlet points can be observed in Figure 87(b) and (d). The pipe pointing upwards is connected to the central pipe while the pipe pointing to the side collects the fluid from five external chambers, as illustrated in Figure 1(c). The external diameter is 82 mm and the inner pipe internal diameter is 39 mm. The external chambers are connected in parallel and then in series with the central channel.

The bottom measurement point is located in one of the outer channels. The stainless steel sheathed thermocouple was heated above the melting point of plastic and inserted through the pipe wall, later protected with a shrinking hose (as pointed in Figure 87(c)). The thermocouples are connected through a temperature reference box (which contains the reference junction in a constant temperature block and a Pt100 sensor) to an Agilent data acquisition unit.

6.3 Summary of paper IV

The title of this paper is “Evaluation of a Coaxial Borehole Heat Exchanger Prototype”. The paper presents a first study of a multi-chamber borehole heat exchanger (BHE3) consisting of one central pipe and five external chambers.

The performance of the particular geometry of the heat exchanger is tested through two thermal response tests, denoted TRT1 and TRT2. The distinction between these tests is that the fluid is circulated in opposite flow directions, i.e. flowing downwards through the central pipe and upwards through the outer channels during TRT1, and vice versa during TRT2.

The operation of BHE3 was closed one week before TRT1 was started. The borehole had not fully recovered and the slope of the temperature baseline was accounted for in TRT1. TRT2 started 17 days after TRT1 was finished and the borehole was not in operation during this interim period. The analysis of TRT2 accounts for the influence of the activities during TRT1.

The flow rate was continuously measured in order to ensure that it was the same during both tests. The supplied power was $10.00 \pm 0.15\text{ kW}$ and the volumetric flow rate about 0.70 l/s . The latter was measured with

two different flow meters, one located in the BHE3 loop and the other in the thermal response test equipment. The standard deviation of all measurements was ± 0.006 l/s. All measurements are shown in Figure 88.

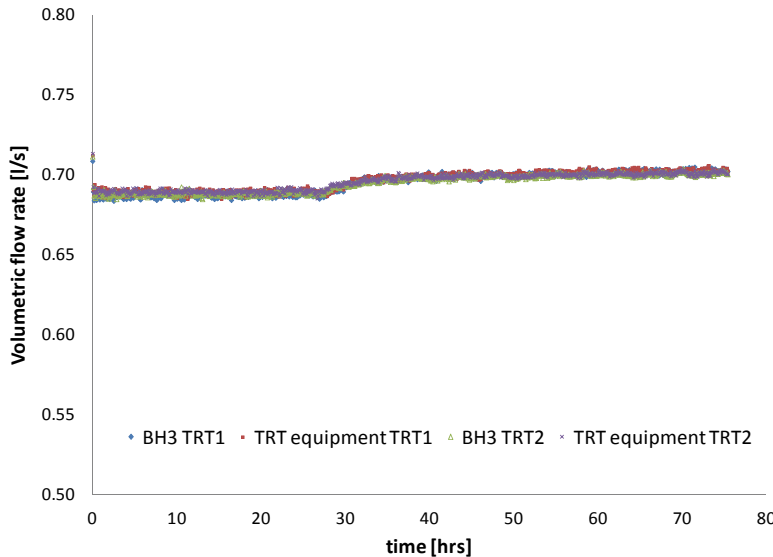


Figure 88. Measured volumetric flow rate with two different meters during TRT1 and TRT2 in BHE3

The fluid temperature has been measured at the inlet, bottom and outlet of the BHE. The temperature at all three measurement points are presented in Figure 89 and Figure 90 for TRT1 and TRT2, respectively.

During approximately the first 24 hours of each test, the fluid was circulated without heat injection, giving a measure of the actual ground temperature surrounding the borehole. This temperature was 8.40°C for TRT1 and 8.79°C for TRT2. There exists a small heat recovery effect behind these measurements (including the effect of TRT1 over TRT2) that influences the TRT analysis. This is taken into consideration by adding a temperature slope term to the undisturbed temperature measurements along the whole duration of both tests.

Figure 89 and Figure 90 show that the inlet and outlet temperatures are nearly the same during both TRTs. The total temperature change in the BHE ($T_{in} - T_{out}$) is about 3.5°C. For a given power supply and volumetric flow rate, it is logical that the total temperature change is independent of the flow direction. However, the bottom temperature reveals that the heat distribution along the downward and upward flow channels changes significantly with the flow direction. During TRT1, with the fluid going

down through the central pipe, $T_{in} > T_{bottom} > T_{out}$, whereas in TRT2, in which the fluid came up through the central pipe, $T_{in} > T_{out} > T_{bottom}$.

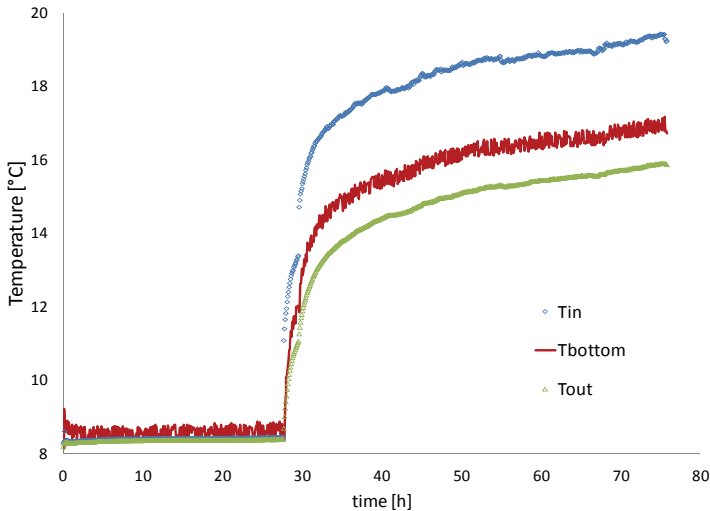


Figure 89. Temperatures during TRT1 in BHE3 (secondary fluid going down through the central pipe)

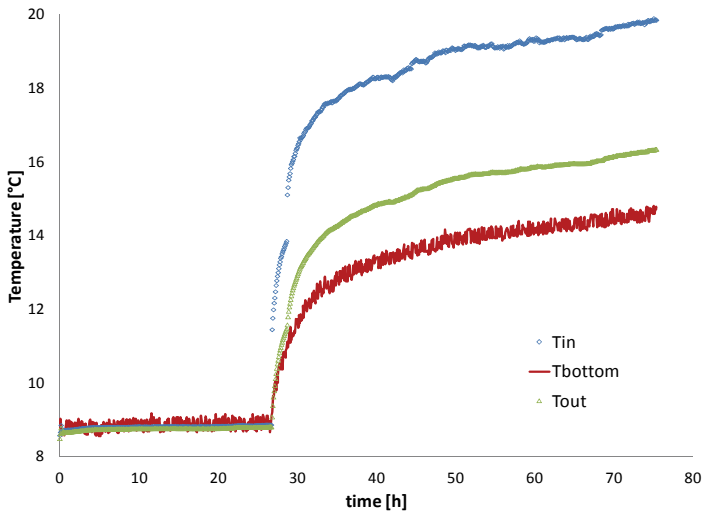


Figure 90. Temperatures during TRT2 in BHE3 (secondary fluid coming up through the central pipe)

This situation is, of course, dependent of the volumetric flow rate. A larger flow rate would have reduced the thermal shunt flow between the channels due to the lower temperature difference between the up- and

downward flows in the BHE. However, 0.7 l/s is already a slightly high secondary fluid flow.

The arithmetic mean temperature difference between the inlet and outlet during TRT1 and TRT2 is used for determining the effective borehole resistance. This is done by minimizing the error between the measured and calculated mean fluid temperature between hour 40 and 70 of the heat injection phase of both tests. The result is shown in Table 6-1.

Table 6-1. Effective ground and borehole resistance during TRT1 and TRT2

Test	TRT1	TRT2
Ground thermal conductivity [W/mK]	3.30	3.24
Effective borehole resistance [Km/W]	0.096	0.094

As expected, the effective borehole thermal resistance and the rock's thermal conductivity were almost the same for both tests. An effective thermal resistance of 0.095 Km/W indicates that the performance of this multi-chamber BHE is similar, or slightly lower, than a U-pipe in a groundwater filled borehole.

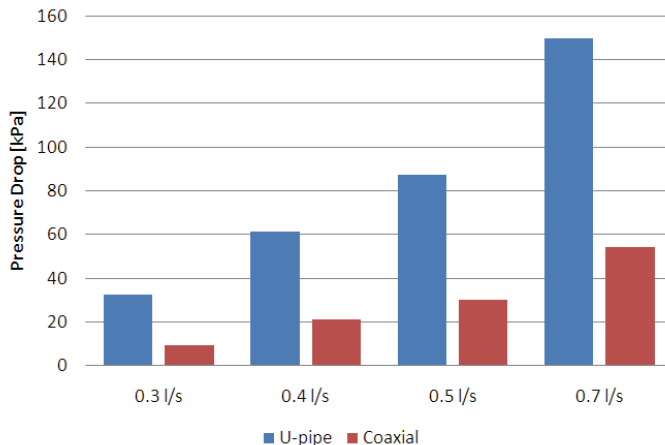


Figure 91. Comparison of pressure drop in U-pipe and Multi-chamber BHE

This performance is attributed to the fact that the pressure drop in this heat exchanger is lower than for a standard U-pipe. For this reason, the optimum flow rate for BHE3 is higher than used in the test. Figure 91 shows an experimental comparison between BHE3 and a U-pipe (BHE4) regarding the pressure drop at four different volumetric flow rates. At all four flow rates, the pressure drop in this coaxial BHE is significantly lower than in the U-pipe (about 60% difference), representing an advantage due to the fact that the necessary pumping power may not

be as high for the coaxial BHE design. The pumping power is however approximately proportional to the cube of the flow rate, which for this design and this borehole depth must be, as mentioned above, higher. If the flow rate had been increased, the borehole thermal resistance would have been reduced, perhaps to a lower value than for a U-pipe BHE.

The measured temperatures and their standard deviations during the pre-circulation phase of the tests are presented in Table 6-2. The thermocouples and Pt500 sensors were previously calibrated in an ice-bath. Unfortunately, the thermocouple connected at the bottom presented some disturbances during the measurements, causing a deviation of ± 0.145 .

Table 6-2. Standard deviation of temperature measurements during TRTs in BHE3

	TRT1	TRT2
T_{in} [°C]	8.426 \pm 0.029	8.819 \pm 0.036
T_{bottom} [°C]	8.587 \pm 0.145	8.852 \pm 0.143
T_{out} [°C]	8.374 \pm 0.028	8.766 \pm 0.038

2-dimensional heat conduction simulations using a finite element method software showed similar results than the thermal response tests. The simulations indicated that a relatively small heat flow through the lateral walls of the external channels took place, and that the thermal contact between the central and the outer channels was high. It was suggested to the manufacturer to increase of the wall thickness of the central pipe and to narrow the contact area between the peripheral and the central channels, in order to decrease the thermal shunt flow between the channels.

6.4 Thermal power distribution

As shown in section 6.2, the temperature distribution along the depth is different when changing the flow direction in this BHE. Thermal power levels have been calculated for the central and external chambers taking advantage of the temperature measurement point at the bottom of the borehole. Figure 92 and Figure 93 show the result of this calculation at each instant during TRT1 and TRT2, respectively.

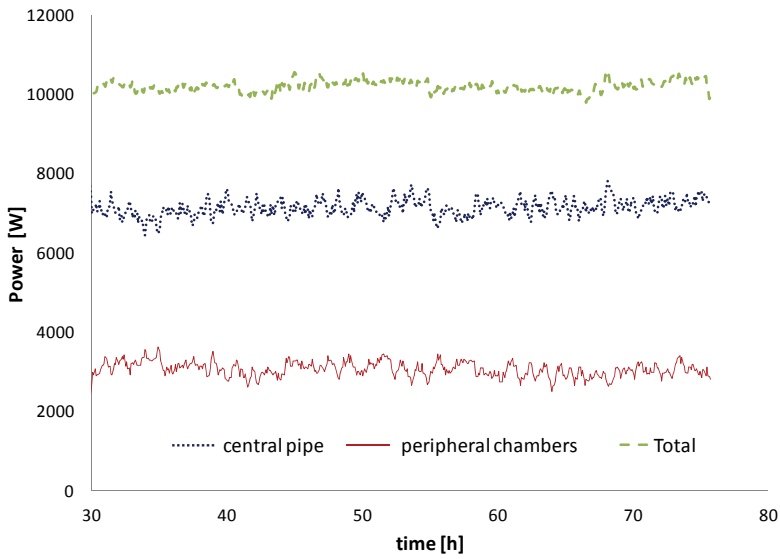


Figure 92. Net thermal power distribution in Multi-chamber BHE (BHE3) during TRT1

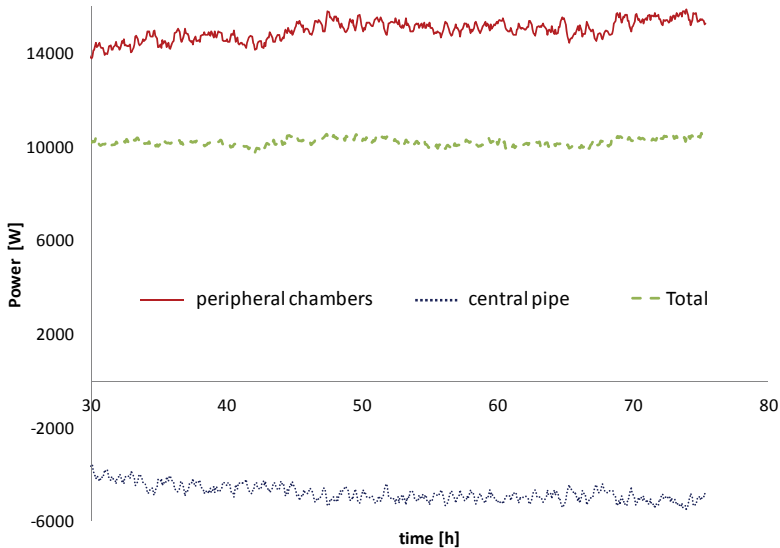


Figure 93. Net thermal power distribution in Multi-chamber BHE (BHE3) during TRT2

It is found that, when the fluid travels downwards through the central pipe as it does during TRT1, the fluid in the central pipe drops in temperature corresponding to 70% of the total heat flow from the BHE, while remaining 30% is released the peripheral multi-chamber arrangement on the way up, as shown in Figure 92. If the flow rate would have

been higher, a more symmetric power distribution between down- and upward flows would have been achieved.

On the other hand, when the fluid travels downwards through the peripheral chambers, Figure 93 shows how the chambers are capable of transferring all heat as the fluid travels downward through them. However, due to the low flow rate and the low thermal resistance between the channels, the heat transfer contribution of the peripheral chambers is decreased by a large thermal shunt flow to the central pipe. A higher mass flow rate would have allowed the total temperature change (i.e. all injected power) to occur along the peripheral chambers.

In chapters 3 and 5 as well as in several publications presented in the background of this thesis (section 2.3), special attention has been given to the use of different fluid temperature approaches that influence the estimation of local borehole resistances.

Using the temperature measurement at the bottom of BHE3, an alternative mean fluid temperature can be calculated accounting for the temperature measurements at the bottom of the BHE, as for example an arithmetic mean of the in-, outlet, and bottom temperatures. Figure 94 and Figure 95 show a comparison of the fluid mean temperature calculated with this definition during TRT1 and TRT2, respectively, compared to the in- and outlet mean used in conventional thermal response tests.

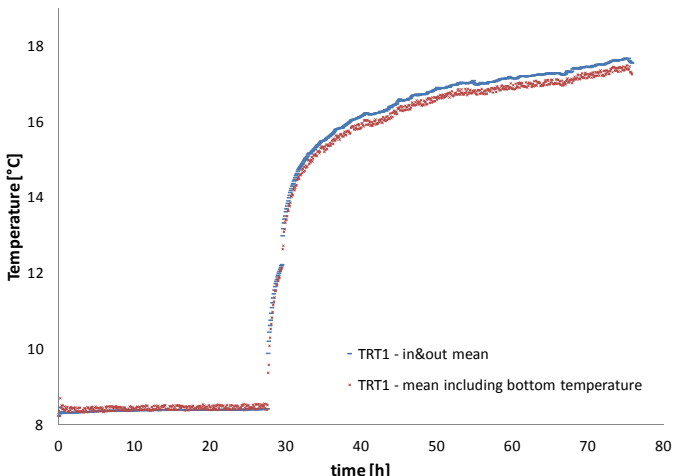


Figure 94. Comparison of two fluid mean temperature approaches during TRT1 in BHE3

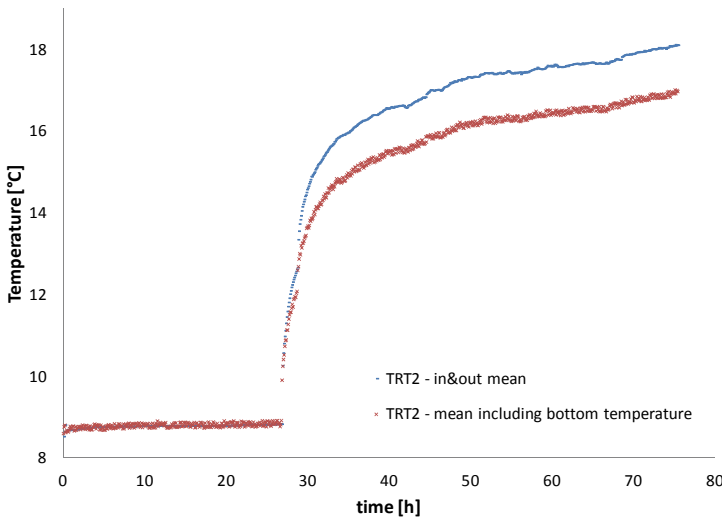


Figure 95. Comparison of two fluid mean temperature approaches during TRT2 in BHE3

The thermal resistance when accounting for the bottom temperature becomes 0.084 and 0.064 Km/W during TRT1 and TRT2, respectively. The ground thermal conductivity remains unchanged. The large difference between the results in TRT2 is due to the temperature gradient created along the depth at this volumetric flow rate. The difference between the mean temperature definitions should decrease with increasing volumetric flow rate.

6.5 Heat Pump operation

During the winter 2008-2009, measurements on BHE3 during heat extraction from the ground were carried out at different flow rates. As for the cases of U-pipe and pipe-in-pipe presented in sections 3.6 and 5.5 respectively, the question about whether the fluid residence time is enough to allow the borehole heat exchanger to operate properly becomes significant due to the short duration of typical heat pump cycles.

In spite of these limitations, indications about how this multi-chamber BHE operates when connected to a heat pump for heat extraction form the ground have been obtained through temperature and flow measurements during heat pump ON periods. Both flow directions have been measured at different volumetric flow rates. Selected parts of heat pump cycles at 0.80 l/s, the highest measured flow rate, are presented and discussed here in order to illustrate what happens along the borehole depth when changing the flow direction.

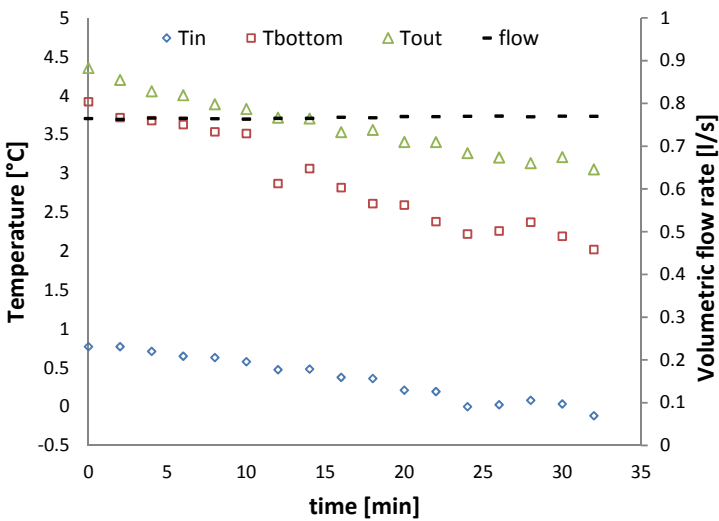


Figure 96. Measurements in BHE3 at 0.80 l/s during heat pump operation. Downward flow in central pipe.

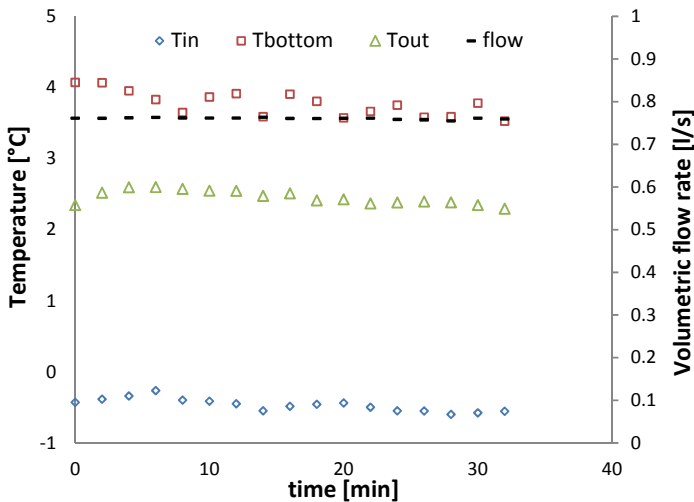


Figure 97. Measurements in BHE3 at 0.80 l/s during heat pump operation. Upward flow in central pipe.

Figure 98 and Figure 99 compare the power distribution as the fluid travels downwards and upwards, respectively. When referring to mode 1-5 it means that the flow travels downwards through the central pipe and upwards through the five external chambers. Mode 5-1 means the opposite direction.

The conclusion regarding the power distribution are the same as those presented for the heat injection cases but now with different heat flow direction, i.e. a temperature increase downwards and upwards occurs when the fluid travels downwards through the central pipe. Both the down-coming and up-going parts of the BHE contribute in the same direction with the heat exchange process. On the other hand, when the fluid travels downwards through the peripheral chambers, these are capable of transferring all heat as the fluid travels downward through them and, due to the low flow rate and the low thermal resistance between the channels, the heat transfer contribution of the peripheral chambers is decreased by a large thermal shunt flow to the central pipe. Again, a higher mass flow rate would have allowed the total temperature change to occur along the peripheral chambers.

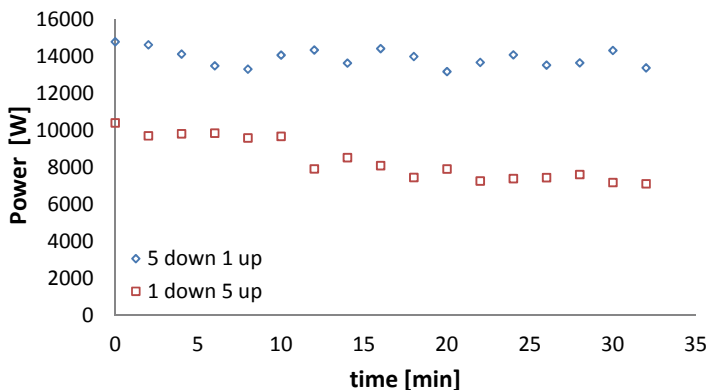


Figure 98. Comparison of the net thermal power absorbed as the fluid travels downwards in two different flow directions at a rate of 0.80 l/s

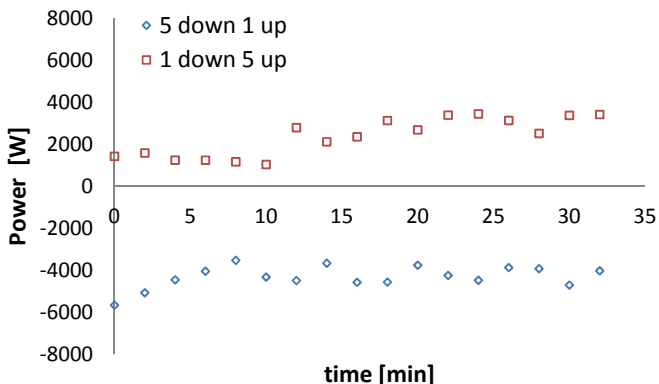


Figure 99. Comparison of the net power absorbed as the fluid travels upwards in two different flow directions at a rate of 0.80 l/s

6.6 Conclusions

- i. The effective borehole thermal resistance of a multi-chamber borehole heat exchanger has been measured to be 0.095 Km/W independently of the secondary fluid flow direction during heat injection tests at 0.70 l/s. The global performance of this BHE is thus similar, or slightly worse, than U-pipe heat exchangers in groundwater filled boreholes.

At the tested conditions, if a thermal resistance during the response test evaluation is calculated including the fluid temperature at the bottom in the arithmetic mean, the result depends on the flow direction and varies between 0.084 Km/W and 0.064. The difference is due to the large temperature gradient created along the depth when the fluid travels downwards through the peripheral chambers, giving a sense of what the surrounding ground sees when changing the flow direction.

When the secondary fluid travels downwards through the central pipe, the down-going fluid is capable of positively contributing to the total temperature change. However, when the fluid travels downwards through the peripheral chambers, all heat is transferred as the fluid travels through them and the heat transfer contribution of the peripheral chambers is decreased by a large thermal shunt flow with the central pipe on the way up.

- ii. Relatively small heat flow through the radial walls of the external channels was identified with 2D finite element simulations of the tested multi-chamber BHE. The thermal contact between the central and the outer channels was high. An increase of wall thickness of the central pipe as well as narrowing the contact area between the peripheral and the central channels has been recommended as an improvement. Moreover, a higher mass flow rate should be used in order to have a more even distribution of the heat along this heat exchanger. The optimum flow rate for this BHE is higher than used in the tests due to its low pressure drop, measured to be about 60% lower than in U-pipes.

7 Measurements on a Multi-pipe BHE

The general purpose of this chapter is to experimentally test a multi-pipe borehole heat exchanger and to contribute to a better understanding of its function and local thermal performance. The specific objectives are presented in section 7.1.

7.1 Specific objectives

- i. Evaluation of the thermal performance of a novel type of multi-pipe BHE including the local thermal conductivity of the surrounding ground
- ii. Assessment of the effect of insulating the central pipe in a multi-pipe BHE and quantification of the thermal power distribution vs. depth
- iii. Measurement of local thermal resistances at different volumetric flow rates

7.2 The experimental rig, BHE11

The experimental work studied in this chapter was carried out in a multi-pipe BHE consisting of an insulated central pipe and 12 peripheral small channels (external pipes), denoted as BHE11 in this thesis. The secondary fluid is an aqueous solution of 13% ethanol by weight.

The cross section of this heat exchanger is illustrated in Figure 100 including the pipe and borehole dimensions (external pipes of type PE16x2mm.). An optical fiber cable for secondary fluid temperature measurements was installed inside the central and one of the external pipes.

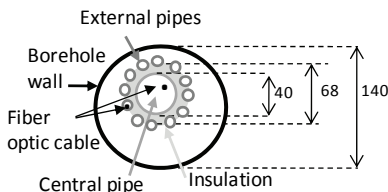


Figure 100. Cross section of BHE11

Due to installation difficulties, the dimension of the peripheral pipe containing the optical fiber was changed to PE20x2mm down to a depth of 66 m. The remaining 11 peripheral pipes are of type PE16x2mm.

The groundwater level measured before installation was 4 m from the top of the casing. The total depth is 105 m. The heat exchanger is 100 m long and the bottom weights are about 5 m long.

Figure 101 shows a picture of this type of Multi-pipe heat exchanger including the bottom and top parts, connecting pipes, as well as the central and peripheral pipes. Figure 102 shows photos from the installation: Figure 102(a) shows the inner part of the BHE bottom where a fiber cable on the secondary fluid side bends between the central and the external pipes. Figure 102(b) shows a photo taken while inserting the heat exchanger into the borehole. Figure 102(c) and Figure 102(d) show the top part of BHE11 after the installation was almost finished.



Figure 101. Photo of BHE11

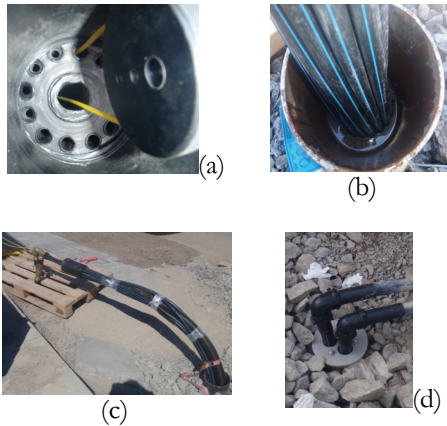


Figure 102. Installation of BHE11

BHE11 was connected to a TRT equipment and later to a heat pump placed indoors.

The fiber cable was pulled through the fluid path into this room through T-junctions seen in Figure 102(c), which were moved to the inlet and outlet connecting lines as shown in Figure 103.

Although not shown here, an inductive flow meter of the type Brunata HGS9-R6, two Pt500 sensors for measurement of the inlet and outlet fluid temperatures, and a STA-D flow regulation valve were also installed.

The measured undisturbed temperature in BHE11 before starting the experiments was almost constant and about 6.85°C between 20 and 50 m depth, with a successively increasing gradient between 50 and 100 m.

The wide larger range of measured temperatures along the first 20 m was partially attributed to the periodic ambient conditions and thermal processes in this region. The undisturbed temperature profile is shown in Figure 104.

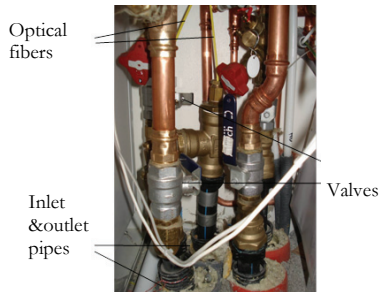


Figure 103. Connection points to BHE11

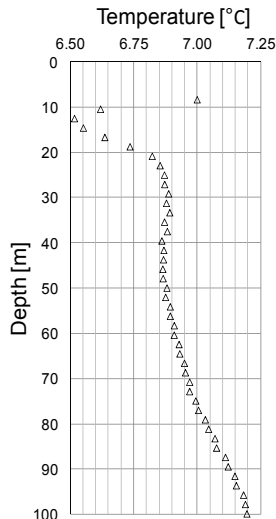


Figure 104. Undisturbed temperature profile in BHE11

7.3 Summary of paper V

The title of this paper is “Distributed thermal response tests on a multi-pipe coaxial borehole heat exchanger”. The paper presents six distributed thermal response tests carried out on BHE11.

Six continuous DTRTs, chronologically named DTRT1 to DTRT6, were carried out and evaluated along four borehole sections. The different borehole sections are illustrated in Figure 105. During DTRT1, the fluid enters the heat exchanger through the central pipe, while for DTRT2 to DTRT6 it enters through the peripheral pipes, i.e. the flow direction in

DTRT2 to DTRT6 is reversed as compared to DTRT1. The injected power and the secondary fluid flow rate were intentionally varied between DTRT2 and DTRT6. The total duration of the experiment was 375 hours and the different test phases are chronologically presented in Table 7-1.

Table 7-1. Chronology of the different parts of the heat injection test in BHE11

Test phase	Time interval [h]
Undisturbed	0-41
DTRT1	47-89
Thermal recovery	89-160
DTRT2	161-208
DTRT3	209-235
DTRT4	235-256
DTRT5	256-333
DTRT6	333-375

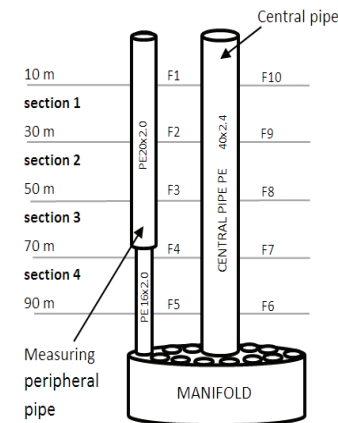


Figure 105. Section division of BHE11 during DTRT analysis

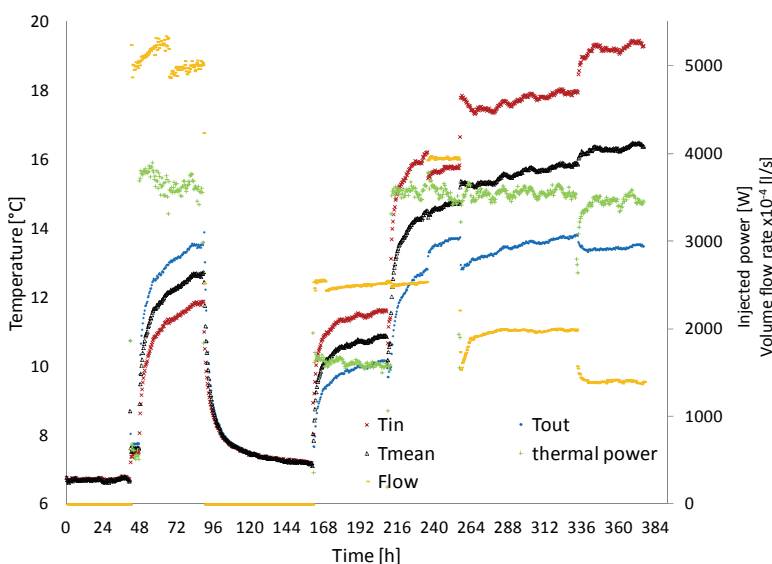


Figure 106. Temperature and thermal power evolution during all DTRTs in BHE11

Figure 106 presents the inlet (T_{in}) and outlet (T_{out}) temperatures as well as their mean value (T_{mean}) during the whole test period. The opposite flow direction used during DTRT1 is intentionally illustrated by keeping the same symbol and colors of the temperature curves. The injected power and the volumetric flow rate are also plotted referred to the secondary vertical axis.

As mentioned above, the BHE was divided in four 20 m sections for the local analyses. The heat flow distribution confirmed that almost no thermal shunt flow occurs regardless of the flow rate and that the distribution of the power is uneven along this BHE at almost all tested conditions, being highest in the upper part of the boreholes.

The resulting uneven power distribution is exemplified as a contrast between section 1 and section 4 in Figure 107 and Figure 108, respectively (where q_{1-12} , q_0 , and q_{total} stand for the heat lost from the peripheral pipes, central pipe, and their sum, respectively).

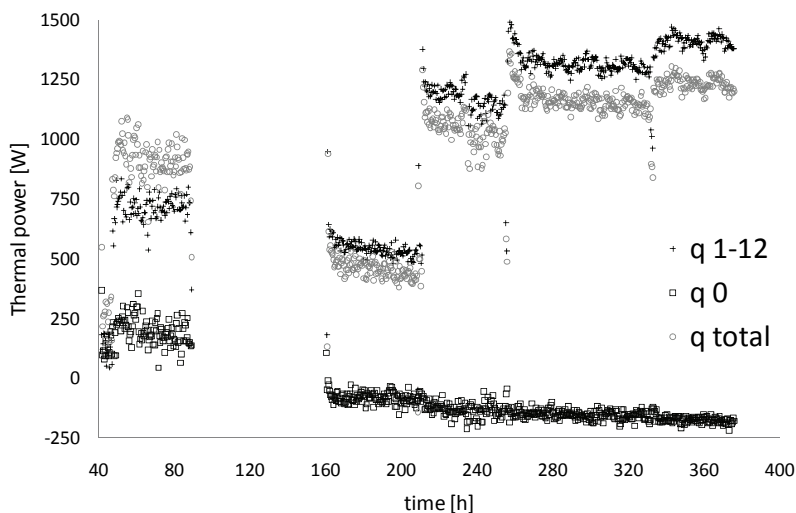


Figure 107. Heat flow from section 1

As the fluid enters the BHE through the peripheral pipes during heat injection, the heat flow is highest at the top of the borehole and decreases with depth. Even when the flow entered the central pipe, the heat flow is slightly higher at the top of the borehole, having a modest contribution from the central pipe in spite of the insulation.

Depending on the undisturbed ground temperature levels and the local thermal conductivities, this uneven heat flow distribution found during

relatively short time periods can, in the long term, cause a redistribution of the temperature levels in the surrounding ground and thereby a different power distribution than found here.

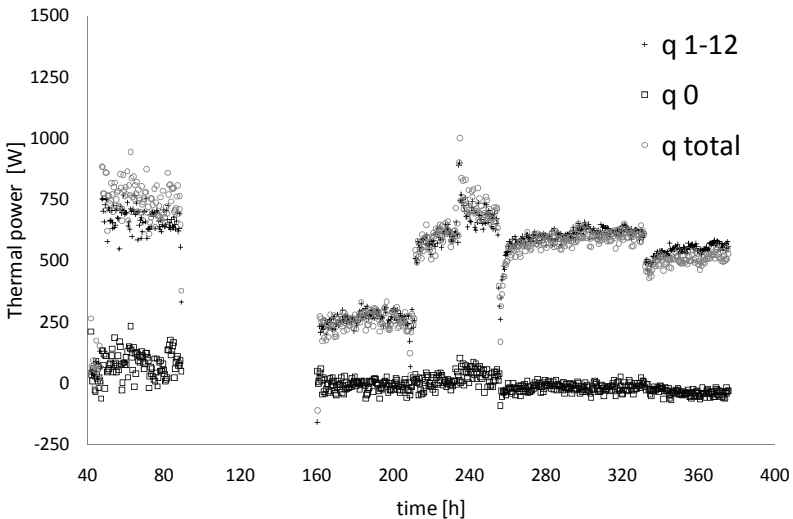


Figure 108. Heat flow from section 4

Thanks to the thermal insulation of the central pipe the thermal shunt flow was relatively low also at low volumetric flow rates. This is illustrated with the temperature profiles during steady flux conditions at a low and high volumetric flow rate in Figure 109.

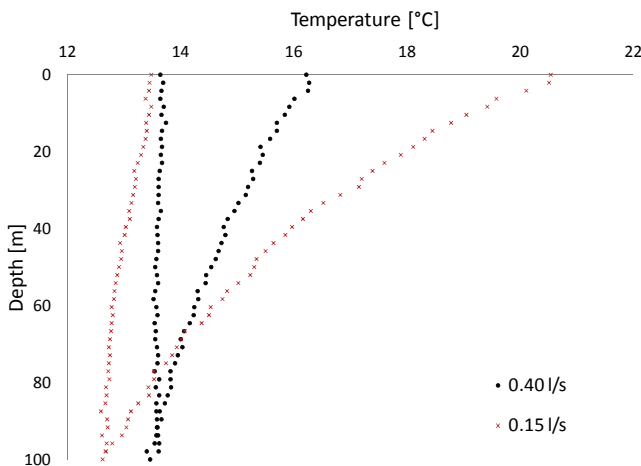


Figure 109. Fluid temperature profiles at two different volumetric flow rates. Secondary fluid travels downwards through the external pipes

As presented in Table 7-1, there was a thermal recovery period of 71 hours without any heating or fluid circulation between DTTRT1 and DTTRT2. The measured temperatures from this period were used to calculate local ground thermal conductivities by using the line source model. The result showed a large difference between the upper part and the rest of the borehole, being highest at the top of the borehole.

The result for sections 1 to was 4.09, 3.29, 2.98, and 2.80 W/mK, respectively. The calculated error margins for these values increased with increasing depth, ranging from 10 to 13%.

These local thermal conductivities were used as an input for determining local variations of the borehole thermal resistance. The resulting local borehole resistances are presented in Figure 110 (a) to (f) for DTTRT1 through DTTRT6.

The flow regime in the peripheral pipes is laminar during all DTTRTs and average borehole thermal resistances remain around 0.04 Km/W almost independently of the volumetric flow rate.

Constant Nusselt numbers and almost constant heat transfer coefficients make the average borehole thermal resistance of the multi-pipe design vary very little with the flow rate.

The borehole section between 50 and 70 m depth presents the lowest thermal resistance, possibly indicating that the peripheral pipes are arranged closer to the borehole wall in this section.

A strong indication of the effect of natural convection in the borehole groundwater on the local borehole resistances was observed when comparing DTTRT2 with DTTRT3, two tests having the same flow rate and different supplied powers. The effect of natural convection is suspected to be larger in multi-pipe designs given their larger heat exchange area exposed to the borehole water as compared to U-pipe BHEs.

A simple finite element method study based on heat conduction only (not accounting for free convection in the groundwater) also showed that the borehole resistance of the multi-pipe design is low and that it drastically changes between 0.018 to 0.093 Km/W with the position of the BHE inside the borehole.

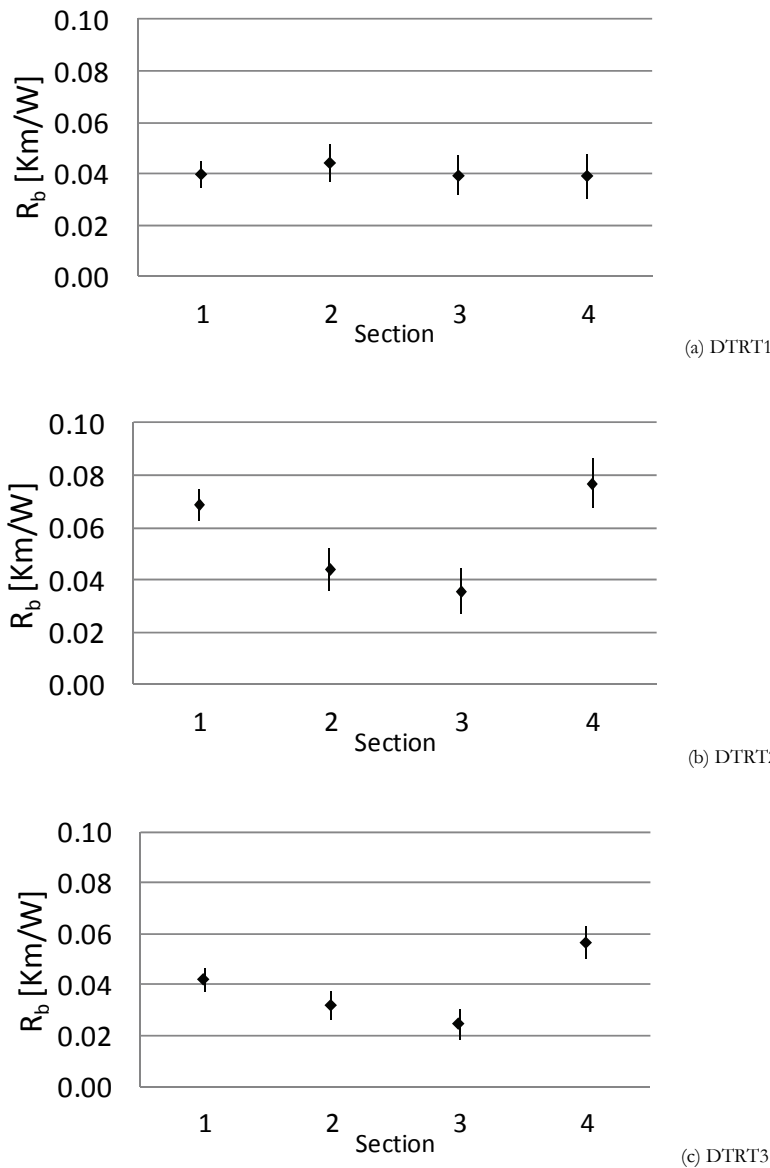


Figure 110. Local borehole resistance results obtained after analyzing all DTRTs

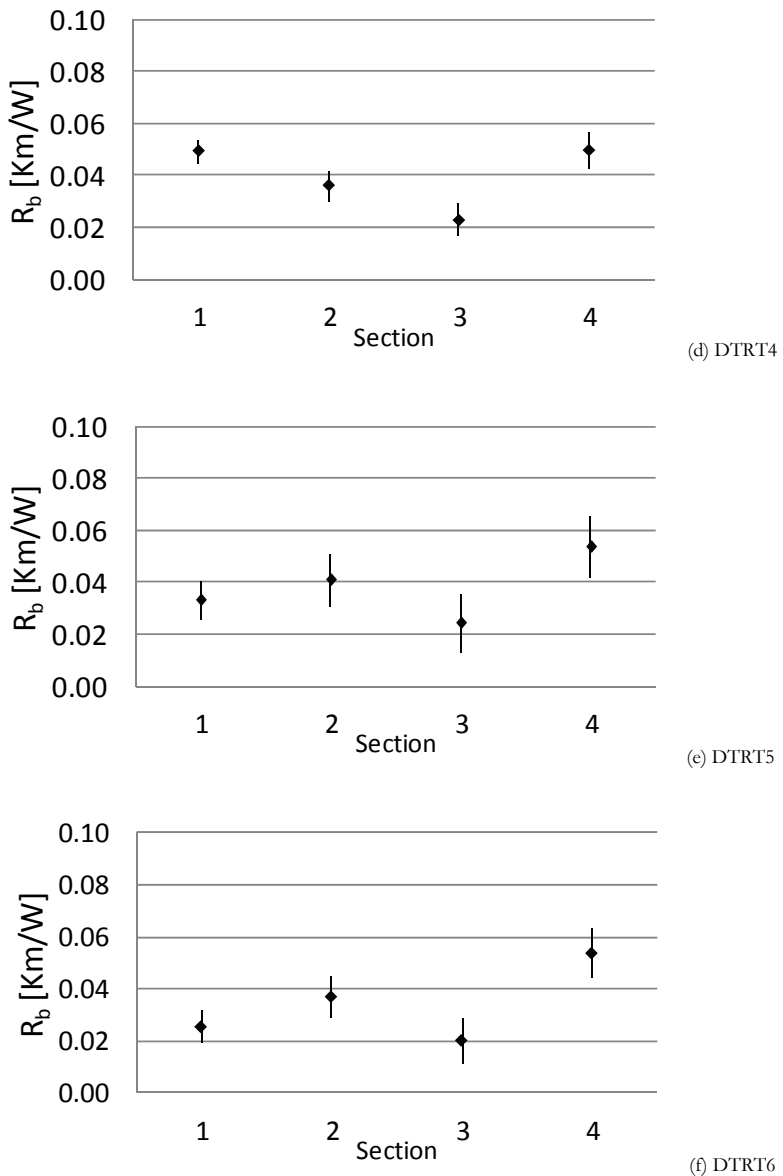


Figure 110. Local borehole resistance results obtained after analyzing all DTRTs

7.4 Flow regime in Multi-pipe BHEs

The expected heat transfer coefficients along the peripheral pipe in which the temperature was measured have been calculated from classical theory for laminar flow for all instants during the experiments. They are found to vary from 180 to 260 W/m²K, as shown in Figure 111.

Since the flow regimes are laminar and the Nusselt number at these conditions is constant, smaller diameters result in larger heat transfer coefficients. This explains the differing results in section 4 (Figure 111), in which the external pipe had a smaller diameter.

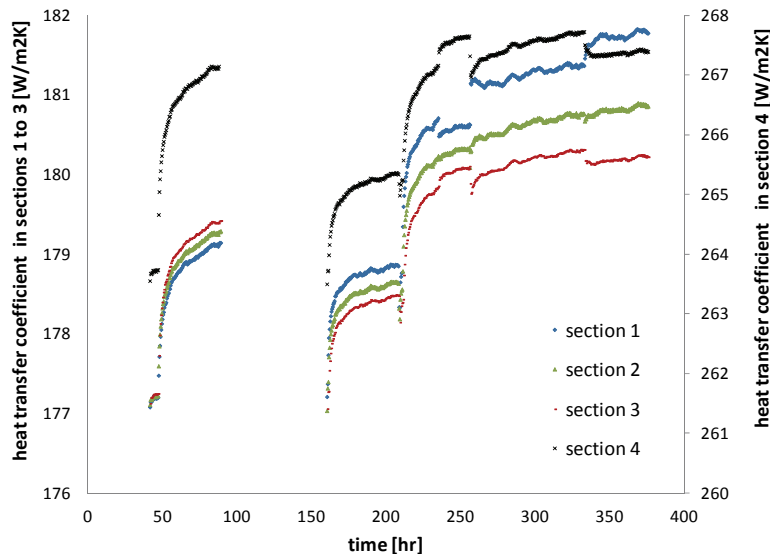


Figure 111. Heat transfer coefficient along the measured peripheral pipe in each section

The vertical distribution of the heat transfer coefficient is exemplified in Figure 112 for the two flow rates presented in Figure 109. Figure 113 shows the Reynolds numbers for the corresponding cases.

The change from laminar to turbulent conditions when passing from the peripheral channels to the central pipe is obvious. This happens at all flow rates tested in paper V except for the 0.14 l/s case where the flow regime in the central pipe is laminar.

Although similar flow transition effects were observed in pipe-in-pipe BHEs, only this multi-pipe BHE is designed to operate at laminar conditions.

It is worth mentioning here that the value of the local thermal resistances resulting from these DTRTs would have been significantly lower if the temperature of the fluid in the central pipe had not been taken into account, considering that it almost does not have any thermal contact with the ground, just like the central pipe in BHE9 and BHE10 (see section 5.3).

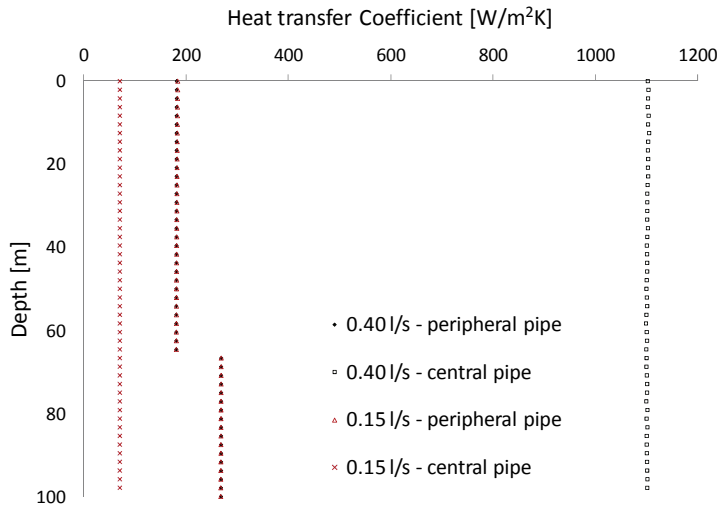


Figure 112. Heat transfer coefficient at two different flows along BHE11

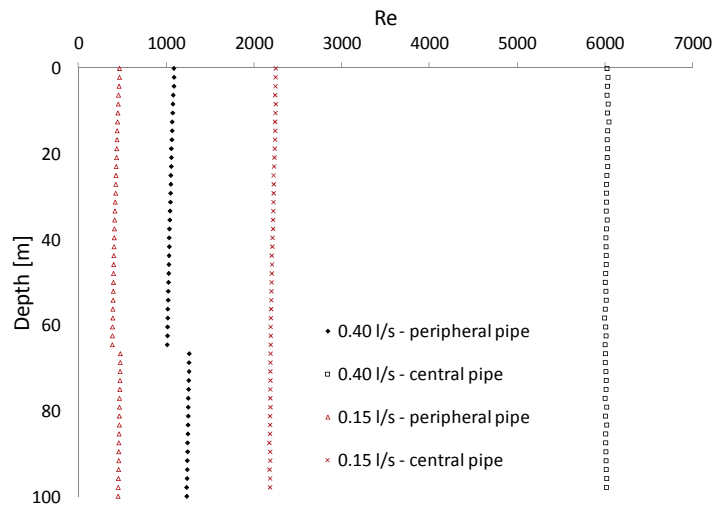


Figure 113. Reynolds number distribution at two different flows along BHE11

7.5 Heat Pump Operation

This BHE has been operating during two winter seasons covering the heating demand of one family house in eastern Stockholm. The secondary fluid flow goes down through the central pipe. The aim with this section is to assess the performance of this multi-pipe BHE connected to a conventional heat pump under normal operating conditions.

Three monitoring periods have been investigated with three different volumetric flow rates (0.13, 0.20 and 0.25 l/s). Table 7-2 presents these periods. The fluid residence time at these flows is about 30, 24, and 18 minutes, respectively, also taking into account the length and size of the piping between the BHE and the heat pump.

Table 7-2. Monitoring periods of Multi-pipe BHE

Measurement period [date and time]	Flow rate [l/s]
2011-10-18 13.45 to 2011-10-28 14.43	0.13
2011-10-28 14.43 to 2011-11-04 12.15	0.20
2011-11-04 12.15 to 2011-11-23 15.00	0.24

Since the same heat pump is used, the extracted power from the ground during ON periods is similar in all cases. The inlet to outlet temperature difference and the vertical temperature profile change depending on the flow rate. Figure 114 show the temperatures in BHE11 during heat pump ON and OFF periods at 0.13 l/s. The operation periods were about 15 to 25 minutes long (at least 5 minutes shorter than the fluid residence time for this BHE).

The duration of the heat pump cycles were similar during the other two measurement campaigns. However, the relatively higher flow rates allowed the observation of more clear temperature profiles along the depth. As an example, Figure 115 shows the temperature development along the depth at 0.20 l/s, and Figure 116 compares the measured temperatures at a last instant before the heat pump shuts down for each tested flow rate.

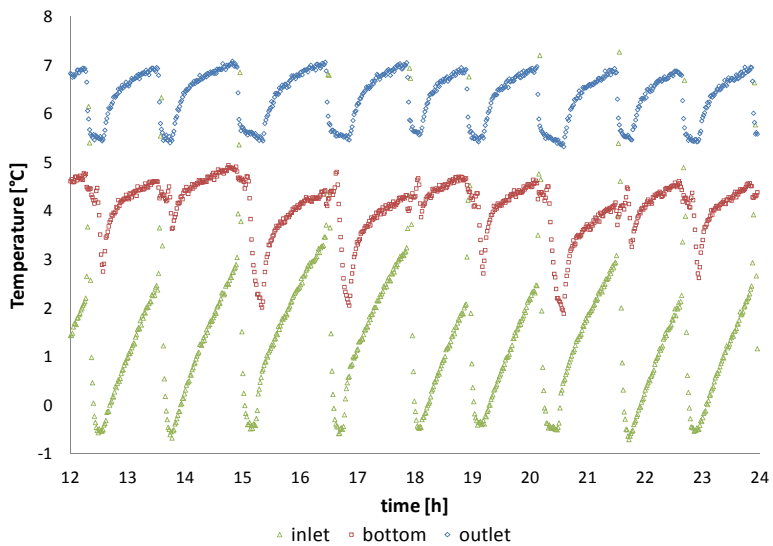


Figure 114. Secondary fluid temperatures at the inlet, bottom and outlet points of the multi-pipe BHE during a day of measurements at 0.13 l/s

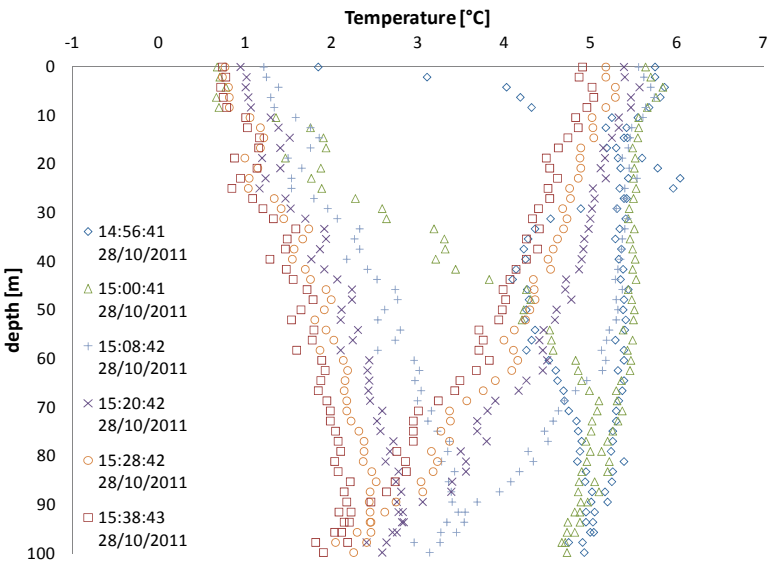


Figure 115. Temperature profiles during heat pump start up at 0.20 l/s

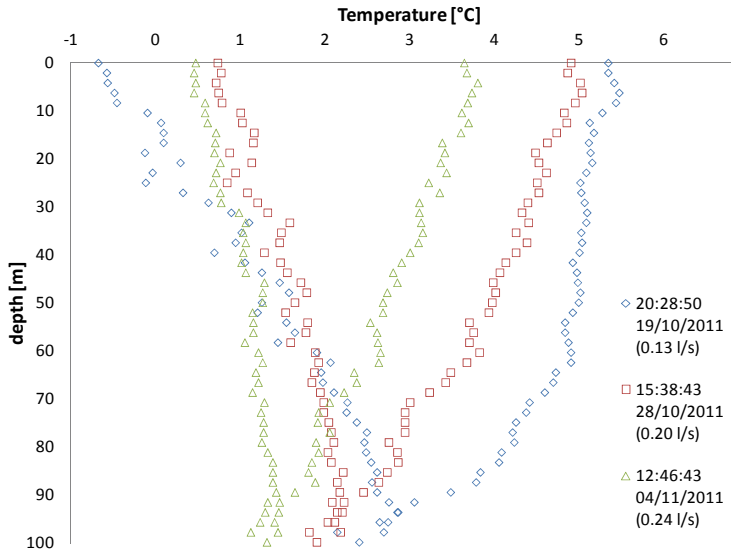


Figure 116. Comparison of measured temperature profiles in BHE11 at different flow rates during heat pump operation (residence time has not elapsed at 0.13 l/s)

Although not shown in Figure 115 the temperatures inside the central pipe during OFF heat pump periods recover very slowly, not as fast as the three measurement points shown in Figure 114, attributed to its relatively higher thermal capacity. This trend is not as abrupt when the fluid enters the BHE through the peripheral pipes. Short term effects are not the subject of this thesis and the study of this phenomenon is suggested for future work.

The effects of insulating the central pipe are not fully observable in Figure 116 (as during heat injection in section 7.3) at any of the flow rates, since the heat transfer process has not yet achieved the steady flux regime in the BHE. It is observed that the inlet temperature decreases with decreasing flow rate, which surely lowers the evaporation temperature in the heat pump.

7.6 Conclusions

- i. A novel type of multi-pipe BHE consisting of one insulated central and 12 peripheral pipes has been tested through 6 distributed thermal response tests and during heat pump operation. This BHE showed good local thermal performance at large temperature differences and low volumetric flow rates.

Temperature measurements inside this BHE were taken with an optical fiber cable and local thermal conductivities were found to vary abruptly along the depth, being larger at the upper parts of the borehole.

- ii. Almost no thermal shunt flow occurs along the tested multi-pipe BHE during steady flux conditions in thermal response tests, thanks to the thermal insulation of the central pipe. The temperature along the central pipe barely changed even at low volumetric flow rates.

The effects of insulating the central pipe are not fully visualized during short heat pump operation periods, and the large temperature difference when running on low flow rates may lower the evaporation temperature in the heat pump.

As the fluid enters the BHE through the peripheral pipes during heat injection, the distribution of the injected power is uneven along this BHE, being highest at the top of the borehole and decreasing with depth. During a thermal response tests, the difference in heat flow can be higher than 50% between the upper and lower borehole sections.

- iii. The flow regime in the peripheral pipes is laminar and the local thermal borehole resistances vary somewhat with depth, being in average about 0.04 Km/W. A finite element method simulation supported the hypothesis that shifting radial pipe location along the depth may be the reason why the measured local borehole resistance varies with depth. In addition, the effect of natural convection on the groundwater reduced the local borehole resistances in the tested multi-pipe BHE by about 30% as the temperature levels changed from about 10 to 14 °C when increasing the injected power by a factor of two.

Almost constant heat transfer coefficients make the local borehole thermal resistance at each section vary little with the flow rate. The flow regime shifts from laminar to turbulent conditions as the fluid moves from the external to the central pipe.

References

- Acuña J. (2008). *Characterization and Temperature Measurement Techniques of Energy Wells for Heat Pumps*. MSc thesis Energy Technology 2008:450. Stockholm: KTH.
- Acuña J. (2010). *Improvements of U-pipe Borehole Heat Exchangers*. Licentiate thesis. Energy Technology. Stockholm: KTH.
- Anbergen H, Frank J, Sass I. (2012). Quality assurance of grouting for Borehole Heat Exchangers. *12th International Conference on Energy Storage* (INNO-U-71). Lleida: ECES.
- Bandos T, Montero A, Fernández de Cordoba P, Urchueguía J. (2011). Improving parameter estimates obtained from thermal response tests: effect of ambient air temperature variations. *Geothermics*, *40*, 136-143.
- Bandyopadhyay G, Gosnold W, Mann M. (2008). Analytical and semi-analytical solutions for short-time transient response of ground heat exchangers. *Energy and Buildings*, *40* (10), 1816-1824.
- Bauer D, Heidemann W, Drück H. (2012). Validation of a groundwater flow and transport modeling tool for borehole thermal energy stores based on FEFLOW. *12th International Conference on Energy Storage* (INNO-U-01). Lleida: ECES.
- Bauer D, Heidemann W, Drück H. (2011). Transient 3D analysis of borehole heat exchanger modeling. *Geothermics*, *40*, 250-260.
- Beier R. A. (2011). Vertical temperature profile in ground heat exchanger during in-situ test. *Renewable Energy*, *36*, 1578-1587.
- Beier R. A., Smith M. D., Spitzer J. D. (2011). Reference data sets for vertical borehole ground heat exchanger models and thermal response test analysis. *Geothermics*, *40*, 79-85.
- Beier R., Smith M. (2003). Minimum duration of in-situ tests on vertical boreholes. *ASHRAE Transactions*, *109*, 475-486.

Bose J, Smith M, Spitler J. (2002). Advances in Ground Source Heat Pump Systems - An International Overview. *7th IEA Heat Pump Conference*. 1:313-324. Beijing.

Carslaw H.S, Jaeger J.C. (1959). *Conduction of Heat in Solids* (2nd uppl.). London: Oxford University Press.

Claesson J, Eftringn B, Eskilson P, Hellström G. (1985). *Markvärme - En handbok om termiska analyser*. Lund: Avd för Matematisk fysik och byggnadsteknik LTH.

Chiasson A, Rees S, Spitler J. (2000). A preliminary assessment of the effects of groundwater flow on closed-loop ground source heat pump systems. *ASHRAE Winter Meeting*. 106, ss. part 1, 929. Dallas, TX.

Claesson J, Bennet J. (1987). Multipole method to compute the conductive heat flows to and between pipes in a cylinder.

Claesson J, Eskilson P. (1988). Conductive Heat Extraction to a Deep Borehole: Thermal Analyses and Dimensioning Rules. *Energy* 13-6, 509-527.

Claesson J, Hellström G. (1988). Theoretical and Experimental study of the local heat transfer in a borehole with heat exchanger pipes. *IV International conference on energy storage for building heating and cooling*. 1, ss. 139-143. Versailles: JIGASTOCK.

Claesson J, Hellström G. (2000). Influence of Regional Groundwater Flow on the Performance of Borehole Heat Exchangers - Detailed Analytical Studies. Department of mathematical physics. University of Lund.

Claesson J, Hellstöm G. (2011). Multipole method to calculate borehole thermal resistances in a borehole heat exchanger. *HVAC&R* 17:6 895-911.

Claesson J, Javed S. (2011). An analytical method to calculate borehole fluid temperatures for time-scales from minutes to decades. *ASHRAE Transactions*, 117 (2), 279-288.

De Carli, Tonon M, Zarrella A, Zecchin R. (2010). A computational capacity resistance model (CaRM) for vertical ground coupled heat exchangers. *Renewable Energy*, 35 (7), 1537-1550.

Diao N, Zeng H, Fang Z. (2004). Improvement in modeling of heat transfer in vertical ground heat exchangers. *HVAC&Research* 10 459-470.

Du C, Chen Y. (2011). An average fluid temperature to estimate borehole thermal resistance of ground heat exchanger. *Renewable Energy*, 36, 1880-1885.

Eskilson P. (1986). Superposition Borehole Model: Manual for Computer Code. University of Lund, Sweden.

Eskilson P. (1987). *Thermal Analyses of Heat Extraction Boreholes*. Department of Mathematical Physics, LTH. Lund, Sweden.

Eskilson P, Hellström G, Wängren B. (1987). *Response Test for a Heat Store with 25 Boreholes*. University of Lund, Mathematical Physics and Building Technology. Lund: Notes on Heat Transfer 9-1987.

EWS. (2006). *GROUNDHIT - brief report on deliverable No. 8 - Design drafts - description of pre-prototype borehole heat exchanger*. Lichtenau: Erdwärmesystemtechnik GmbH & Co. KG.

Fossa M. (2011). The temperature penalty approach to the design of borehole heat exchangers for heat pump applications. *Energy and Buildings* (43), 1473-1479.

Fossa M., Cauret O, Bernier M. (2009). Comparing the Thermal Performance of Ground Heat Exchangers of Various Lengths. *EFFSTOCK*, (s. 113). Stockholm.

Fujii H, Okubo H, Itoi R. (2006). Thermal Response Tests Using Optical Fiber Thermometers. *GRC Transactions 30*, Kyushu University, Fukuoka.

Fujimoto M, Fujii H, Komaniwa Y, Chou N. (2012). Experiments and numerical study on the effects of filling materials in ground heat exchangers. *12th International Conference on Energy Storage* (ss. INNO-U-63). Lleida: ECES.

Gehlin S, Nordell B. (2003). Determining Undisturbed Ground Temperature for Thermal Response Test. *ASHRAE*, Vol. 109, Pt.1.

Gehlin S. (2002). *Thermal Response Test - Method, Development and Evaluation [Doctoral Thesis]*. Luleå: Luleå University of Technology.

GEOTEC. (2012). *Geoenergin i samhället - En viktig del i en hållbar energiförsörjning*.

Gnielinski, V. (1976). New equations for heat and mass transfer in turbulent pipe and channel flows. *Int. Chem. Eng.* 16, 359-368.

Grab T, Storch T, Braune S, Gross U. (2011). Performance of a geothermal heat pipe using propane. *VIII Minsk International Seminar "Heat Pipes, Heat Pumps, Refrigerators, Power Sources"*.

Gustafsson A.M, Westerlund L, Hellström G (2010). CFD-modelling of natural convection in a groundwater-filled borehole heat exchanger. *Applied Thermal Engineering* 30 , 683-691.

Gustafsson A.M. (2010). *Thermal response test: Influence of convective flow in groundwater filled borehole heat exchangers*. Luleå: Doctoral Thesis LTH. ISBN 978-91-7439-143-5.

Gustafsson A.M, Gehlin S. (2008). Influence of natural convection in water-filled boreholes for GCHP. *ASHRAE Transactions* 114-1, 416-423.

Gustafsson A.M, Gehlin S (2006). Thermal Response Test - power injection dependence. *10th int. conf. on thermal energy storage Ecostock*. NJ.

Gustafsson, A.M, Westerlund L. (2010). Multi-injection rate thermal response test in groundwater filled borehole heat exchanger. *Renewable Energy* , 35 (5), 1061-1070.

Hellström G, Kjellsson E. (2000). Laboratory measurements of heat transfer properties of different types of borehole heat exchangers. *Proc. of Terrastock, 2000*. Stuttgart, Germany.

Hellström G, Sanner B. (1997). *EED - Earth Energy Designer. Version 1. User's manual*.

Hellström G. (2002). *Borehole Heat Exchangers - State of the art*. in Hummelshöj, R., Hansen, J. & Lorenzen, K. (eds.), ECES: Annex 13. Subtask 2, International Energy Agency (IEA).

Hellström G. (1994). Fluid to ground thermal resistance in duct ground heat storage. *6th international conference on thermal energy storage* (pp. 373-380). Espoo: CALORSTOCK.

Hellström G. (1991). *GROUND HEAT STORAGE, Thermal Analyses of Duct Storage Systems [Doctoral Thesis]*. Lund: LTH.

Hellström, G. (1998). Thermal Performance of Borehole Heat Exchangers. *The Second Stockton International Geothermal Conference*.

Hjulström J. (2012). Återfyllning av borrhål i geoenergisystem: konventioner, metod och material. Examensarbeten i geologi vid Lunds universitet, kandidatarbete, nr 298. LTH.

Incropera F, De Witt F. (2007). *Fundamentals of Heat and Mass Transfer*. NJ: John Wiley & Sons.

Ingersoll, L. R, Plass. H. J. (1948). Theory of the Ground Pipe Heat Source for the Heat Pump. *ASHVE Transactions*, Vol. 54.

Javed S, Claesson J. (2011). New analytical and numerical solutions for the short-term analysis of vertical ground heat exchangers. *ASHRAE Transactions* (117), 3-12.

Kavanaugh, Rafferty. (1997). *Ground Source Heat Pumps, Design of Geothermal Systems for Commercial and Institutional Buildings*. ASHRAE.

Kharseh M. (2011). *Reduction of prime energy consumption by ground source heat pumps in a warmer world*. Doctoral thesis: Luleå University of Technology.

Kjellsson E, Hellström G. (1997). Laboratory study of the heat transfer in a water-filled borehole with a single U-pipe. *7th International conference on thermal energy storage* (ss. 509-514). Sapporo: MEGASTOCK.

Kruse H, Peters S. (2008). Earth Heat Pipe Working with Carbon Dioxide Status of Development. Zurich: 9th Int. IEA Heat Pump Conference.

Kruse H, Russmann H. (2005). Novel CO₂-Heat Pipe as Earth Probe for Heat Pumps without Auxiliary Pumping Energy. 8th International IEA Heat Pump Conference. Las Vegas.

Lamarche L, Beauchamp B. (2007). A new contribution to the finite line source model for geothermal boreholes. *Energy and Buildings* 39 (2) 188-198.

Lamarche L, Kajl S, Beauchamp B. (2010). A review of methods to evaluate borehole thermal resistances in geothermal heat-pump systems. *Geothermics* 39, 187-200.

Liebel H. (2012). *Influence of groundwater on measurements of thermal properties in fractured aquifers*. Doctoral thesis. Trondheim: NTNU.

Liebel H, Javed S, Vistnes G. (2012). Multi-injection rate thermal response test with forced convection in a groundwater-filled borehole in hard rock. *Renewable Energy* 48, 263-268.

Lund J, Derek H, Tonya L. (2010). Direct Utilization of Geothermal Energy 2010 Worldwide Review. (s. 007). Bali: Proceedings IGA World Geothermal Congress 2010.

Marcotte D, Pasquier P. (2008). On the estimation of thermal resistance in borehole thermal conductivity test. *Renewable Energy*, 33, 2407-2415.

Mei V, Fischer S. (1983). Vertical Concentric Tube Ground-Couple Heat Exchangers. *ASHRAE Transacciones*, 89 (part 2B), 391-406.

Melinder Å, Berendson J, Granryd E, Kyrk B. (1989). Köldbärare för värmepumpstillämpningar. Byggforskningsrådet R18:1989.

Melinder Å. (2007). *Thermophysical Properties of Aqueous Solutions Used as Secondary Working Fluids [Doctoral Thesis]*. KTH.

Mogensen P. (1983). Fluid to Duct Wall Heat Transfer in Duct System Heat Storages. *The International Conference on Subsurface Heat Storage in Theory and Practice*. Appendix, Part. II, p. 652-657. Stockholm.

Montero A, Martos J, Martínez G, Urchueguía J. (2012). Experimental measurement of the ground temperature recovery time after borehole heat exchanger insertion. *12th International Conference on Energy Storage* (ss. INNO-U-37). Lleida: ECES.

Ochsner K. (2008). Carbon Dioxide Heat Pipe in Conjunction with a Ground Source Heat Pump. *Applied Thermal Engineering*, 2077-2082.

Oliver J, Braud H. (1981). Thermal Exchange to Earth with Concentric Well Pipes. *Transactions of the ASABE*. 24 (4), 0906-0910.

Paul (1996). *The effect of Grout Thermal Conductivity on Vertical U-tube Heat Exchanger Design and Performance*. Vermillion, USA: MSc. thesis, South Dakota University.

Platell P. (2006). Developing Work on Ground Heat Exchangers. *ECOSTOCK 2006 Conference Proceedings* (pp. 7A-1). NJ. ECOSTOCK.

RHC. (2012). *Strategic Research Priorities for Geothermal Technology*. Brussels: European Technology Platform on Renewable Heating and Cooling.

Rieberer R, Mittermayr K, Halozan H. (2002). CO₂ Heat Pipe for Heat Pumps. *IIR/IIF-Commission B1,B2,E1 and E2*, (ss. 200-207). Guangzhou.

Rieberer R, Mittermayr K, Halozan H. (2005). CO₂ Thermosyphons as Heat Source System for Heat Pumps - 4 Years of Market Experience. *8th IEA Heat Pump Conference*, (s. o6_5). Las Vegas, Nevada, USA.

- Rieberer R, Mittermayr K, Halozan H. (2004). CO₂ Two-phase Thermosyphon as Heat Source System for Heat Pumps. *6th IIR - Gustav Lorentzen Conference on Natural Working Fluids*. Glasgow.
- Rieberer, R. (2005). Naturally Circulating Probes and collectors for Ground Couple Heat Pumps. *Int. Journal of Refrigeration* 28, 1308-1315.
- Risorto, L. (2012). *Modeling and validation of U-pipe thermosyphon borehole heat exchanger with CO₂*. Energy Technology. Stockholm: KTH.
- Sanner B, Karytsas K, Abry M, Coelho L, Goldbrunner J, Mendrinos D. (2007). GROUNDHIT - Advancement in ground source heat pumps through EU support. *European Geothermal Congress*. Unterhaching.
- Sanner, B. (1991). In-Situ Corrosion Test for Ground Heat Exchanger Materials in Schwalbach, GCHP Research Station. *IEA Heat Pump Centre newsletter*, 9 (3), 27-29.
- Sharqawy M, Mokheimer E, Badr H. (2009). Effective pipe-to-borehole thermal resistance for vertical ground heat exchangers. *Geothermics* 38, 271-277.
- Shonder J, Beck J. (1999). Determining effective soil formation properties from field data using a parameter estimations technique. *ASHRAE Transactions* 105 (1), 458-466.
- Spitler J. (2000). GLHEPRO - A design tool for commercial building ground loop heat exchanger. (s. 115). Aylmer, QC, Canada: Proceedings of the 4th International Conference on Heat Pumps in Cold Climates.
- Spitler J, Bernier M. (2011). Ground-source heat pump systems: The first century and beyond. *HVAC&R*, 17:6, 891-894.
- Storch T, Grab T, Zieger C, Schreiter S, Kupka M, Gross U. (2011). Visual observations inside a geothermal heat pipe. *VIII Minsk International Seminar "Heat Pipes, Heat Pumps, Refrigerators, Power Sources"*.
- Storch T, Weickert T, Grab T, Gross U. (2012). Wetting and film behaviour of propane inside geothermal heat pipes. *16th International Heat Pipe Conference*. Lyon, France.
- SVEP. (2012). Hämtat från <http://www.svepinfo.se/aktuellt/statistik/>
- Witte H. (2012). The GEOTHEX geothermal heat exchanger, characterisation of a novel high efficiency heat exchanger design. *12th International Conference on Energy Storage* (ss. INNO-U-32). Lleida: ECES.

- Witte H, Van Gelder A. (2006). Geothermal response tests using controlled multi-power level heating and cooling pulses: quantifying groundwater effects on heat transport around a borehole heat exchanger. *10th International Conference on Thermal Energy Storage (Ecostock)*. New Jersey.
- Yang W, Mingheng S, Guangyuan L, Zhenqian C. (2009). A two-region simulation model of vertical U-tube ground heat exchanger and its experimental verification. *Applied Energy* 86, 2005–2012.
- Yavuzturk C, Spitler J. (1999). A short time step response factor model for vertical ground loop heat exchangers. *ASHRAE Transactions* (105) 475-485.
- Yavuzturk C, Spitler J. (2001). Field validation of a short time step model for vertical ground loop heat exchangers. *ASHRAE Transactions* (107) 751-759.
- Yavuzturk C, Chiasson A. (2002). Performance analysis of U-tube, concentric tube, and standing column well ground heat exchangers using a system simulation approach. *ASHRAE Transactions* 108 (1), 925-938.
- Yavuzturk C, Chiasson A, Nydahl J. (2009). Simulation model for ground loop heat exchangers. *ASHRAE Transactions* (115) 45-59.
- Zanchini E, Lazzari S, Priarone A. (2010a). Effects of flow direction and thermal short-circuiting on the performance of small coaxial ground heat exchangers. *Renewable Energy* (35), 1255–1265.
- Zanchini E, Lazzari S, Priarone A. (2010b). Improving the thermal performance of coaxial borehole heat exchangers. *Energy* (35), 657–666.
- Zarrella, Scarpa M, De Carli M. (2011). Short time step analysis of vertical ground-coupled heat exchangers: The approach of CaRM. *Renewable Energy*, 36 (9), 2357–2367.
- Zeng H, Diao N, Fang Z. (2002). A finite line source model for boreholes in geothermal heat exchangers. *Heat Transfer - Asian Research* (31), 558-567.
- Zeng H, Diao N, Fang Z. (2003). Heat transfer analysis of boreholes in vertical ground heat exchangers. *Heat and Mass Transfer* 46, 4467-4481.